7-12-2014

A New CFRP-UHPC System for Strengthening Reinforced Concrete T-Beams

Moneeb Genedy

Moneeb Genedy
Candidate

Civil Engineering
Department

This thesis is approved, and it is acceptable in quality and form for publication:

Approved by the Thesis Committee:

Mahmoud Reda Taha , Chairperson

Arup Maji

Yu-Lin Shen

A New CFRP-UHPC System for Strengthening Reinforced Concrete T-Beams

BY

Moneeb Genedy

B.S. CIVIL ENGINEERING, Alexandria University, Egypt, 2008

M.S., CIVIL ENGINEERING, University of New Mexico, 2014.

THESIS

Submitted in Partial Fulfillment of the
Requirements for the Degree of

Master of Science

Civil Engineering

The University of New Mexico
Albuquerque, New Mexico

May, 2014

DEDICATION

I would like to dedicate this work to my parents, Gamal Genedy and Samyah Genedy, and my wife, Rania Ghallab, who have provided me with everything that I have needed to succeed.

ACKNOWLEDGMENTS

I would like to thank my advisor and committee chair, Dr. Mahmoud Reda Taha for his help, support, and motivation through this program. Without Dr. Taha's guidance and advice, I would not have been able to finish this work. I am honored to work under his supervision. I would also like to thank my committee members, Dr. Arup Maji and Dr. Yu-Lin Shen, for their support.

I would further acknowledge Mr. Ken Martinez for his sincere help to conduct these experiments. I would like also to thank Andrew Garner for his help and advice. In addition, I would like to extend a special thanks to my colleagues, Sherif Aboubakr, Sherif Daghash, Andrew Griffin, Michelle Begaye, Elisa Borwsky, and Rahulreddy Chennareddy for their help and assistance with the concrete batching and testing required for this project. And thanks to everybody else in my group.

I would also like to acknowledge Department of Energy for funding my assistantship and research.

Preface

During the course of this thesis (2013-2014) the following papers have been submitted for publication in reviewed proceedings.

1- Genedy, M., Kim, J. J., and Reda Taha, M., *Strengthening of RC T-Beams Using CFRP and UHPC*, in *International Conference on Construction Materials and Structures*. 2014: Johannesburg, South Africa.

2- Genedy, M., Kim, J. J., and Reda Taha, M., *Innovative Strengthening of RC Beams Using CFRP-UHPC Composite*, in *The 7th International Conference on FRP Composites in Civil Engineering*. 2014: Vancouver, Canada.

3- Genedy, M., Daghash, S., Soliman, E., and Reda Taha, M., *Improving Tensile Strength of GFRP Using Carbon Nanotubes*, in *The 7th International Conference on FRP Composites in Civil Engineering*. 2014: Vancouver, Canada.

4- Soliman, E., Genedy, M., and Reda Taha, M., *Altering the Tension behavior of GFRP Using Carbon Nanotubes*, in *The twenty-second International Conference on Composites/Nano Engineering*. 2014: Malta.

A New CFRP-UHPC System for Strengthening Reinforced Concrete T-Beams

by

Moneeb Genedy

B.S. CIVIL ENGINEERING, Alexandria University, Egypt, 2008

M.S., CIVIL ENGINEERING, University of New Mexico, 2014.

ABSTRACT

Since Fiber Reinforced Polymer (FRP) was introduced to the construction field, strengthening of reinforced concrete beams using FRP laminates became a common repair and retrofit technique. Traditionally, Reinforced Concrete (RC) beams are strengthened by adhering FRP laminates to the tension side of the beam to work as an additional tensile reinforcement. Although this technique has been proven as an efficient strengthening technique, in many cases reaching the tension side of the beam is challenging due to the existing of ducts, pipes or cables underneath the beam in buildings. This challenge is magnified in bridges crossing water canals or major highways where expensive scaffolding is needed to reach the underside of beams.

This research investigates a flexural strengthening system for T-beams that avoids the need to reach the tension underside. In this technique, the top 51 mm cover of the beam is removed, and Carbon Fiber reinforced polymer (CFRP) laminates are attached to the existing concrete surface after which an Ultra High performance Concrete (UHPC) overlay is then cast on top of the CFRP. The hypothesis of this technique is that the very

high compressive strength of the UHPC overlay will push the neutral axis up and allow the CFRP laminates to be under tension. Four RC beams were cast and tested under four-point bending until failure. The proposed strengthening technique showed an increase in the load capacity while strengthening beam with only UHPC overlay had no significant effect on the load capacity of the beam. Unlike the expected, replacing the UHPC overlay with Latex Modified Ultra High Performance Concrete (LMUHPC) overlay did not increase the bond between the overlay and the T-beam and resulted in low load capacity. These results indicate that the proposed technique might be beneficial for shallow to medium T-beams and slabs.

.

Contents

LIST OF TABLES

LIST OF FIGURES

CHAPTER 1. Introduction

1.1. Motivation and problem statement

Concrete is the most used material in construction and holds the second highest consumption rate of a material after water [1]. The estimation of the value of concrete used in 2012 is $41 billion [2]. Concrete used in construction purposes is normally reinforced with steel rebars due to its weak tensile strength. Reinforced Concrete (RC) is a favorable construction material due to its relatively long life cycle. During its lifetime, a concrete structure most likely will need to be repaired or strengthened. Deterioration of concrete, corrosion of steel rebars, and the increase of the expected loads on structures are the main causes for the need for concrete strengthening [3-5].

Traditionally, flexural strengthening of a reinforced concrete beam is used to mean increase its cross section area and add additional steel reinforcement. Additional reinforcement is arranged at the tension side and additional concrete is cast to increase the beam's cross section area. Since Fiber Reinforced Polymer (FRP) was introduced to the construction industry, a flexural strengthening technique using FRP laminates has gained wide acceptance. High strength to weight ratio and corrosion resistance has made FRP a more favorable strengthening material than steel. FRP laminates are attached to the tension side of the beam using flexible adhesive, typically epoxy, to work as additional tension reinforcement [6-9].

Although flexural strengthening of RC beams by applying FRP laminates at the tension side is an efficient technique of strengthening, in many cases reaching the tension side of

the beam is a challenge in building. This challenge is attributed to obstacles by existing ducts, pipes, or electrical wires and cables underneath the beam. Special expensive arrangements are typically needed to reach the tension side of the beam. Moreover, in bridges crossing water canals or major highways, access to the underside of the beams requires large and typically very expensive scaffolds. These special arrangements or scaffolds make this strengthening technique very expensive [4, 5]. Thus, an innovative flexural strengthening technique is required to overcome this challenge.

1.2. Contribution

A composite flexural strengthening system for beams without the need to reach the tension side based on the work done by [3, 4, and 5] is suggested and investigated in this thesis. The proposed system is a combination of Ultra High Performance Concrete (UHPC) and Carbon Fiber Reinforced Polymer (CFRP). In this technique, the top 50 to 75 mm cover of the RC beam is removed and CFRP laminates are attached to the existing concrete surface using epoxy. Afterward, the top cover is replaced with UHPC overlay. The very high strength of UHPC overlay will make the area of the compression zone required for equilibrium smaller than that in normal concrete. Therefore, using UHPC will push the neutral axis up causing the CFRP to be under tension. This will allow the CFRP to work as an additional tension reinforcement and increase the moment capacity of the beam.

To investigate the efficiency of the technique in strengthening T-beams in flexure, four T-beams were made and tested. Many factors including reinforcement arrangement, distance between the supports and properties of the concrete affect the capacity of the

beam. Thus, very high precision was adopted to normalize all the factors that could affect the results to ensure that an absurd change in behavior or capacity of the T-beam is due to the modifications made intentionally in the strengthened system. Moreover, the possible modes of failure in beams were a challenge to investigate this technique. A flexure failure in all beams was favorable to evaluate the efficiency of the proposed flexural strengthening technique.

The proposed strengthening technique was investigated on simply supported slabs by [3] and on continuous slabs by [4 and 5]. The strengthening technique showed very promising results in strengthening slabs. However, the efficiency of the proposed system with T-beams was never investigated. Moreover, many arguments were raised on the benefits of incorporating CFRP laminates in the strengthening technique and the potential enhancement in the capacity of the flexural elements could be due to the UHPC overlay. Thus, four T-beams were cast and tested to validate the suggested strengthening technique. The first T-beam is a control beam to compare results. The second beam is only strengthened with UHPC overlay with no CFRP laminates. This second beam will validate contribution of the CFRP laminates to flexural strengthening. The third beam is strengthened with CFRP and UHPC overlay to investigate the efficiency of the proposed system in flexural strengthening of T-beams. In the fourth beam, the UHPC overlay was replaced by Latex Modified Ultra High Performance Concrete (LMUHPC) to investigate the effect of adding SBR polymer latex to UHPC on the bond between the overlay and existing concrete surface. Our hypothesis was that using LMUHPC will overcome the potential debonding issue appeared in strengthening slabs [3].

Testing observations and analysis showed that strengthening beams with only UHPC overlay had almost no effect on the flexural capacity of the T-beam. The increased flexural capacity of the beam strengthened with only the UHPC overlay is less 1%. On the other hand, the contribution of the CFRP laminates in the strengthened beam was able to increase the load capacity, but this increase was limited to 9.2%. The limitation in the load capacity increase was due to the change of failure mode to be governed by shear failure instead of flexure governed failure. Failure was governed by shear due to the additional tension demand of the shear force and the insufficient developing length of the tension rebars at the support area. Unlike the expected, the T-beam strengthened with CFRP and LMUHPC failed earlier due to debonding between the LMUHPC overlay and the normal concrete surface. This was due to the low Young's modulus of elasticity of MLUHPC. From this research and the work done by [3, 4, and 5] it can be concluded that this technique is efficient with slabs and shallow, like ribbed T-beams, and medium depth T-beams. As the depth of the beam increases, the efficiency of the strengthening technique decreases due to the limited moment arm of CFRP compared to the beam depth.

1.3. Outline of the thesis

Chapter 2 of the thesis presents a literature review on strengthening techniques of RC flexural elements. Moreover, a brief literature review on Ultra High Performance Concrete (UHPC) and Latex Modified Concrete (LMC) is provided.

Chapter 3 describes the experimental methods for this research. The chapter begins with explaining the experimental program. Then, information for the materials used is

presented. Next, the dimensions of the beams, casting of concrete, applying CFRP laminates and shear dowels, mixing and casting UHPC and LMUHPC, and curing process are described. Finally, the test setup and information on test preparation are discussed.

A comparison between normal concrete, UHPC, and LMUHPC is presented in Chapter 4. After that, detailed calculations for the expected behavior of the four beams are presented. This is followed by an analysis of the test results. The chapter ends with a comparison and discussion of the analyzed results of the four T-beams. Finally, conclusions are drawn and a set of recommendations for future research is presented in Chapter 5.

CHAPTER 2. Literature Review

2.1. Strengthening RC beams

Traditionally, flexural strengthening of a reinforced concrete beam used to mean increasing its cross section area and adding additional steel reinforcement. Additional reinforcement is arranged at the tension side and additional concrete is cast to increase the beam's cross section area as shown in **Figure 2.1**. In 1960s, strengthening of RC beams using externally attaching steel plates to the tension side of the beam was presented in South Africa [10]. Although externally attaching steel plates to the tension side of the beam proved effective in flexural strengthening, external exposure of a steel plate outside the beam makes it more prone to environmental deterioration mechanics such as corrosion. Furthermore, the heavy weight of steel made installation of these plates difficult and relatively expensive. Thus, an alternative strengthening technique was required [6, 10].

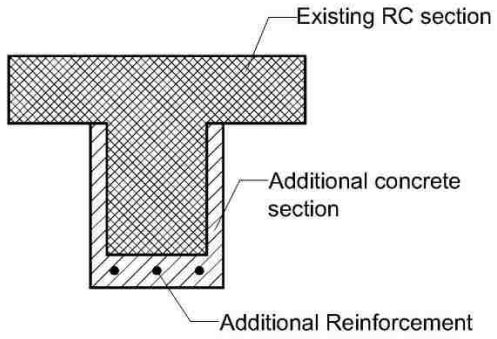

Figure 2.1: Schematic for traditional strengthening technique

2.2. Convention strengthening technique for RC beams with FRP

Since FRP was introduced to the construction industry, flexural strengthening technique using FRP laminates gained wide acceptance. Using FRP laminates in repairing and strengthening beams and slabs was presented in 1980s [8]. The concept of FRP strengthening technique is to attach the FRP laminates to the tension side of the beam to work as additional tension reinforcement [11-12]. This technique showed high efficiency and was able to increase the load capacity of the beams above 100% [7]. Strengthening beams with externally attached FRP laminates showed no change in the mechanics of the beam. Stress and strain distributions on strengthened section are presented in **Figure 2.2** [11]. For the purpose of estimating the load capacity of the strengthened section, it was assumed that FRP is perfectly bonded to the concrete surface, relative deformation in the adhesion is negligible, and the FRP behavior is linear-elastic until failure [3]. Guidelines were developed worldwide to enable economical and safe design of FRP strengthening systems [11].

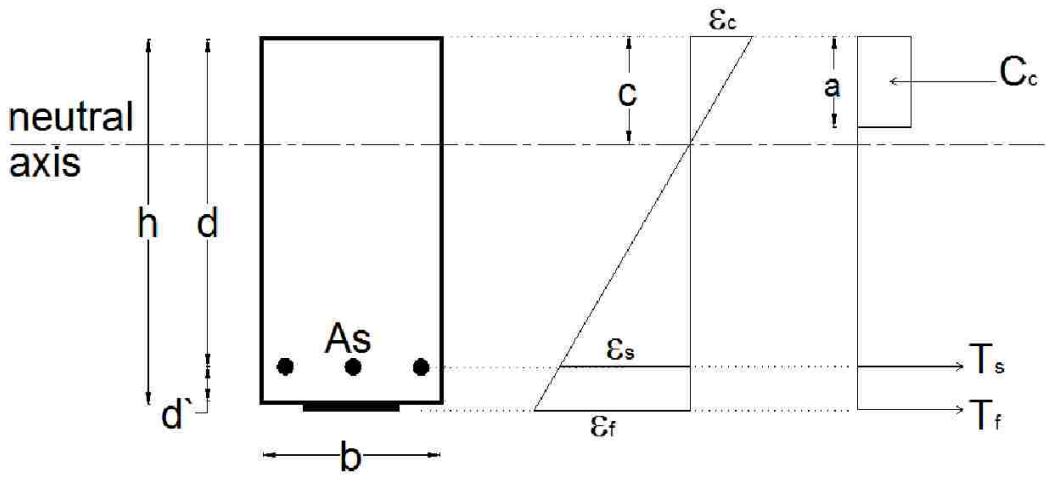

Figure 2.2: Stress and strain distribution for strengthened section [26]

2.3. Fiber Reinforced Polymer (FRP)

Fiber Reinforced Polymer (FRP) is a composite material made of polymer (typically epoxy) matrix reinforced with certain types of fibers. FRP laminates can be categorized according to the type of fiber reinforcement used. Carbon, glass, kevlar or aramid are the main types of fibers used to fabricate FRP laminates [3]. Another way of classifying FRP laminates is the orientation of the reinforcement fibers inside the polymer matrix. Unidirectional FRP is that FRP that all its reinforcement fibers are oriented in the same direction. On the other hand, FRP is defined as bi-directional when the reinforcement fibers are oriented to two orthogonal directions.

FRP was presented and accepted as a construction material in the construction industry due to its high strength/weight ratio and its high corrosion resistivity. Among the three types of FRP, Carbon Fiber Reinforced Polymer (CFRP) has higher modulus of elasticity and ultimate tensile strength than Glass Fiber Reinforced Polymer (GFRP) and Aramid Fiber Reinforced Polymer (AFRP). On the other hand, the rupture strain of CFRP is lower than both GFRP and AFRP [11]. Although, FRP is able to carry compression forces, its fibers are prone to buckle. This makes compression not a favorable stress state for FRP [4]. The absence of the plasticity in the stress-strain behavior of FRP resulted in its sudden failure. Although FRP has very high corrosive resistance, its polymer matrix makes it sensitive to some environmental conditions like change in temperature and humidity. These disadvantages necessitated developing special design provisions to provide ductility and durability in RC structures strengthened or reinforced with FRP [3].

2.4. Innovative strengthening technique

Although flexural strengthening of RC elements by applying FRP laminates at the tension side is an efficient technique of strengthening, in many cases reaching the tension side of the flexure element is a challenge in buildings and bridges crossing water canals or major highways. Special arrangements and large scaffolds are typically needed to reach the tension side of the element. These special arrangement or scaffolds make this strengthening technique very expensive [3-5]. Thus, an innovative flexural strengthening system was proposed by Mosallam, et al to overcome this challenge [4, 5].

A composite system was made of CFRP and High Performance Concrete (HPC) for strengthening continuous one way RC slabs without the need to reach the tension side of the slab. The CFRP laminates were applied to the top side of the slab. Afterwards, a thin layer of HPC is cast on the top of the CFRP laminates [4, 5]. The system is modified by Garner by replacing the HPC overlay with UHPC overlay [3]. Cross section of the strengthened slab with the proposed system by Garner is presented in **Figure 2.3**.

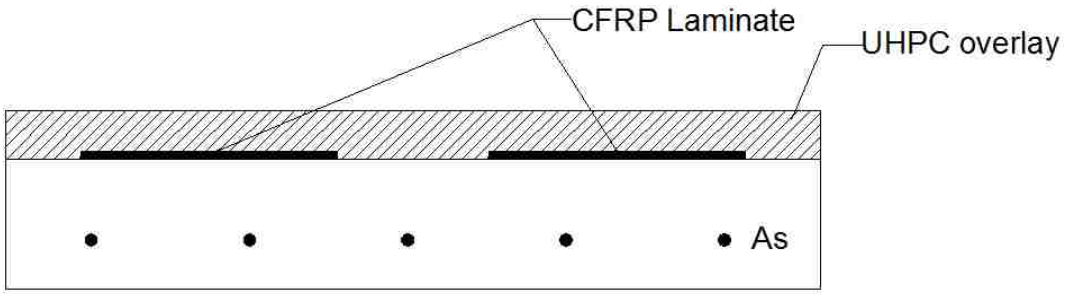

Figure 2.3: Strengthened slab cross-section [3]

The concept of the proposed technique is that using a high strength of UHPC overlay will push the neutral axis up making CFRP to act under tension. This will allow CFRP to

work as additional tension reinforcement and increase the moment capacity of the slab. The proposed strengthening technique showed increase of the nominal capacity of one way slabs by 41% [3].

2.5. Latex Modified Concrete (LMC)

The definition of Latex Modified Concrete (LMC) according to ACI is mixing the concrete components with organic polymer dispersed in mixing water [15]. Polymer latex has a very high using rate among concrete polymer admixtures [16]. Adding polymer latex to concrete mix to produce LMC was first patented in 1924. Since the first patent, many patents and researches of LMC system were conducting until now [17]. LMC systems are mainly used as a repair material or as overlays in bridges [16 – 21].

Adding polymer latex to concrete mix forms elastic membranes in the concrete and reduces the formation of voids and cracks and increase the impermeability of concrete [21, 22]. This improvement increases LMC durability and makes it more suitable to serve in extreme condition than normal concrete [18, 22]. Moreover, polymer latex gives LMC high bond strength making it preferable alternative for application requiring high adhesion [23]. LMC required deferent curing conditions than normal concrete to allow forming polymer inside concrete. LMC need to be cured in water for 2days followed by air curing.

2.6. Ultra High Performance Concrete (UHPC)

UHPC was first produced in early 1980s. To be able to consider concrete as Ultra High Performance Concrete (UHPC), its compressive strength have to be at least 125 MPa (18,000 Psi) [3]. The high cement content, low water/cement ratio, silica fume, and well

graded materials are main factors contributing in the UHPC high strength. Silica fume has two roles in UHPC mix as it works as filler and as pozzolanic material [24-26]. The nominal size of the aggregate used in UHPC mixes is small and typically in the range of 5 mm [24].

To achieve the very high compressive strength in UHPC, very low water/binder ratio is needed. Typically, the water/binder ratio in UHPC mixes is less than 0.2 [3, 24. 25]. To keep UHPC workable with this low water/binder ratio, large amount of superplastisizers is required. With this low water content, mixing procedure and time of the normal concrete is not suitable for mixing UHPC. Although mixing time of UHPC depends on the mixer type and the energy supplied by mixer, 15 minutes is the average time required to obtain homogeneous UHPC mix [24, 25, 27]. Although fresh UHPC is workable and can be cast, it loses workability very quickly after casting [28, 29]. Moreover, curing conditions has major effect of UHPC properties and it can gain very high early strength with hot water or steam curing [24, 29]. In the last decade, UHPC has been used in construction projects in USA, Canada, and South Korea [3, 30].

CHAPTER 3. Experimental Methods

This chapter describes the experimental methods for the research starting with the experimental program. Then, the properties of the materials used are discussed. Afterwards, dimensions of the beams, casting of concrete, applying CFRP laminates and shear dowels, and curing process are described. Finally, test setup and preparation is discussed.

3.1 Experimental program

This research program included testing of four flexural T-beams under static bending. The first beam is the control beam (Beam-C). This beam is used as reference beam to investigate the effect of the strengthening system and modifications on the flexural capacity of T-beams. Beam-C only contains regular concrete and steel reinforcement. The second beam is the beam in which the top 51 mm layer was replaced by Ultra-High Performance Concrete (UHPC) overlay and called (Beam-U). This beam is tested to investigate the effect of UHPC overlay only on the flexural capacity of the beam. The third beam is the beam strengthened with the Carbon Fiber reinforced Polymers (CFRP) laminates and UHPC overlay denoted (Beam-UF). This beam was tested to investigate the effect of new proposed strengthening system on the flexural capacity of the T-beam. The forth beam has the same strengthening system as Beam-UF with the UHPC overlay replaced with Latex Modified Ultra-High Performance Concrete (Beam-MUF). This beam it was tested to investigate the effect of incorporating polymer latex with UHPC on the bond between the LMUHPC and the regular concrete. All the four beams were tested at age of 10 weeks (70 days).

3.2 Materials

The regular concrete used is a ready mix concrete obtained from a local ready mix plant in Albuquerque, New Mexico. The concrete has a maximum nominal aggregate size of 12.7mm. The slump of the concrete was 164 mm and it had a 28 days compressive strength of 33 MPa. Further discussion on the concrete properties is presented in Chapter 4. For the reinforcement of the four beams, steel rebars with diameters of 13 mm and 10 mm were used. The yield strength of the steel is 414 MPa. For Beam-UF and Beam-MUF unidirectional Carbon Fiber Reinforced polymer (CFRP) laminate sheets provided by Graphtec LLC were used. The laminates have a thickness of 1.14mm and width of 51mm. The tensile strength of the laminates is 2689 MPa and the young's modulus of elasticity (E) is 131.3 GPa. **Figure 3.1** shows the stress-strain curve for the CFRP laminates.

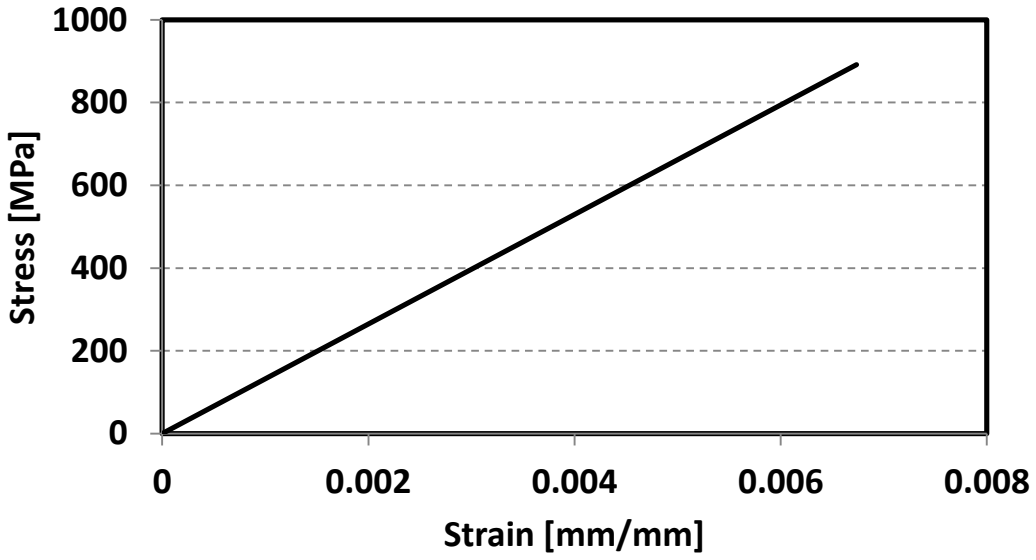

Figure 3.1: Stress-strain curve for CFRP laminates

For attaching the CFRP sheets and the shear dowels to the concrete, a low viscosity epoxy system manufactured by Euclid Chemical Company was used. The epoxy system has a resin to hardener mixing ratio of 3:1.

3.3 Beams dimensions and reinforcement

All the four T-beams were identical in dimensions. The beams had a total length of 2438 mm and the span between the supports is 2290 mm. The beams were loaded under two concentrated loads spaced at 914mm. Each beam was reinforced with two longitudinal number 4 bars (D = 13mm) with cover of 50 mm and number 3 stirrups (D = 10mm) spaced at 127 mm. Two number 3 bars was place 75 mm from the top of the beam to ensure the stability of the reinforcement cage during casting the concrete. These rebars were intentionally interrupted at mid-span to eliminate their contribution in beam's moment capacity. **Figure 3.2** shows a longitudinal section of the beam illustrating the reinforcement arrangement.

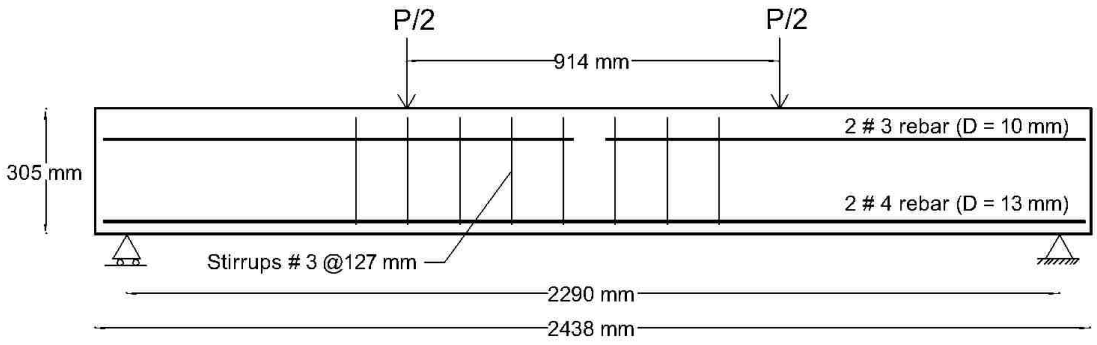

Figure 3.2: Longitudinal section and reinforcement arrangement

The total height of each beam is 305 mm and the web width is 152 mm. The flange of the beam has a thickness of 102mm and its width is 457mm. Beam-U has a top layer of

UHPC with a thickness of 51mm. Beam-UF has two CFRP laminate sheets with width of 51mm and thickness of 1.14 mm attached to the regular concrete and a 51 mm layer of UHPC on top of the CFRP sheets. Beam-MUF is the same like Beam-UF but the UHPC layer was replaced with a LMUHPC layer with the same thickness. **Figure 3.3** shows the cross section for the four beams.

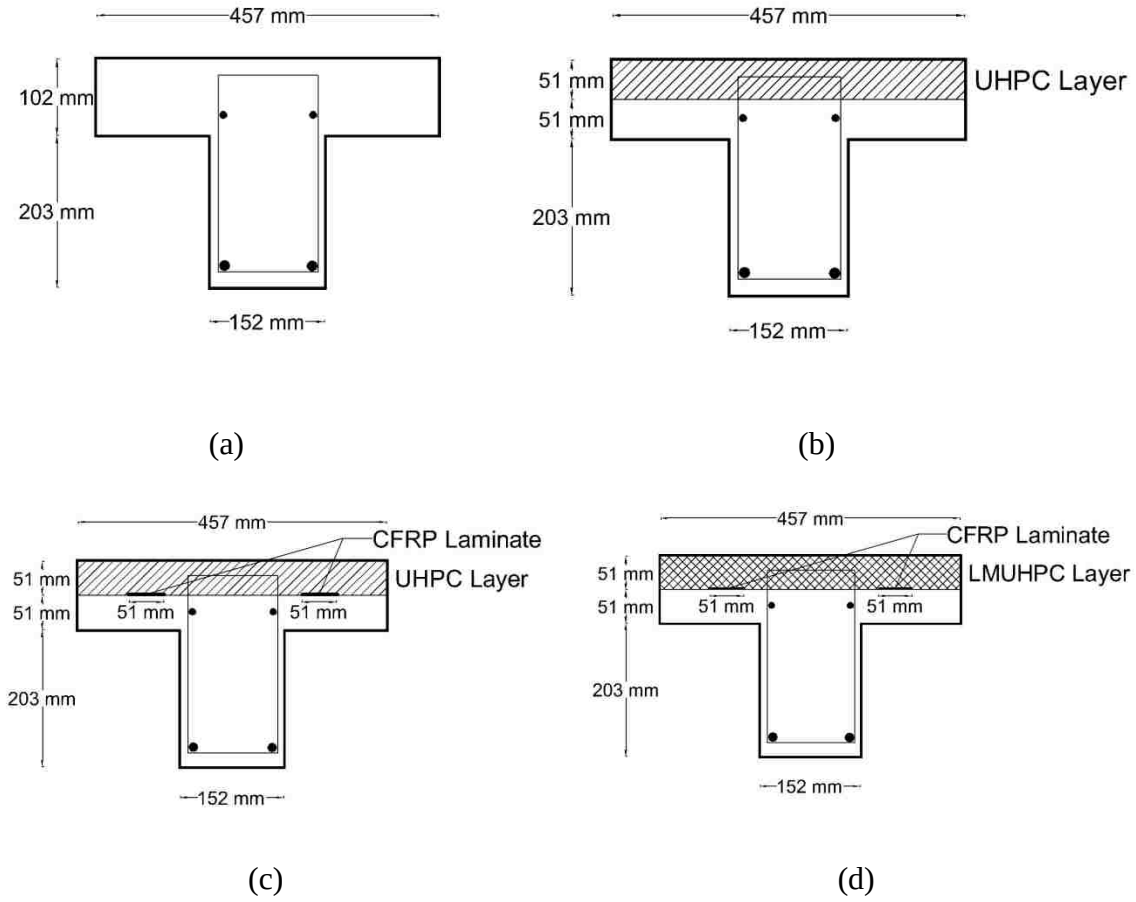

Figure 3.3: Cross section for (a) Beam-C (b) Beam-U (c) Beam-UF (d) Beam-MUF

3.4 Strain gauges location

To monitor the strain in the beams, two types of strain gauges manufactured by Vishay Inc. were used. "C2A-06-125LW-120/C-33F" strain gauges were used to monitor the

strain in the steel rebars and "N2A-06-40CBY-350/P" strain gauges were used to measure the strain in the CFRP sheets and the concrete. For Beam-C and Beam-U, four strain gauges were used. One strain gauge was installed at the center of each steel rebar to monitor the maximum strain in the steel and two strain gauges were installed at the top of each beam at mid-span at both sides of the beam to measure the maximum strain in concrete. **Figure 3.4** and **Figure 3.5** shows the strain gauges installed on the rebars and concrete respectively.

For Beam-UF and Beam-MUF, six strain gauges were used to monitor the strains. Four strain gauges were installed on the steel rebars and concrete as in Beam-C and Beam-U in addition to one strain gauge installed at the center of each CFRP sheets to monitor the strain in the CFRP laminates. To attach the strain gauges to rebars, CFRP, or concrete, surface preparation procedure following Vishay Notes was applied [31, 32].

Figure 3.4: Strain gauge installed on steel rebar

Figure 3.5: Strain gauge installed on top of the concrete

3.5 Concrete casting

For casting, four wooden forms were fabricated with inner dimensions equal to the beams dimensions. The steel cage was erected and then moved to the wooden form. Plastic chairs were used to provide the 50 mm cover required for the reinforcement. Before placing the reinforcement cage in the forms, form oil was used to oil the four forms to prevent the wood from sticking to the concrete. **Figure 3.6** shows the four wooden forms before placing the steel cage. **Figure 3.7** shows the steel cage placed in the wooden form.

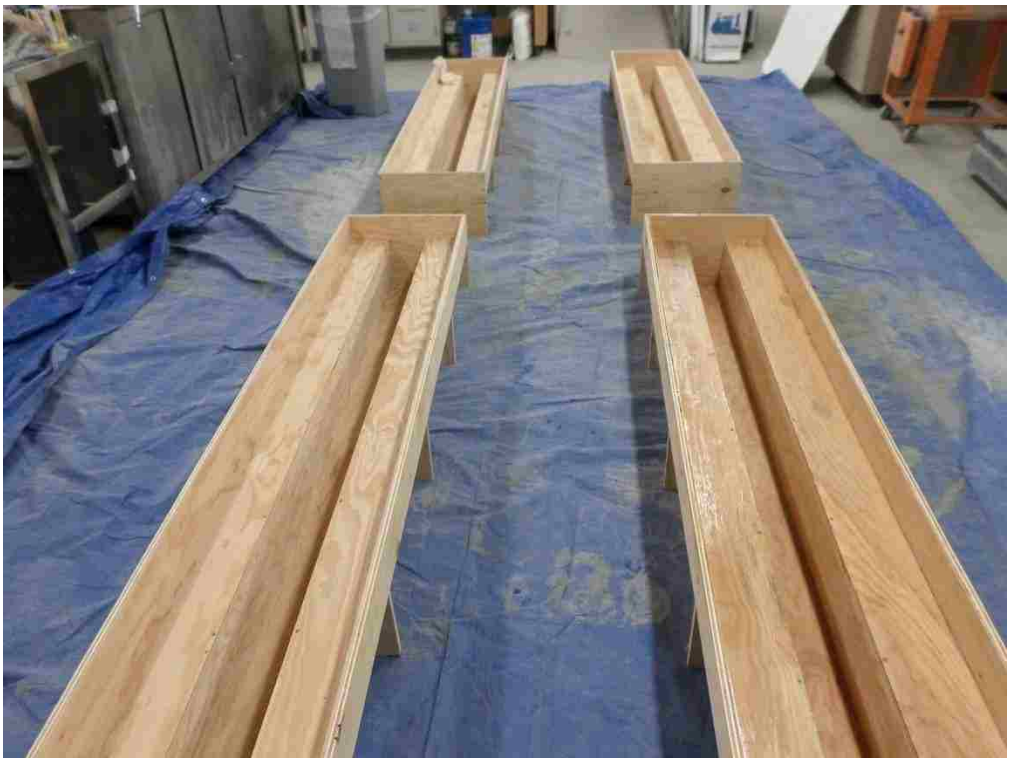

Figure 3.6: The four wooden forms

Figure 3.7: The steel cage placed in the oiled wooden form

After the steel cages were placed in the wooden forms, the concrete was poured in the four forms. For Beam-C, the concrete was casted for the whole height of the beam (305 mm). Thereafter, the top surface of Beam-C was finished. For the other three beams, the concrete was casted to height of 254 mm not including the top 51 mm layer. During concrete casting, a mechanical vibrator was used to ensure compaction of concrete and prevent any cavitation. **Figure 3.8** shows vibrating the concrete. **Figure 3.9** shows the four beams after casting the regular concrete.

Figure 3.8: Concrete vibrating

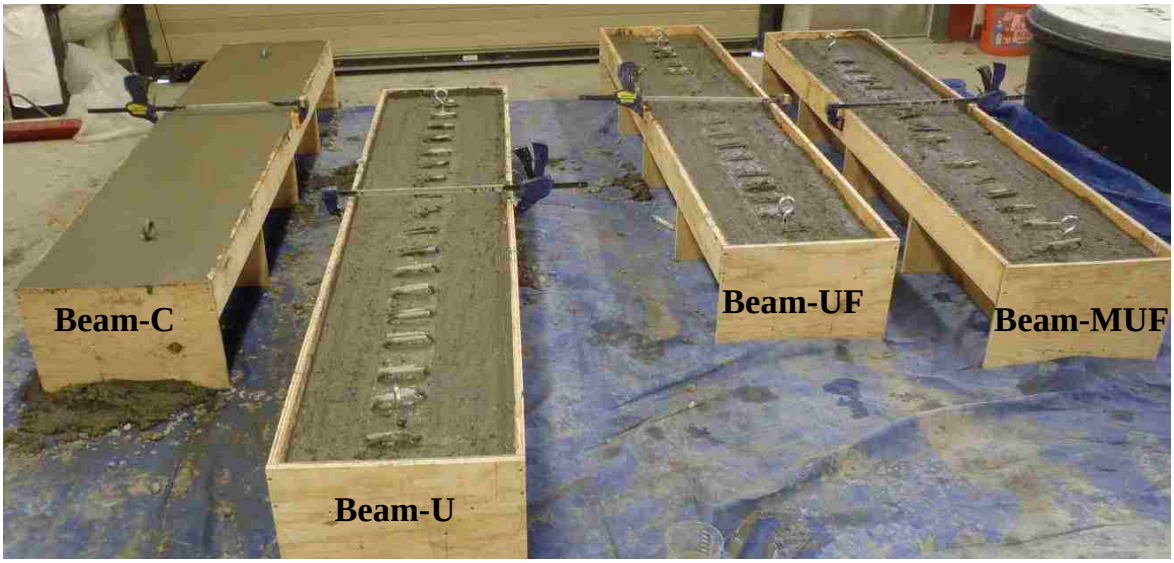

Figure 3.9: The four beams after casting the regular concrete

After 5 hours, the surfaces of Beam-UF and Beam-MUF were slightly roughened prior to attaching the CFRP laminates to ensure good bond between the concrete and the CFRP sheets as shown in **Figure 3.10**.

Figure 3.10: The roughened surface of Beam-UF

3.6 CFRP and shear dowels application

After 3 days of concrete casting, shear dowels were installed in the flange of Beam-U to provide shear transfer between the UHPC layer and the regular concrete. 26 holes with 10 mm diameter and 25.4 mm depth were drilled in the already casted concrete. The epoxy was poured in the holes to fill about two third of the holes' depth then, 9.5 mm diameter 51 mm length steel dowels were implanted into the holes filled with epoxy. **Figure 3.11** shows the shear dowels installed in Beam-U.

Figure 3.11: Shear dowels installed in top surface of normal concrete in Beam-U

At the same concrete age, two CFRP laminates sheets with length of 1829 mm and width of 51 mm were attached to each beam using epoxy. Any excessive amount of epoxy was removed to provide rough surface before applying the UHPC or the LMUHPC. After applying the CFRP sheets, the shear dowels were installed in the flange of both beams

with the same dimensions and procedure in Beam-U. **Figure 3.12** shows Beam-UF after installing CFRP sheets and shear dowels. The CFRP laminates were provided from the manufacturer with one roughened surface and one smooth surface. Thus, the smooth surface of the CFRP sheet was sand-plasted before it was attached to the concrete surface to allow good mechanical bond between CFRP and concrete.

Figure 3.12: CFRP sheets and shear dowels installed in Beam-UF

As shown in Figure 3.12 and Figure 3.11, the stirrups of the reinforcement cage at the web were exposed to provide shear transfer in the web area.

3.7 UHPC and LMUHPC layers

After the shear dowels were installed in Beam-U and shear dowels and CFRP laminates in Beam-UF, a 51 mm thick layer of UHPC was casted on top of both beams. The UHPC

has a mean compressive strength after 28 days of 140 MPa. For Beam-MUF, a 51 mm thick layer of LMUHPC was casted on top of the beam after installing the shear dowels and attaching the CFRP laminates sheets. The mean compressive strength after 28 days for the LMUHPC was 62.1 MPa. Further investigation of the UHPC and LMUHPC is presented in Chapter 4.

To produce the UHPC and the LMUHPC, a Sicoma planetary shear mixer was used. **Figure 3.13** shows the shear mixer used to mix the UHPC and the LMUHPC.

(a) (b)

Figure 3.13: (a) Planetary shear mixer (b) inside view

To be able to achieve this very high strength, a very low water to binder ratio of 0.17 was used for the UHPC mix. The maximum nominal size for the aggregate used for the mix was 5 mm. For the LMUHPC the mix used for the UHPC was modified by adding SBR polymer latex. The latex was adding as ratio of the cement content. The polymer latex to cement ratio used for the LMUHPC mix was 0.15. As the polymer latex is 50% water, the amount of water added to the mix in the latex was subtracted from the water amount

in the mix. **Table 3.1 and Table 3.2** show the mix design for the UHPC and LMUHPC respectively.

Table 3.1: Mix proportions of 1 m^3 of UHPC

Cement	1029 kg/m^3
Water	227.5 kg/m^3
Aggregate	910 kg/m^3
Silica Fume	306.6 kg/m^3
Superplasticizer (Glenium 3030 NS)	26.7 kg/m^3

Table 3.2: Mix proportions of 1 m^3 of LMUHPC

Cement	1029 kg/m^3
Water	146.3 kg/m^3
SBR Polymer Latex	154.3 kg/m^3
Aggregate	910 kg/m^3
Silica Fume	306.6 kg/m^3
Superplasticizer (Glenium 3030 NS)	26.7 kg/m^3

For mixing the UHPC and the LMUHPC, a specific procedure was used [3]. The following procedure for mixing the UHPC was slightly modified than Garner used in 2011.

- The aggregate was placed in the shear mixer and the mixer was turned on.

- The cement and the silica fume were added slowly while mixing each over two minutes.
- All the dry components were allowed to mix for five minutes.
- 45% of the water and superplasticizer were added over one minute.
- The components were allowed to mix for five minutes.
- Another 45% of water and superplasticizer were added over one minute.
- The components were allowed to mix until the cement accumulates and forms small balls.
- The remaining 10% of water and superplasticizer were added and the concrete was mixed until the desired consistency was achieved.

For mixing the LMUHPC the following procedure was used.

- The cement and the silica fume were added to the aggregate slowly while mixing each over two minutes and allowed to mix for 5 minutes.
- 50% of the water, superplasticizer, and polymer latex were added over one minute and mixed for five minutes.
- More 30% of the water, superplasticizer, and polymer latex were added over one minute and mixed for five minutes.
- Another 10% of the water, superplasticizer, and polymer latex were added over one minute.
- The components were allowed to mix until the cement accumulates and forms small balls.

- The remaining 10% of water and superplasticizer were added and the concrete was mixed until the desired consistency was achieved.

3.8 Curing of the beams

After casting the regular, the four beams were immediately covered with plastic sheets to keep water inside the beams and eliminate any water evaporation from the beams. After five hours, the beams were covered with wet burlap to provide water for cement hydration process and covered with the plastic sheets. The burlap was watered twice a day for three days. **Figure 3.14** shows Beam-C covered with wet burlap and plastic sheet. Afterwards, Beam-C was moved to the curing tank and submerged in hot water for 28 days. The water temperature during the curing process was 55 ±3 °C. Three electrical heaters were used to heat and circulate water in the tank. Then the tank was covered with thick fume boards to keep heat inside the tank and reduce water evaporating rate. **Figure 3.15** shows the curing tank used. The same curing conditions were used for Beam-U and Beam-UF after casting the UHPC layer.

Figure 3.14: Beam-C covered with wet burlap and plastic sheet for curing

For Beam-MUF, a deferent curing procedure was used because the polymer latex in the LMUHPC needs to be air cured. The beam was covered with wet burlap and plastic sheet for three days after casting the LMUHPC as in the other three beams. Afterwards, the beam was moved to the curing tank and submerged in the hot water for 7 days only. Then, the beam was removed from the curing tank and it was allowed to be air cured until testing.

Figure 3.15: Curing tank used in the curing process

3.9 Test setup and preparation

3.9.1. Four point bending setup

The four beams were tested and four point bending set-up. MTS load actuator attached to steel reaction frame was used for applying the load on the beams. **Figure 3.16** shows the load actuator attached to the reaction steel frame. Two steel cylinders spaced at 914 mm with a diameter of 100 mm were used as loading points. For equal distribution of the load on the two loading points, a wide flange steel beam W 10 × 49 was attached to the load actuator and rested on the two loading cylinders. More two steel cylinders rested on wide flange steel beams W 12 × 40 were used as the supports of the beam. One of the supporting steel cylinders was allowed to move horizontally to work as a roller support. The second cylinder was welded to the wide flange steel beam to be restricted from the horizontal movement to work as pin support for the beam. The two supports were placed so that the distance between the center lines of the two supporting cylinders would be 2.29 m. The two supports were tied down as shown in **Figure 3.17** to eliminate any unexpected movement of the supports.

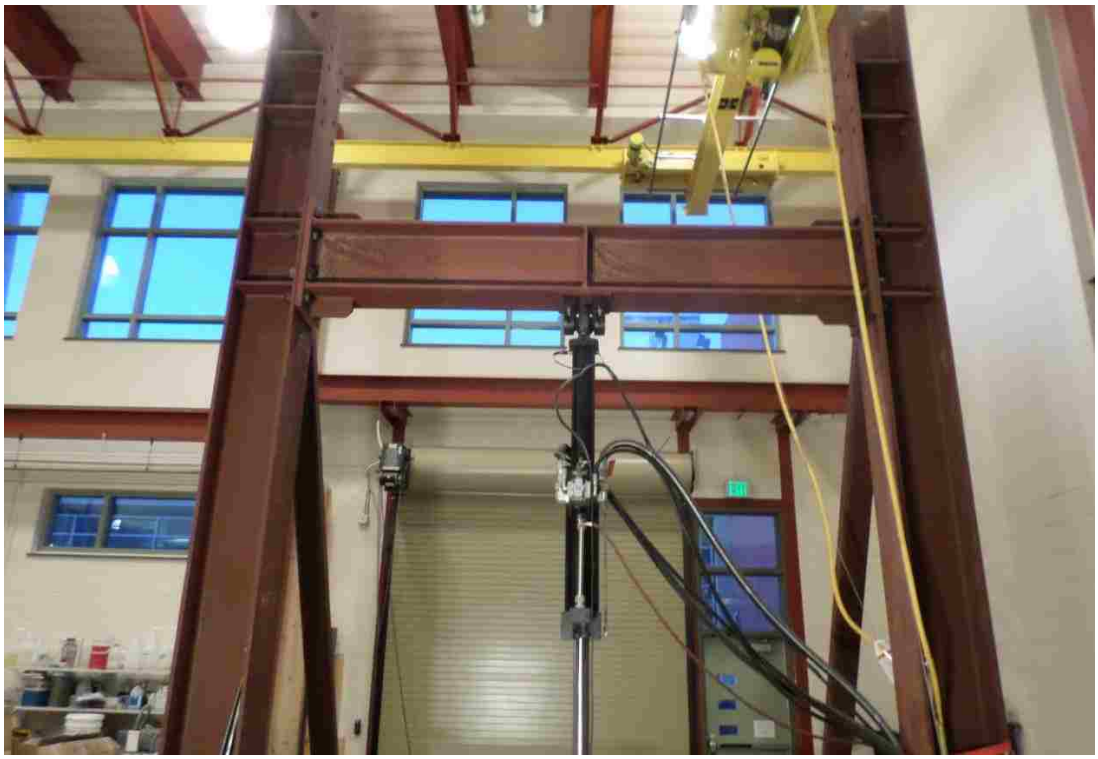

Figure 3.16: Load actuator attached to the reaction frame

Figure 3.17: Support tie down

Two lateral supports were used to support the flange of the beam at mid-span during applying the load on the beams to restrict any lateral movement of the beam. More four lateral supports were used to support the flange and the web at the supports to reduce the possibility of any lateral torsional buckling instability. Silicon sheets and compressible foam were placed between the concrete beam and the lateral supports to eliminate the any friction between the concrete and the steel and allow the beam to move vertically at mid-span and rotate at the supports without any restrictions. Two Linear Variable Deferential Transducers (LVDTs) were used the vertical displacement at the mid-span. More two LVDTs were used to monitor the vertical displacement at the supports. The LVDTs used to measure the vertical displacement at mid-span of the beams were continually adjusted during conducting the experiment to keep the reading of the LVDTs within their accurate reading rang. **Figure 3.18** shows the test setup for the beams. **Figure 3.19** shows the lateral supports of the beams at the supports area. **Figure 3.20** and **Figure 3.21** show schematic diagram for lateral support setup.

Figure 3.18: Four point bending setup for beams testing

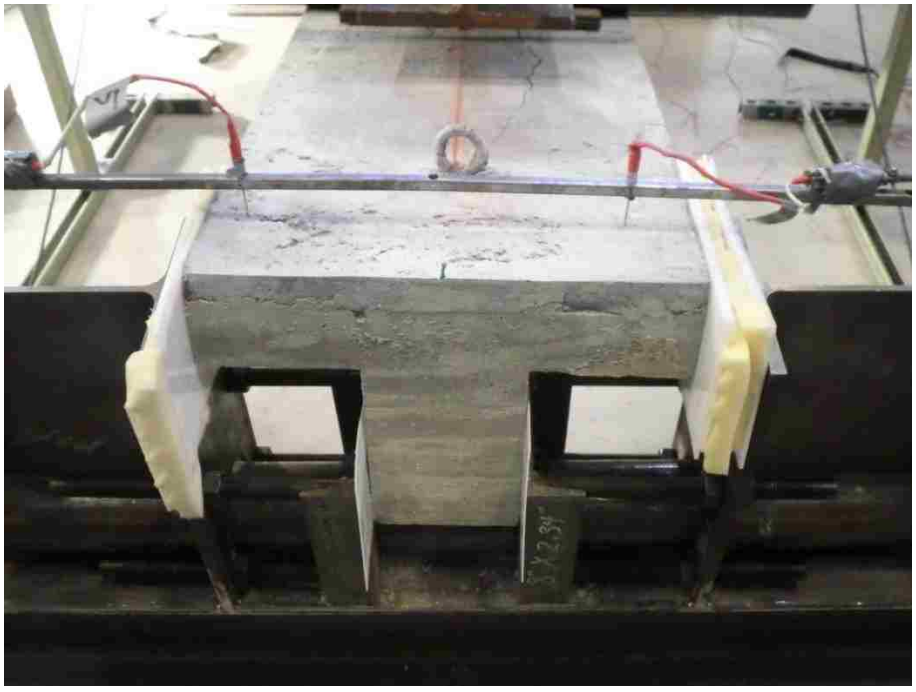

Figure 3.19: Beams lateral support at the support area

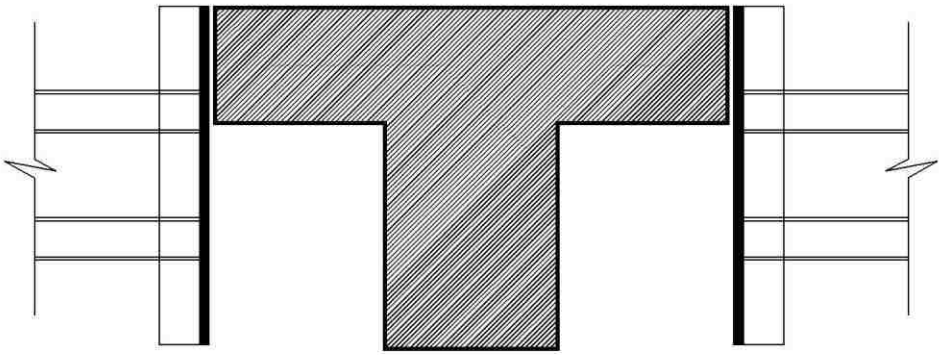

Figure 3.20: Lateral support of the beam at mid-span

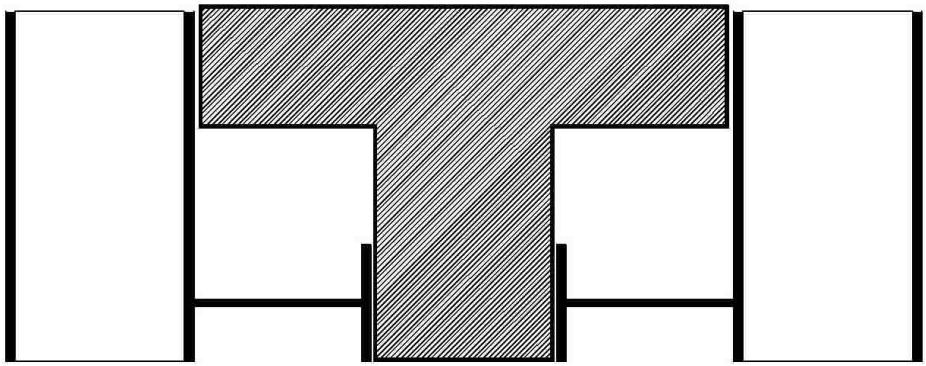

Figure 3.21: Lateral support of the beam at support area

3.9.2. Test preparation

Three days before the test date, the top surface of the beam was at mid span was cleaned and grinded as a preparation for attaching the Strain gauges. Afterwards, the center of the beam is marked to help in adjusting the beam. Then, an overhead crane and a hydraulics jack were used to move the beam under the loading setup. Then, the beam was placed on the supports and the hydraulics jack was used to center the beam under the wide flange loading beam. Leveling device was used to ensure the adjustment of the beam as shown in **Figure 3.22.**

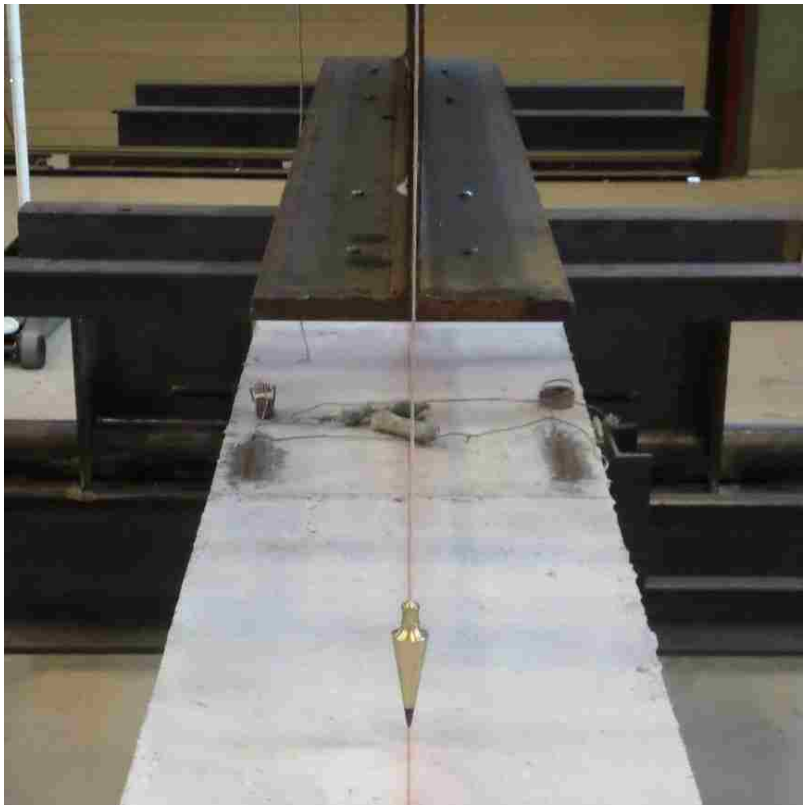

Figure 3.22: Beam centered under the loading beam showing also leveling device

3.9.3. Loading rate and collecting data

To test the four beams, displacement control test was used with a loading rate of 1mm/min. After each 1 mm displacement, the loading was hold for 1 minute to allow monitoring and marking the cracks propagate in the beams. After displacement of 25 mm, the holds were carried out each 3 mm displacement. When the displacement of the actuator reached 40 mm, the loading step between the holds was increased to be 5 mm and it was increased again to be 10 mm after actuator total displacement reaches 70 mm. At the point of 100 mm total displacement, the loading rate was increased to 3 mm/min and the step between the holds was increased to 30 mm until failure.

To collect the date of the test, the load actuator and the LVDTs were connected to MTS data accusation system which record the data simultaneously every 1 sec. As for the strain gauges, they were connected to Vishay 2100 Signal Conditioning Amplifier system was used to provide the excitation level required for the strain gauges. All the strain gauges were excited to 5 Volts DC. The signal conditioning amplifier was connected to the MTS data accusation system to record the data from the strain gauges.

CHAPTER 4. Results and Discussion

In this chapter, a comparison of the properties of normal concrete, the Ultra High Performance Concrete (UHPC), and the Latex Modified Ultra High Performance Concrete (LMUHPC) is presented. Afterwards, the expected behavior of the four beams is provided. This is followed by analysis of the experimental observations of the four beams. Furthermore, we end this chapter by an in-depth discussion and comparison of the experimental observations of the four beams.

4.1 Concrete properties

In this section, the fresh concrete properties and the mechanical properties for the normal concrete, the UHPC, and the LMUHPC is presented. The stress-strain curves for the three types of concrete are discussed.

4.1.1 Normal concrete

The normal concrete was obtained from a local ready mix concrete mixing plant in Albuquerque, New Mexico. The maximum nominal size of the aggregate used in the concrete was 12.7 mm. The slump of the concrete was 164 mm as shown in **Figure 4.1**. The volume of the air entrained in normal concrete was 2.1% as shown in **Figure 4.2**. The temperature of the concrete was measured immediately after it was discharged from the mixing truck to be 10°C.

Figure 4.1 Slump of normal Concrete

Figure 4.2 Air entrapped device

While casting the beams, twelve concrete cylinders 100 mm × 200 mm were cast. After 7 days, the compressive strength was tested. After 28 days, the compressive strength, the tensile strength, and Young's modulus of elasticity were tested. **Table 4.1** presents the results of the normal concrete.

Table 4.1: Mechanical properties for normal concrete

	Mean Value [MPa]	Standard Deviation [MPa]
Compressive strength (7 days)	24	0.4
Compressive strength (28 days)	33	1.8
Modulus of Elasticity	25,354	N/A
Tensile strength (28 days)	2.3	0.7

4.1.2 Ultra High Performance Concrete (UHPC)

The UHPC was mixed in the planetary shear mixer as discussed previously in Chapter 3. Because the top layer in both Beam-U and Beam-UF were UHPC, two deferent mixes of the UHPC were mixed. The first mix was used in Beam-U (UHPC1) and the second mix was used in Beam-UF (UHPC). The fresh properties for both mixes is presented in **Table 4.2**

Table 4.2: Fresh concrete properties for UHPC1 and UHPC2

	UHPC1	UHPC2
Slump (mm)	229	216
Temperature (°C)	18.3	18.3

Figure 4.3 Slump of UHPC1

The mechanical properties for both mixes are presented in **Table 4.3**. The stress-strain curves for both concretes are presented in **Figure 4.4**. As shown in the stress-stain curve, both mixes UHPC1 and UHPC2 were identical.

Table 4.3: Mechanical properties for UHPC1 and UHPC2

	UHPC1		UHPC2	
	Mean Value [MPa]	Standard Deviation [MPa]	Mean Value [MPa]	Standard Deviation [MPa]
Compressive Strength (7 days)	114	14.5	120	14.9
Compressive Strength (28 days)	133	16.9	140	21.1
Modulus of Elasticity	30,417	N/A	30,023	N/A
Tensile Strength	5	0.4	6.3	0.9

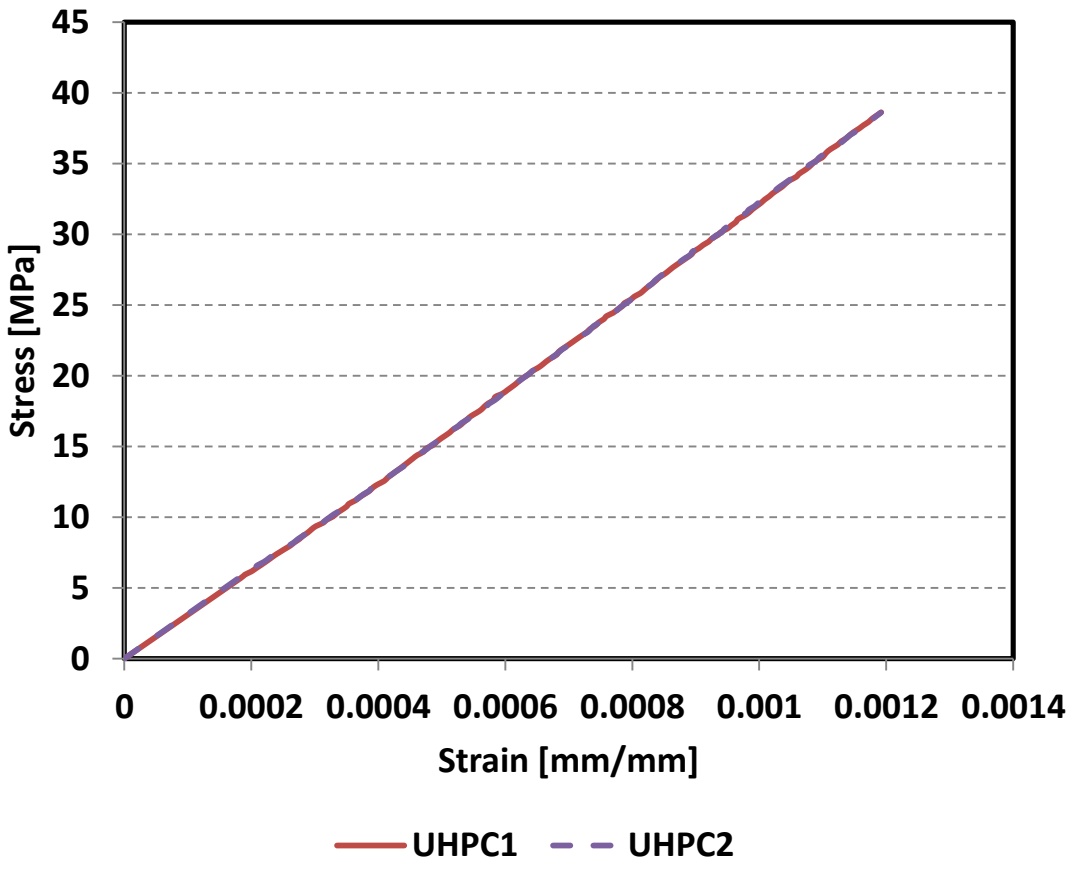

Figure 4.4 Stress-strain curves for both UHPC mixes

4.1.3 Latex Modified Ultra High Performance Concrete (LMUHPC)

The LMUHPC was mixed as discussed previously in Chapter 3. The slump of the LMUHPC was 60 mm and the temperature was 17.2°C. **Figure 4.5** shows the slump of the LMUHPC. The compressive strength after 7 days and 28 days, modulus of elasticity after 28 days, and tensile strength were tested. **Table 4.4** shows the mechanical properties of the LMUHPC.

Figure 4.5 Slump of LMUHPC

Table 4.4: Mechanical properties for LMUHPC

	Mean Value [MPa]	Standard Deviation [MPa]
Compressive strength (7 days)	62	15.1
Compressive strength (28 days)	74	0.6
Modulus of Elasticity	16,881	N/A
Tensile strength (28 days)	3.6	0.8

4.1.4 Stress-Strain curves

A 100 mm × 200 mm cylinder of each type of concrete was tested under compression until 449 kN. During the loading, the strain at the middle third of the cylinders was measured. Then, the stress was calculated and the stress-strain curves for each type were plotted as shown in **Figure 4.6**. As shown in **Figure 4.5**, the stress-strain curves for both UHPC1 and UHPC2 are identical. So, only one curve for the UHPC was used in comparison.

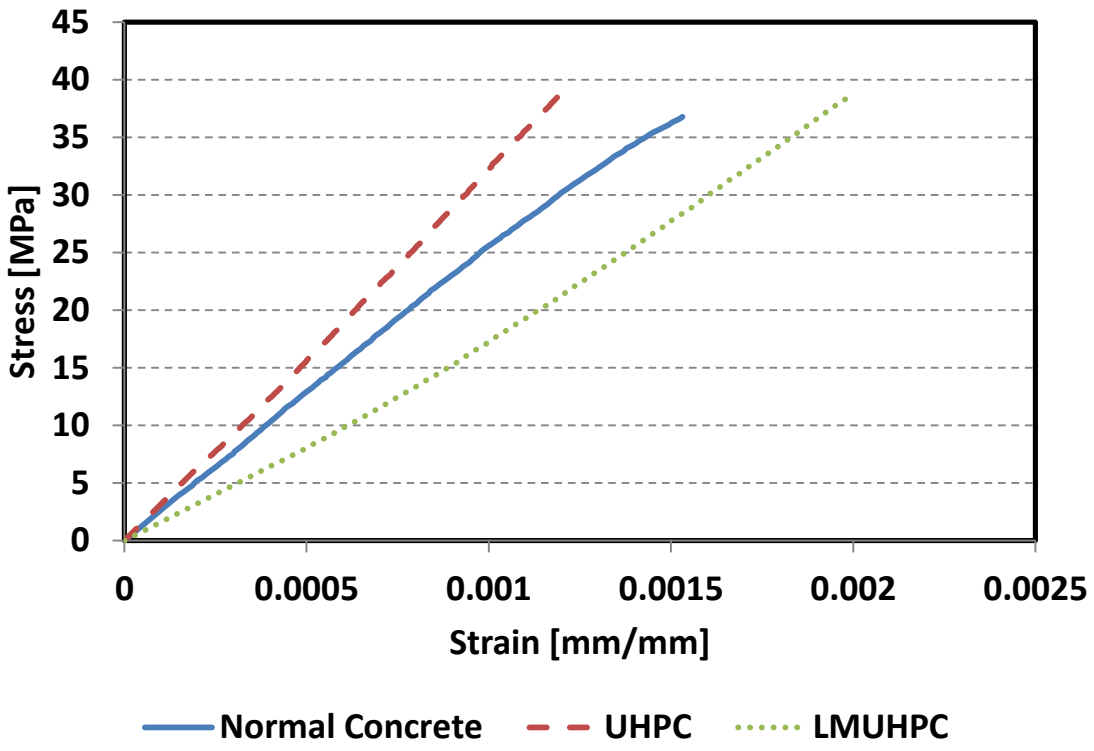

Figure 4.6 Stress-Strain curves for the three concrete types

As shown in Figure 4.6, the modulus of elasticity of the UHPC is 18% higher than normal concrete. However, the compressive strength of the LMUHPC is 126% higher than normal concrete, its modulus of elasticity is 33% less than normal concrete. This decrease of the modulus of elasticity due to the polymer latex added to the LMUHPC. Latex Modified Concrete (LMC) is well known to have a lower modulus of elasticity than normal concrete (ACI 548. Report 2010).

4.2 Test Results

In this section, the expected behavior and the test observation for the four beams are presented. As mentioned in Chapter 3, all the beams were tested under four point bending. The advantage of the four point bending is that there are no shear forces

between the two loading points. Flexural effect can be dominant in perform the four point loads. **Figure 4.7** shows schematic diagram for loading the beam. **Figure 4.8** and **Figure 4.9** show the shear force and the bending moment diagrams respectively.

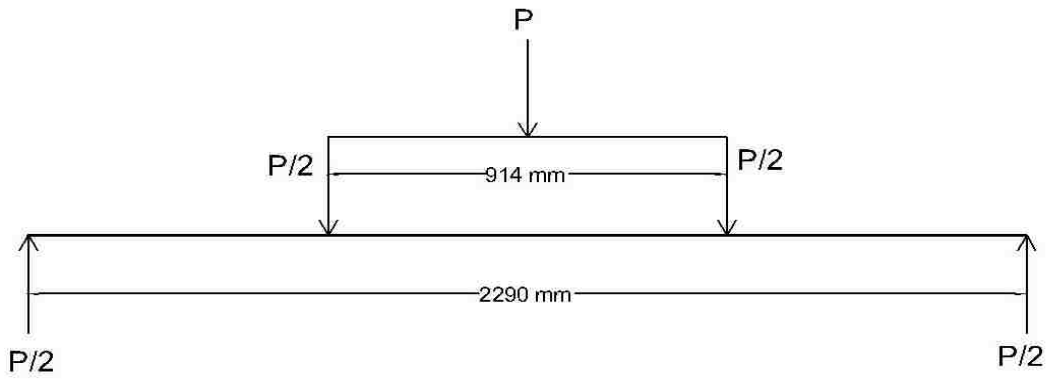

Figure 4.7: Schematic Diagram of the Beam Loading

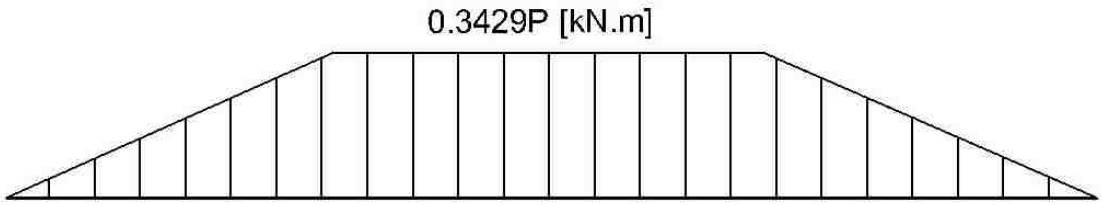

Figure 4.8: Bending Moment Diagram

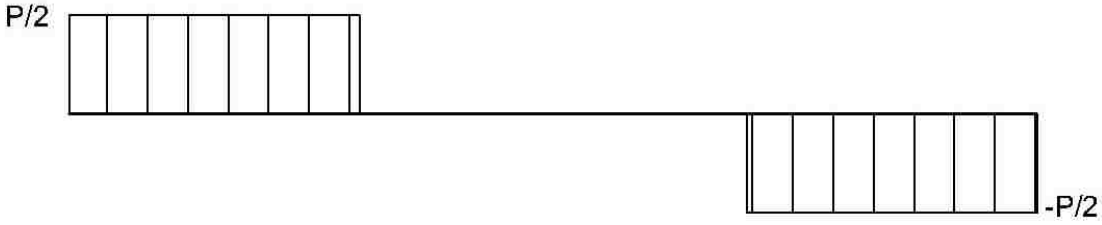

Figure 4.9: Shear Force Diagram

4.2.1. Hypothesis

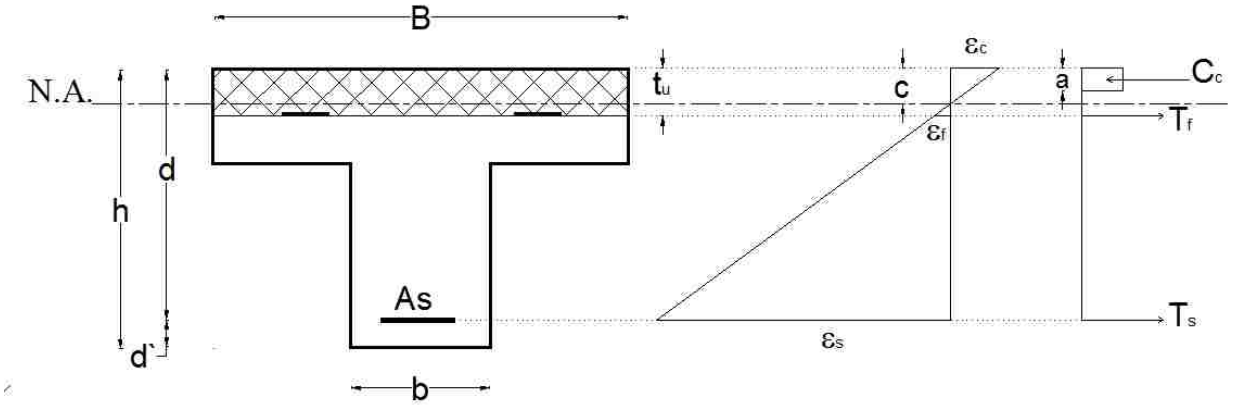

Figure 4.10: Schematic for beam cross section

The corresponding moment was calculated using equation **4.1**. The estimated cracking moment for the beams was calculated using equation **4.2**.

$$M = 0.3429P \quad \textbf{(4.1)}$$

Where:

M: Bending moment [kN.m]

P: Applied Load by the actuator [kN]

4.2.1.1. Service state behavior

$$M_{cr} = \frac{f_{ct}.I_g}{y_t}10^{-6} \quad \textbf{(4.2)}$$

Where:

M_{cr}: Cracking moment [kN.m]

f_{ct}: Tensile strength of the normal concrete [MPa]

I_g: Gross moment of inertia [mm^4]

y_t: Distance from the neutral axis to the bottom of the beam [mm]

To calculate the gross moment of inertia for Beam-U, Beam-UH, and Beam-MUF, the deference in Young's modulus of elasticity between the normal concrete and the UHPC or the LMUHPC and the existing of the CFRP laminates were considered. The distance of the neutral axis from the bottom of the beam was calculated for the four beams as following

For Beam-C

$$y_t = \frac{A_{fl} y_{fl} + A_w y_w + (n_s - 1)A_s d`}{A_{fl} + A_w + (n_s - 1)A_s} \quad \textbf{(4.3)}$$

Where:

A_{fl}: Area of beam flange [mm^2]

y_{fl}: Distance between the centerline of the flange and the bottom of the beam [mm]

A_w: Area of the beam web [mm^2]

y_w: Distance between the centerline of the web and the bottom of the beam [mm]

n_s: Modular ratio between the modulus of elasticity of steel to the modulus of elasticity of normal concrete.

A_s: Cross section area of steel rebars [mm^2]

d`: Distance between the centerline of the rebars and the bottom of the beam [mm]

For Beam-U

$$y_t = \frac{A_{fl} y_{fl} + (n_u - 1)A_u y_u + A_w y_w + (n_s - 1)A_s d`}{A_{fl} + A_w + (n_s - 1)A_s + (n_u - 1)A_u} \quad \textbf{(4.4)}$$

Where:

n_u: Modular ratio between the modulus of elasticity of UHPC to the modulus of elasticity of normal concrete.

A_u: Area of the UHPC layer [mm^2]

y_u: Distance between the centerline of the UHPC layer and the bottom of the beam [mm]

For Beam-UF

$$y_t = \frac{A_{fl} y_{fl} + (n_u - 1)A_u y_u + (n_f - 1)A_f y_f + A_w y_w + (n_s - 1)A_s d`}{A_{fl} + A_w + (n_s - 1)A_s + (n_u - 1)A_u + (n_f - 1)A_f} \quad \textbf{(4.5)}$$

Where:

n_f: Modular ratio between the modulus of elasticity of CFRP to the modulus of elasticity of normal concrete.

A_f: Area of the CFRP laminates [mm^2]

y_f: Distance between the CFRP laminates and the bottom of the beam [mm]

For Beam-MUF

$$y_t = \frac{A_{fl} y_{fl} + (n_m - 1)A_m y_m + (n_f - 1)A_f y_f + A_w y_w + (n_s - 1)A_s d`}{A_{fl} + A_w + (n_s - 1)A_s + (n_m - 1)A_m + (n_f - 1)A_f} \quad \textbf{(4.6)}$$

Where:

n_m: Modular ratio between the modulus of elasticity of LMUHPC to the modulus of elasticity of normal concrete.

A_m: Area of the LMUHPC layer [mm^2]

y_m: Distance between the centerline of the LMUHPC layer and the bottom of the beam [mm].

4.2.1.2. Ultimate state behavior

Based on the reinforcement and the compressive strength for the three concrete types, the expected flexural nominal capacity and the nominal shear capacity were calculated for each beam. For the calculation the ultimate compressive strain in the normal concrete was assumed to be -0.003 and -0.0039 for the UHPC and the LMUHPC [3]. The calculation for the flexural capacity and shear capacity are listed below.

The Flexural Nominal Capacity for Beam-C and Beam-U:

$C_c = T_s$ **(4.7)**

Where:

C_c: Compression force in the concrete [kN]

T_s: Tension force in the rebars [kN]

Equation **4.7** can be expected as following.

$$0.85 f`_c aB = A_s f_y \quad \textbf{(4.8)}$$

Where:

f_c`: Compressive strength of the concrete in the compression zone [MPa]

a: Depth of compression block [mm]

B: Width of the beam flange [mm]

f_y: Yield strength of the steel rebars [MPa]

Equation **4.8** can be reformed as following

$$a = \frac{A_s f_y}{0.85 f`_c B} \quad \textbf{(4.9)}$$

After calculating (a) from equation **4.9**, the value of compression block depth is checked to be less than the thickness of the flange. Moreover, the tensile strain of steel rebars is calculated using equations **4.10** and **4.11** to ensure that the strain in the rebars exceeds the yielding strain. Then, the nominal flexural capacity (M_n) in kN.m is calculated from equation **4.12.**

$$c = \frac{a}{\beta_1} \quad \textbf{(4.10)}$$

Where:

c: Depth of compression zone [mm].

β_1: Concrete stress block coefficient.

According to ACI 318, β_1 is 0.81 for normal concrete and 0.65 for UHPC and LMUHPC.

$$\varepsilon_s = \frac{\varepsilon_{cu}(d-c)}{c} \quad \textbf{(4.11)}$$

Where:

ε_s: Tensile strain in steel.

ε_{cu}: Ultimate compressive strain in concrete at failure.

d: Distance from the center line of the steel rebars to the top of the beam [mm].

$$M_n = A_s f_y \left(d - \frac{a}{2}\right) 10^{-6} \quad \textbf{(4.12)}$$

The nominal flexural capacity for Beam-UF and Beam-MUF:

For both Beam-UF and Beam-MUF the equilibrium equations **4.7** and **4.8** are modified to be equations **4.13** and **4.14** respectively to consider the force in the CFRP laminates.

$C_c = T_s + T_f$ **(4.13)**

Where:

T_f: Tensile force in the CFRP laminates [N]

$$0.85 f`_c \beta_1 c B = A_s f_y + A_f f_f \quad \textbf{(4.14)}$$

Where:

f_f: Tensile stress in the CFRP laminates [MPa]

The tensile stress in the CFRP is unknown so equations **4.15** and **4.16** are used to calculate the stress of the CFRP as a function of the depth of compression zone (c).

$$f_f = \varepsilon_f E_f \quad \textbf{(4.15)}$$

$$\varepsilon_f = \frac{\varepsilon_{cu}(t_u - c)}{c} \quad \textbf{(4.16)}$$

Where:

ε_f: Tensile strain in the CFRP laminates.

E_f: Young's modulus of elasticity of the CFRP laminates.

t_u: Thickness of UHPC or LMUHPC overlay

From equations **4.15** and **4.16**, equation **4.14** will be:

$$0.85 f`_c \beta_1 cB = A_s f_y + A_f E_f \frac{\varepsilon_{cu}(51-c)}{c} \quad \textbf{(4.17)}$$

Equation **4.17** could be written in the quadratic equation formula:

$$J_1 c^2 + J_2 c + J_3 = 0 \quad \textbf{(4.18)}$$

Where:

$$J_1 = 0.85 f`_c \beta_1 B$$

$$J_2 = A_f E_f \varepsilon_{cu} - A_s f_y$$

$$J_3 = -t_u A_f E_f \varepsilon_{cu}$$

$$c = \frac{-J_2 \pm \sqrt{J_2^2 - 4J_1 J_3}}{2J_1} \quad \textbf{(4.19)}$$

The depth of compression zone (c) is checked to be less than t_u=51mm to ensure that the CFRP laminates are under tension. Then, the depth of compression stress block (a) is calculated from equation **4.20** and the nominal flexural capacity (M_n) in kN.m is calculated from equation **4.21**

$$a = c\beta_1 \quad \textbf{(4.20)}$$

$$M_n = \left[A_s f_y \left(d - \frac{a}{2} \right) + A_f f_f \left(t_u - \frac{a}{2} \right) \right] 10^{-6} \quad \textbf{(4.21)}$$

The nominal shear capacity (V_n) in kN for the beams was calculated using the simplified method [33] equation **4.22**.

$$V_n = [V_c + V_s] 10^{-3} \quad \textbf{(4.22)}$$

Where:

V_c: Concrete shear contribution following ACI 318.

V_s: Shear reinforcement contribution with the assumption of steel yields following ACI 318.

$$V_c = \frac{\sqrt{f`_c}}{6} b_w d \quad \textbf{(4.23)}$$

$$V_s = \frac{A_v f_y d}{s} \quad \textbf{(4.24)}$$

Where:

b_w: Width of the beam web [mm].

A_v: Cross section area of the shear reinforcement [mm^2].

s: Spacing between the stirrups [mm].

The above method known as the simplified method might overestimate the shear capacity. **Table 4.5** shows the cracking moment, the flexural moment capacity, and the nominal shear force capacity for the four beams. Moreover, the load corresponding to the cracking moment and the nominal moment capacity are calculated. All the values reported in **Table 4.5** represent load applied by the actuator only after deducting the effect of the own weight of the beam.

Table 4.5: The expected capacity for the four beams

	Beam-C	Beam-U	Beam-UF	Beam-MUF
I_g [mm^4]	616,221,840	649,892,717	651,085,908	546,926,828
Cracking moment [kN.m]	6.3	6.5	6.5	5.8
Cracking force [kN]	18.3	18.9	18.9	16.8
Nominal flexural capacity [kN.m]	26.4	26.7	36.8	31.9
Maximum flexural load capacity [kN]	76.9	77.9	107.3	93.1
Nominal shear capacity [kN]	167.6	173.1	173.3	169.4
Maximum shear load capacity [kN]	335.2	346.2	346.6	338.8

4.2.2. Experimental observations

4.2.2.1 Beam-C

As the control beam was loaded, vertical cracks started to appear. The first crack observed and was located near the loading point at load of 25.6 kN. corresponding to a displacement at mid span of 2.2 mm. This is corresponding to a moment of 8.8 kN.m. Afterwards, flexure shear cracks propagated over the beam span as shown in **Figure 4.11.**

Figure 4.11: Cracks propagated in Beam-C

Beam-C was able to carry maximum moment of 45.7 kN.m associated with a load of 133.2 kN. and failure displacement at mid span of 117.8 mm. the MTS actuator was used to obtain the displacement at loading points. The failure displacement at the loading points was 99.6 mm. **Figure 4.12** shows Beam-C at failure.

Figure 4.12: Beam-C at failure

Failure of Beam-C occurred by concrete crushing at mid-span as shown in **Figure 4.13**. The compressive strain of the concrete reached 0.0043 at failure.

Figure 4.13: Crushing of Concrete at Beam-C

The load-displacement curve for Beam-C is shown in **Figure 4.14**. The curve shows that the beam behavior was linear-elastic until the load reached 80.4 kN and a corresponding displacement of 7 mm. At this point, the tension strain at the steel rebars reached 0.0021 and the rebars were just started to yield. **Figure 4.15** shows the tension strain in the steel rebars vs. the applied load on the beam. The curve shows that the rebars reached yield strain of 0.002 at load of 77.2 kN and displacement of 6.7 mm. The strain gauges connected to the rebars were able to read the tension strain up to 99.1 kN as shown in **Figure 4.15.** After this point, the strain gauges got debonded from the rebars and stopped reading. To calculate the stiffness of the beam, the linear part of the load-displacement curve was used **Figure 4.16**. This part shows changing in beam stiffness.

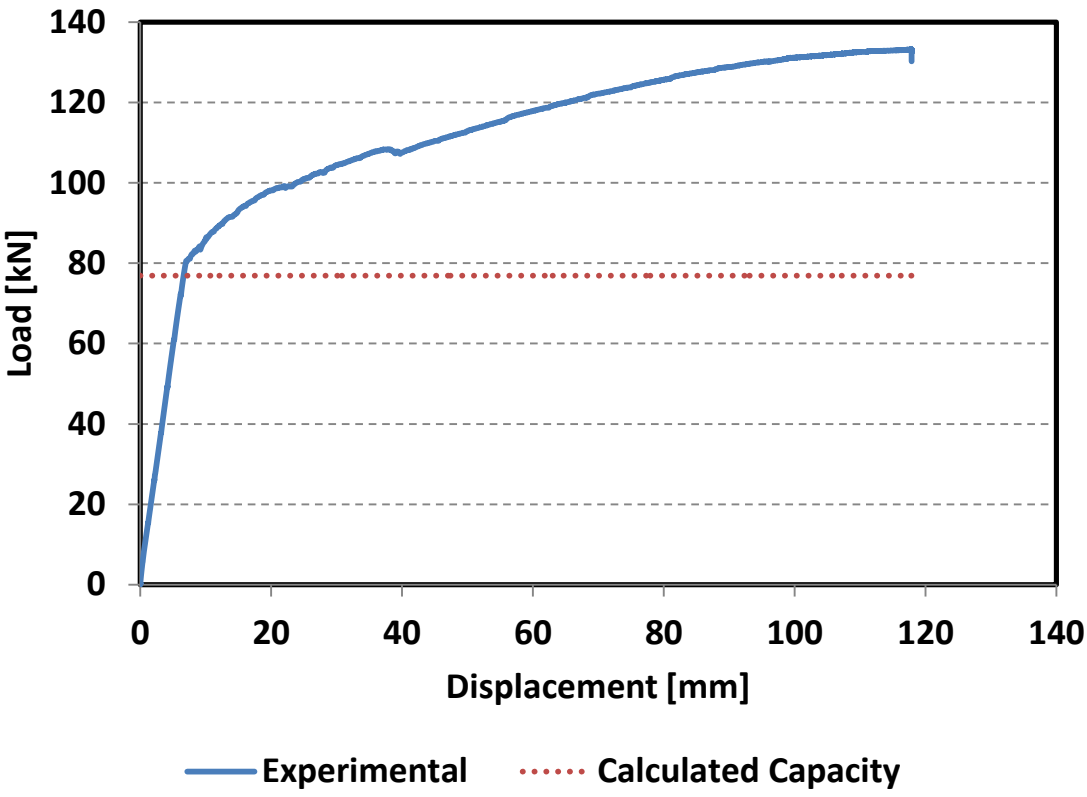

Figure 4.14: Load-Displacement curve for Beam-C

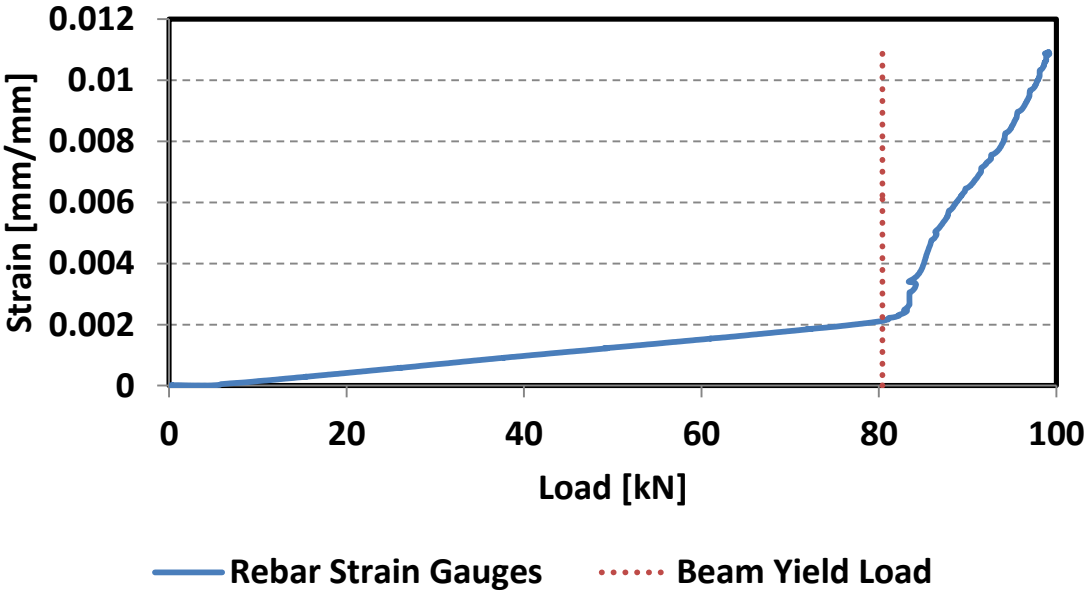

Figure 4.15: Load vs. tension strain in rebars in Beam-C

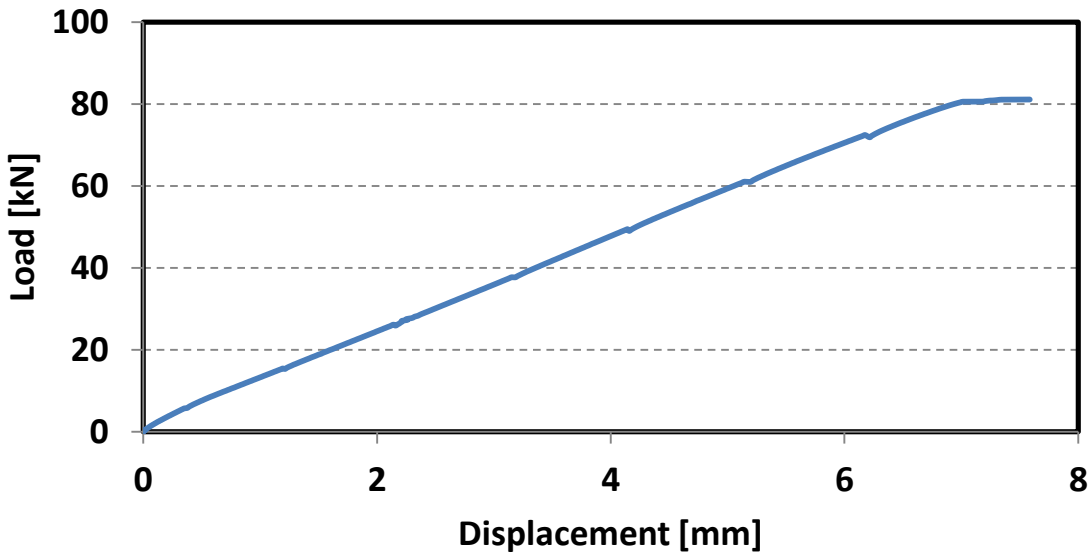

Figure 4.16: Linear part of load-displacement curve used for calculating Beam-C stiffness

The curvature of the beam (Ψ) was calculated using equation **4.25.** To calculate depth of compression zone (c), the strain distribution on the mid-span section was obtained using the compression strain in the **Figure 4.17** and the tension strain in the rebars **Figure 4.15**. The strain distribution at different values of load is shown in **Figure 4.18**, **Figure 4.19,** and **Figure 4.20.**

$$\Psi = \frac{\varepsilon_c}{c} \qquad \textbf{(4.25)}$$

Where

Ψ: Beam curvature [1/mm],

c: Depth of compression zone [mm],

ε_c: Compressive strain in concrete.

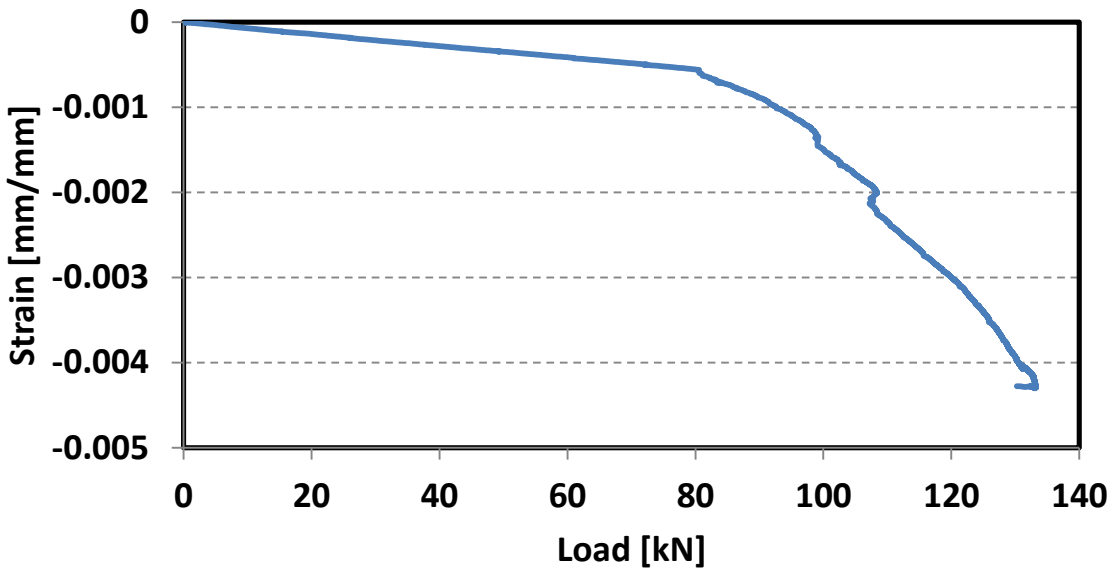

Figure 4.17: Load vs. compression strain in concrete top fiber in Beam-C

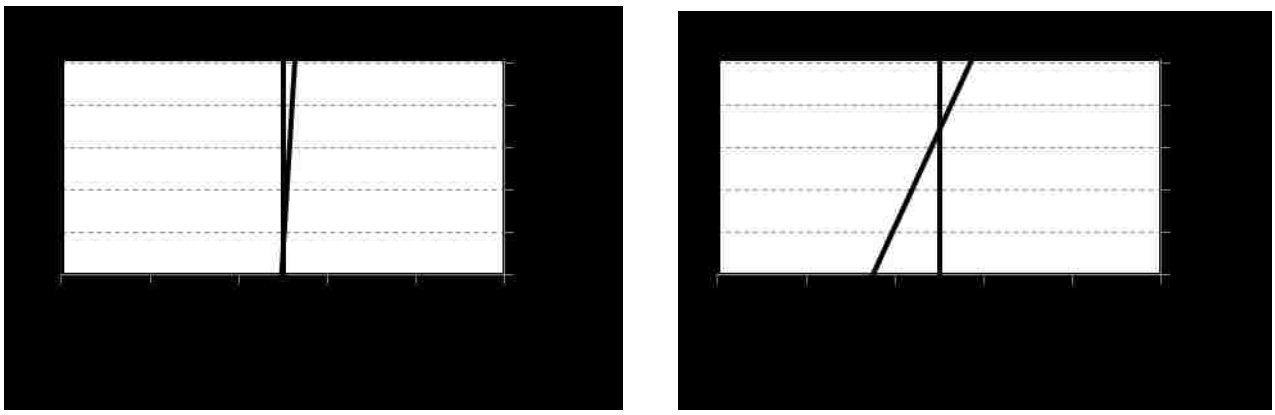

Figure 4.18: Strain distribution at mid-span section of Beam-C at different loads

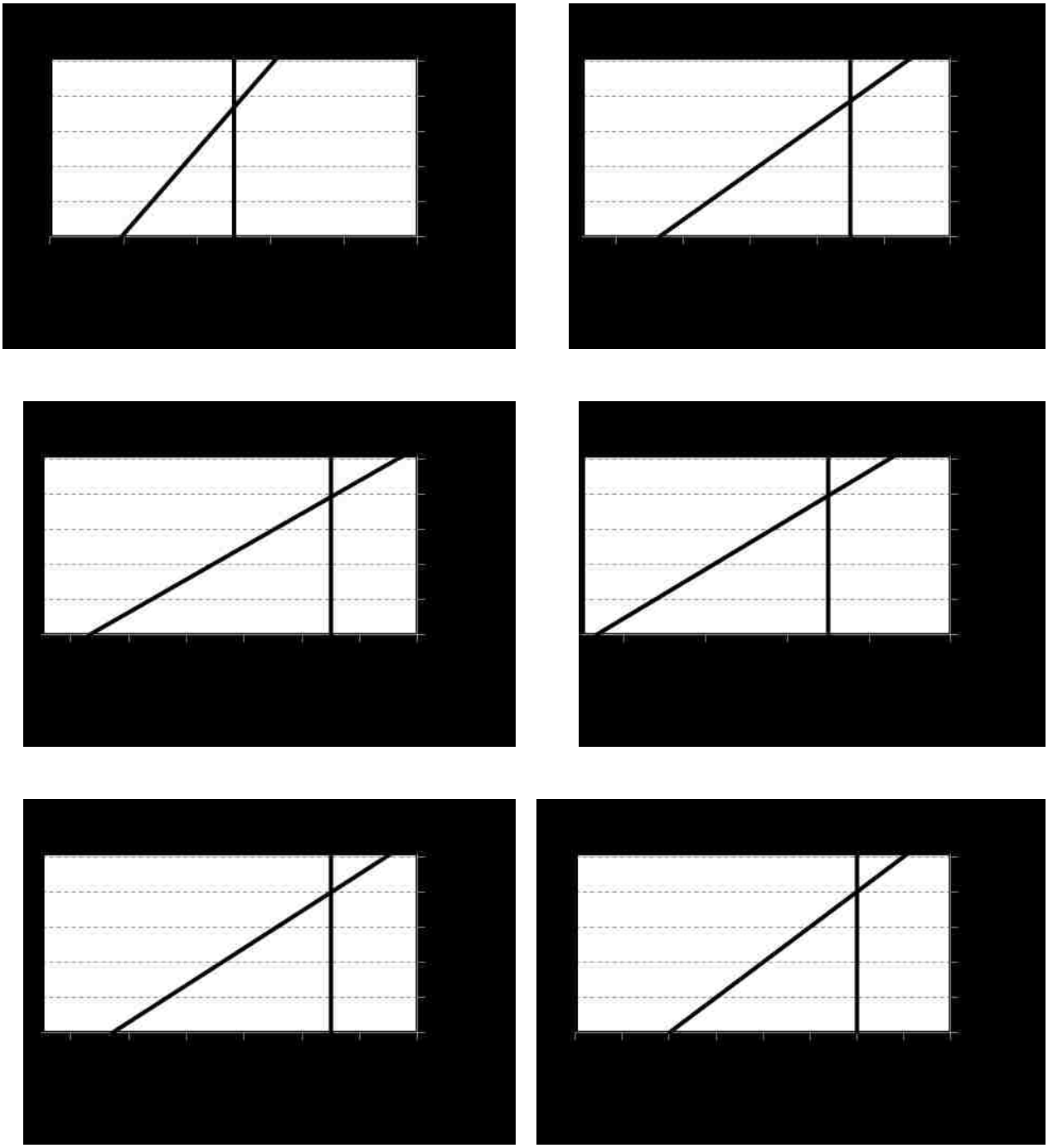

Figure 4.19: Strain distribution at mid-span section of Beam-C at different loads

(Cont.)

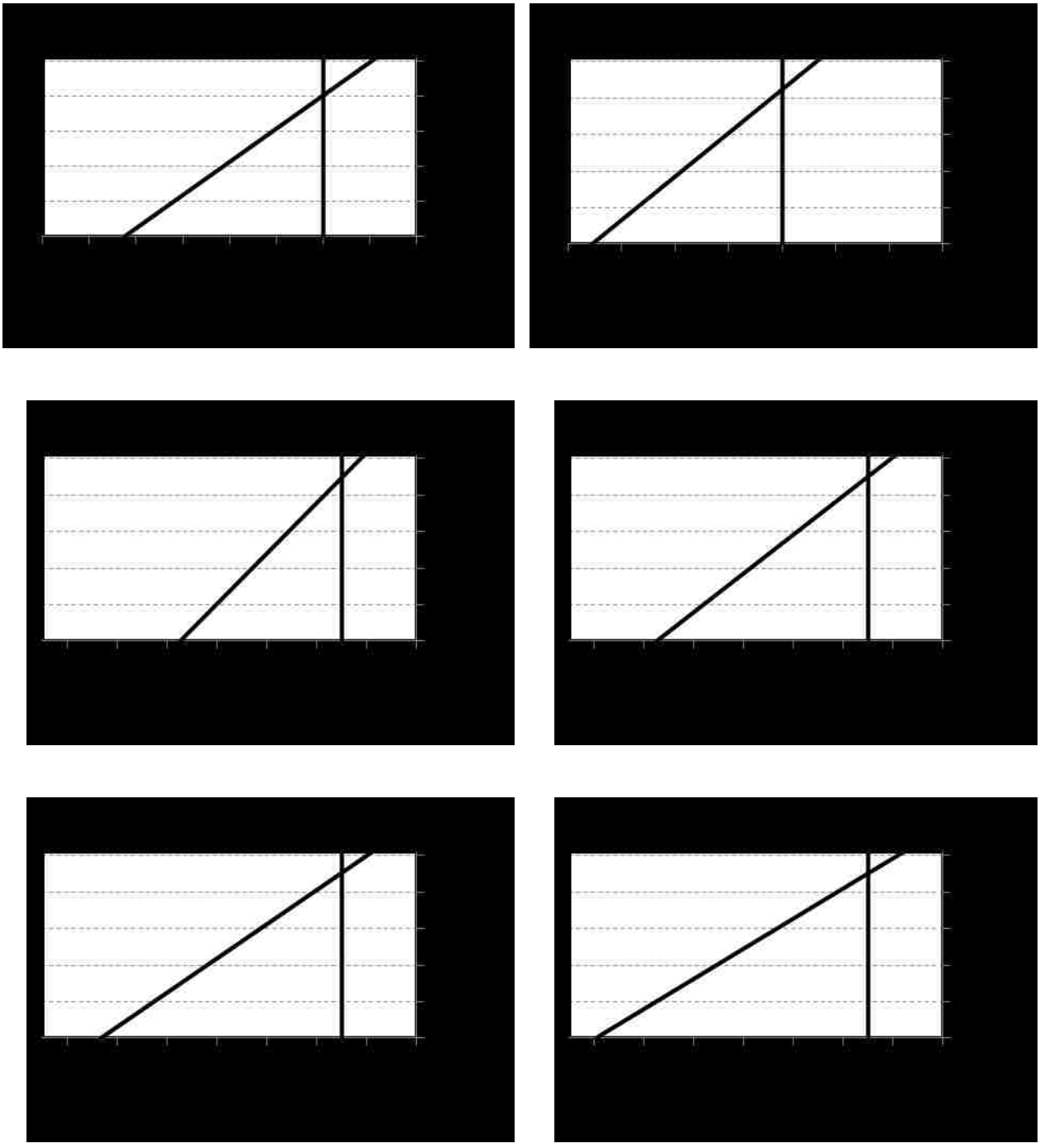

Figure 4.20: Strain distribution at mid-span section of Beam-C at different loads

(Cont.)

Using similar triangles, the depth of compression zone (c) was calculated from the strain distribution using equation **4.26**. The Moment-Curvature curve for the control beam is shown in **Figure 4.21**.

$$c = \frac{\varepsilon_c}{\varepsilon_c - \varepsilon_s} d \qquad \textbf{(4.26)}$$

Where

$\varepsilon_{c:}$ Compressive strain in concrete top fiber,

$\varepsilon_{s:}$ Tensile strain in steel,

d: Depth of the steel bars from the top [mm].

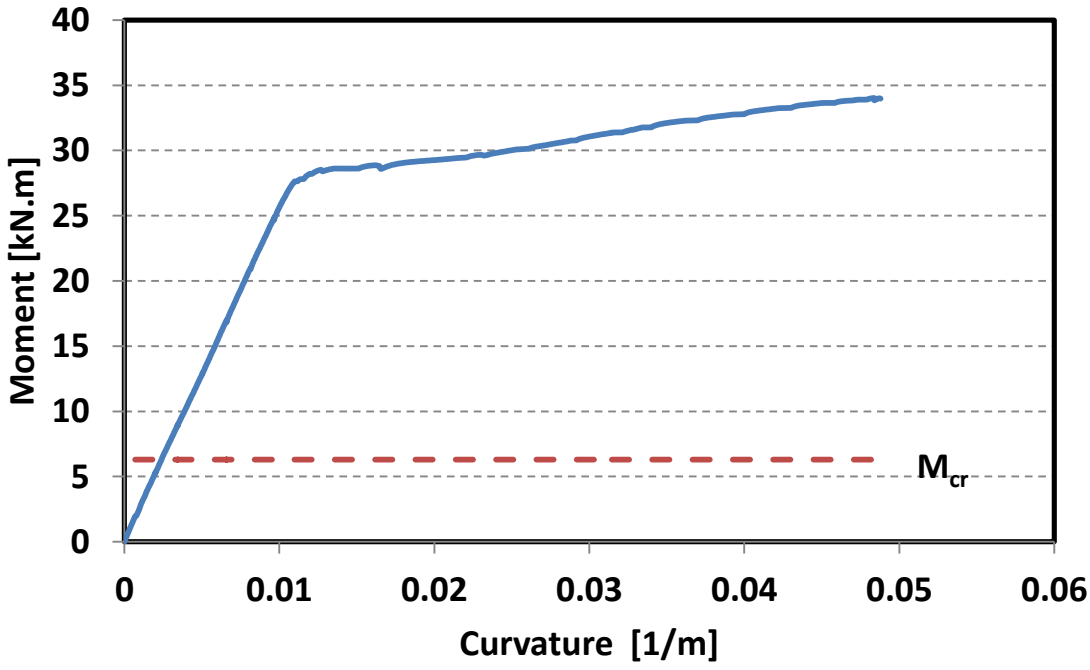

Figure 4.21: Moment-Curvature for Beam-C

As shown in **Figure 4.21** the moment-curvature is only plotted until a moment value of 34 kN.m. This moment is corresponding to a load value of 99.1 kN. At this load, the strain gauges were detached. The slope of the moment-curvature represents the flexural stiffness (EI) of the beam following equation **4.27**. The figure shows that the curvature increased linearly with the applied moment until a moment value of 27.6 kN.m associated to load of 80.4 kN which is the point at which the linear-elastic behavior of the load-displacement ended. The curvature then started to increase nonlinearly with minimal increase in moment. The initial and cracked flexural stiffness (EI) for the control beam were 2860.6 $kN.m^4/m^2$ and 2545.1 $kN.m^4/m^2$ respectively.

$$\Psi = \frac{M}{EI} \qquad \textbf{(4.27)}$$

Where

M: Applied moment on the beam [kN.m].

4.2.2.2 Beam-U.

While conducting the test, the beam side was checked continuously to track crack propagation. The first crack observed was located at the middle third of the beam near the loading point as in Beam-C. The load was of 16.9 kN. corresponding to a mid-span displacement of 0.5 mm while the first crack was observed. This is corresponding to a cracking moment of 5.8 kN.m. As load increased, the cracks propagated over the beam span as shown in **Figure 4.22.**

Figure 4.22: Cracks propagated in Beam-U

The moment capacity of Beam-U was 45.7 kN.m identical to the moment capacity of the control beam. The load, displacement at mid-span, and displacement at loading point at failure were 133.3 kN, 123.6 mm, and 100.3 mm respectively. Failure of the beam occurred due to crushing of the UHPC top layer at mid-span. The compressive strain of concrete at failure was 0.0031. **Figure 4.23 and Figure 4.24** show Beam-U at failure and the crushing of the UHPC respectively.

Figure 4.23: Beam-U at failure

Figure 4.24: Crushing of UHPC top layer in Beam-U

Figure 4.25 shows the load-displacement for Beam-U. The figure shows that the beam behavior was linear-elastic until the load reached 77.8 kN with corresponding displacement of 7.4 mm. The tensile strain at the steel rebars was 0.0021 at the end of the linear-elastic behavior of Beam-U. **Figure 4.26** shows the tension strain in the steel rebars vs. the applied load. The figure shows that the rebars reached yield strain of 0.002 at load of 75.1 kN and displacement of 7.0 mm. The strain gauges connected to the rebars were able to measure the tension strain up to load of 94.1 kN. After this point, the strain gauges were detached from the rebars and stopped reading.

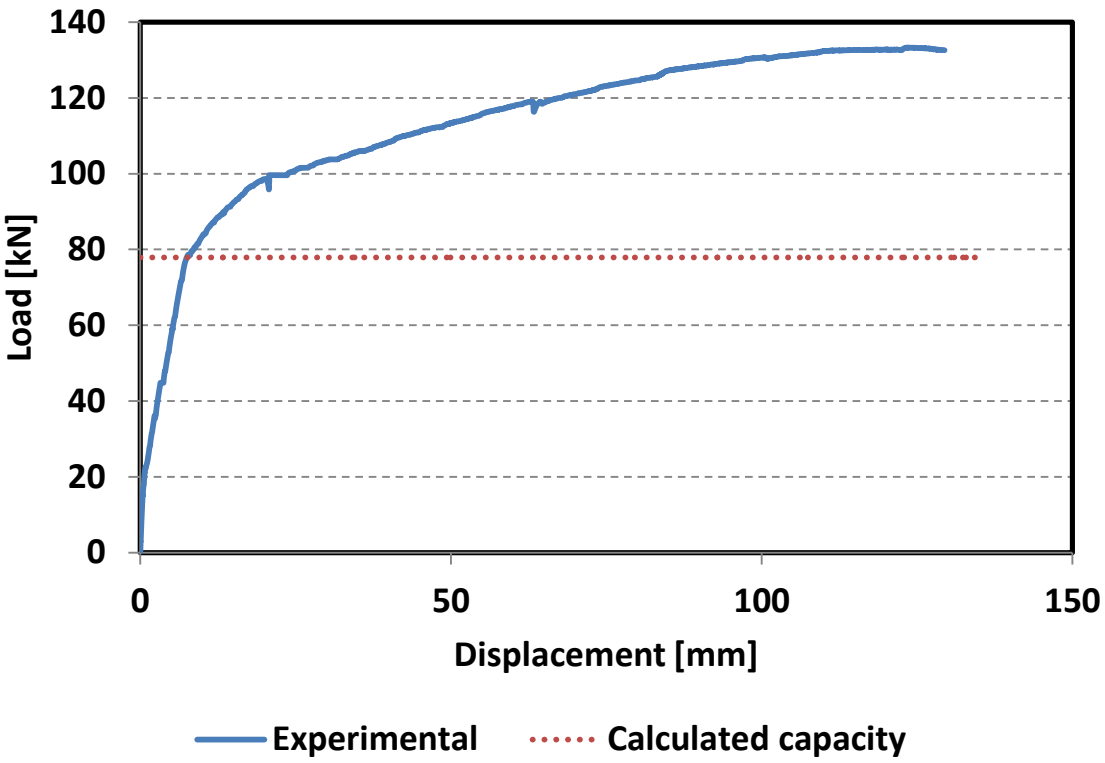

Figure 4.25: Load-Displacement for Beam-U

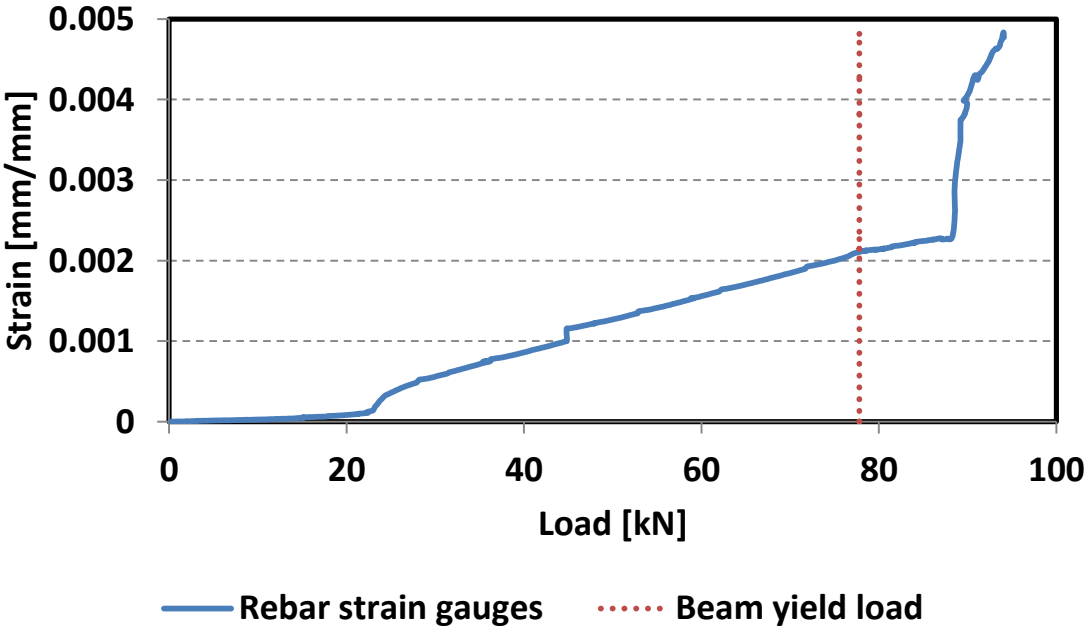

Figure 4.26: Load vs. tensile Strain in rebars for Beam-U

Beam stiffness of Beam-U was calculated similar to the control beam. **Figure 4.27** shows the linear part used to calculate beam stiffness.

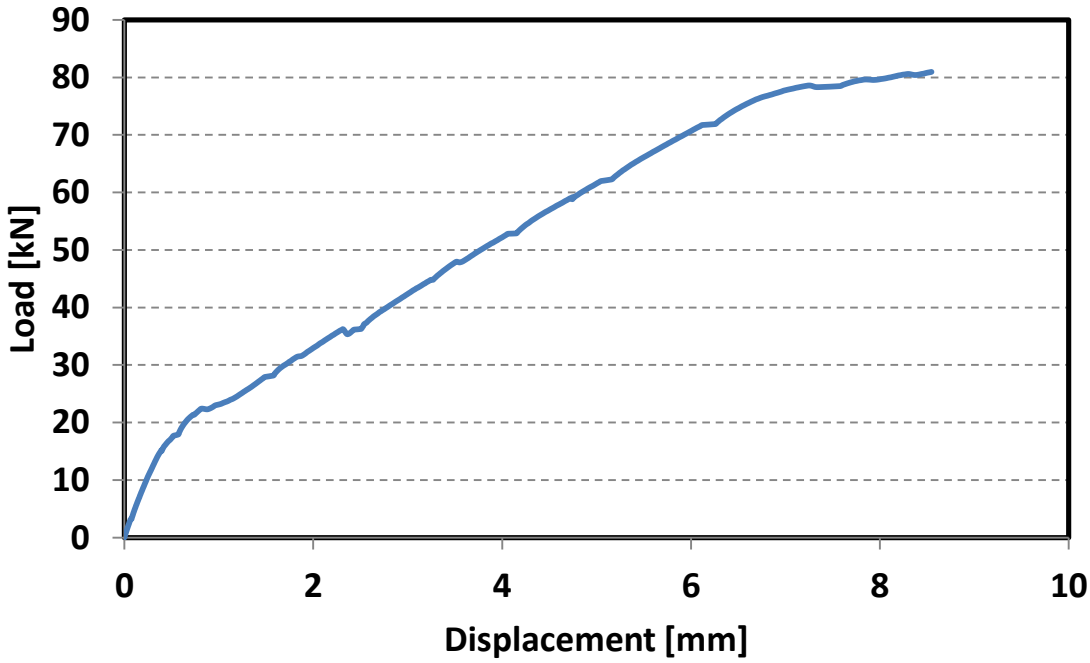

Figure 4.27: Linear part of load-displacement used for calculating stiffness for Beam-U

The curvature of the beam was calculated using equation **4.25.** The depth of compression zone (c) was calculated using the same procedure used in the control beam. **Figure 4.28** shows the load vs compressive strain for Beam-U. **Figure 4.29**, **Figure 4.30,** and **Figure 4.31** show the strain distribution on the mid-span section at different load values.

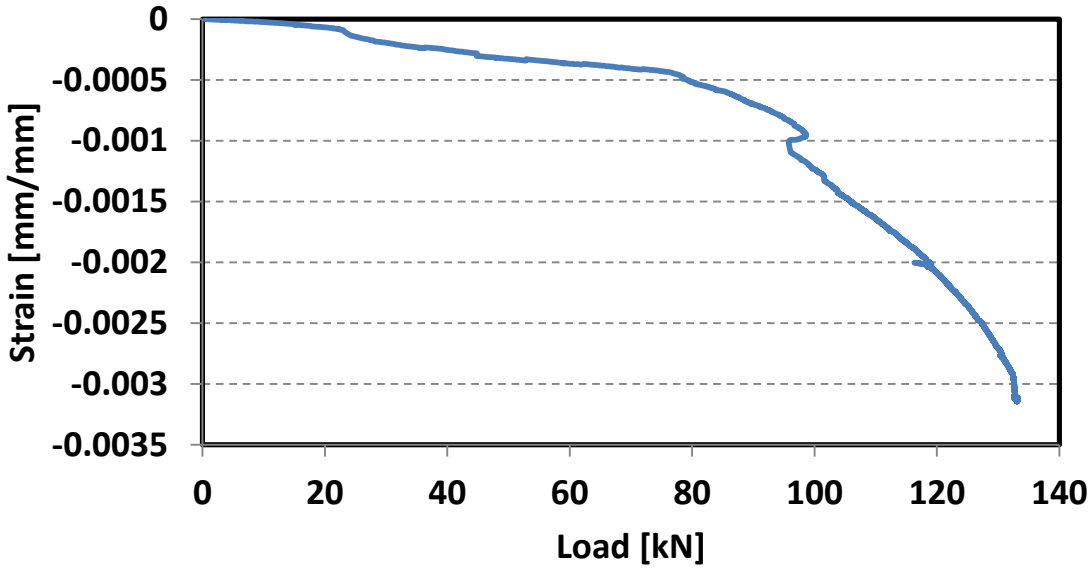

Figure 4.28: Load vs. compression strain in concrete top fiber in Beam-U

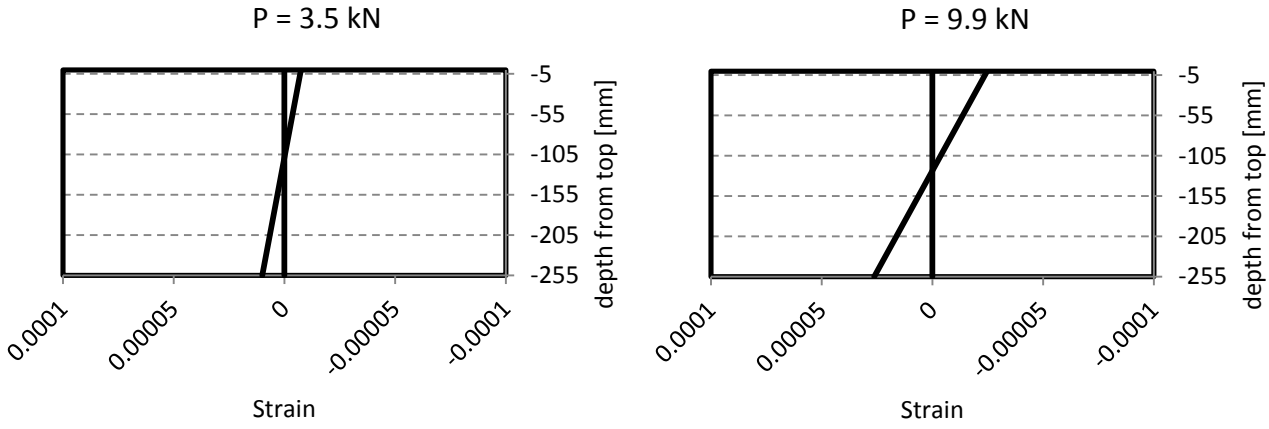

Figure 4.29: Strain distribution at mid-span section of Beam-U at different loads

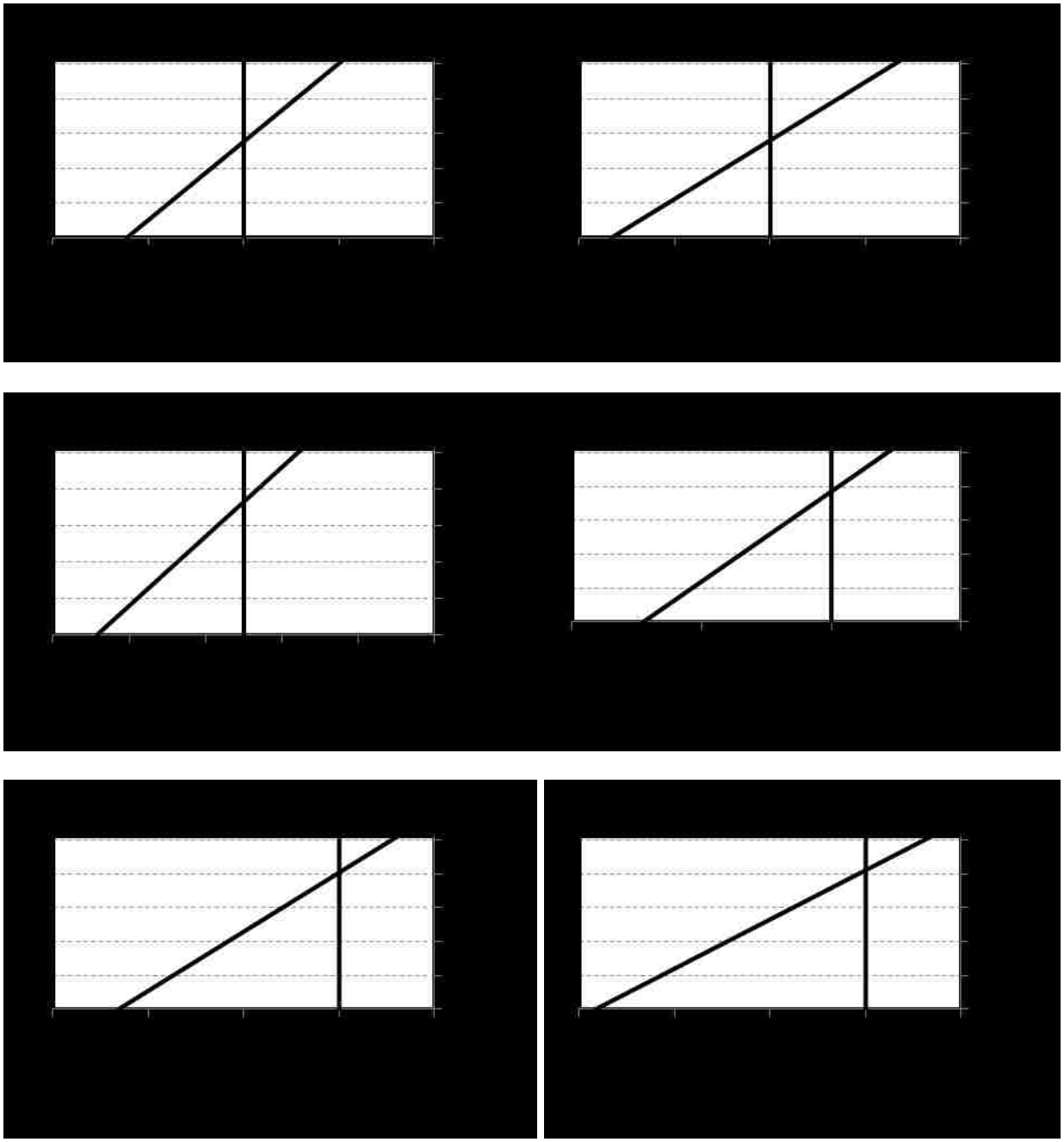

Figure 4.30: Strain distribution at mid-span section of Beam-U at different loads

(Cont.)

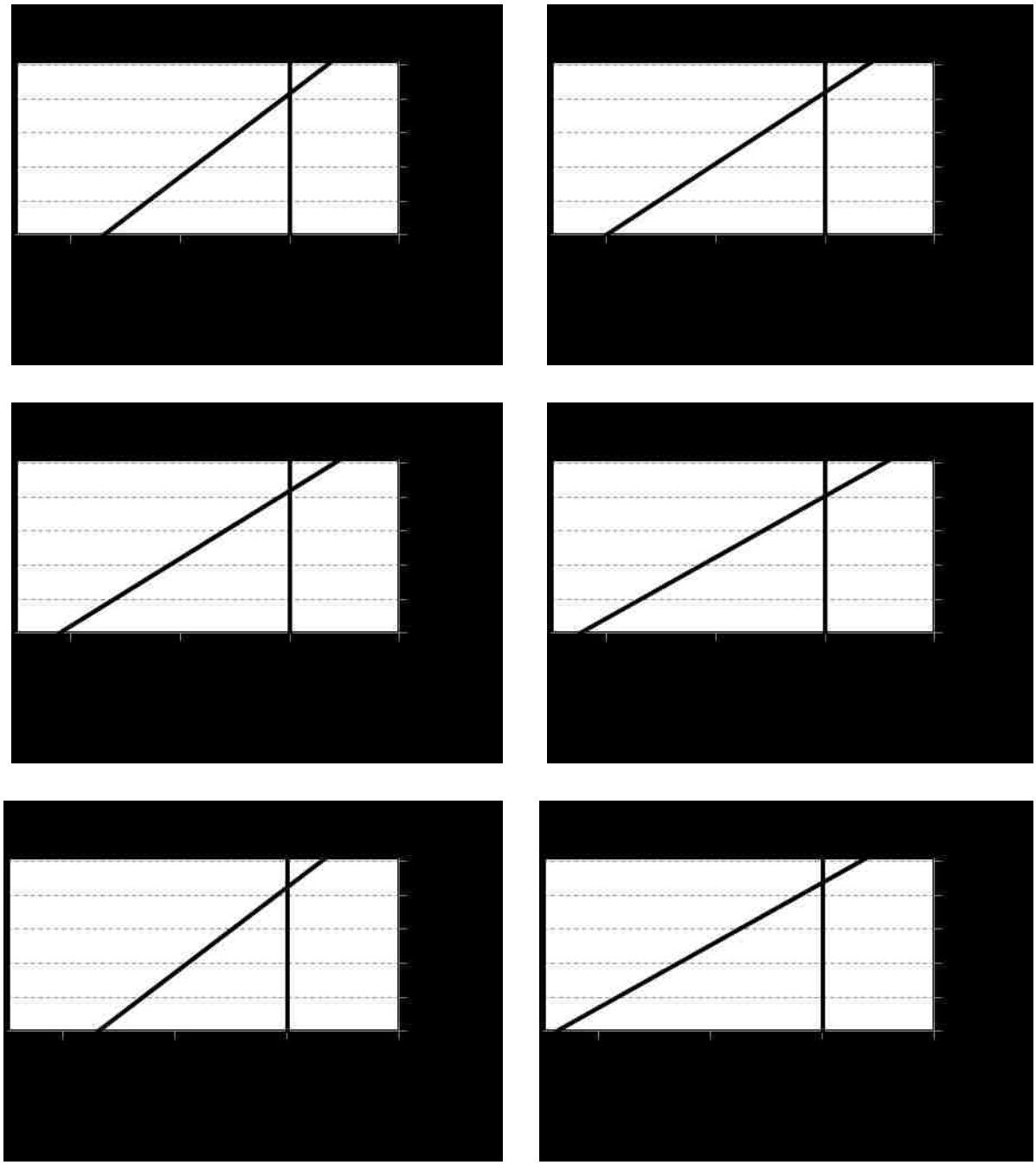

Figure 4.31: Strain distribution at mid-span section of Beam-U at different loads

(Cont.)

The depth of compression zone (c) was calculated from the strain distribution using equation **4.26**. **Figure 4.32** shows the moment-curvature for Beam-U. Unlike the control beam, the linear part of the Moment-Curvature curve has two different slobs. The first slope is from the start of the loading until moment of 4.9 kN.m corresponding to load value of 14.2 kN. This load relatively small value is very close the first crack observed at 16.9 kN. The second slope is from 8 kN.m until 30 kN.m corresponding to load of 23.4 kN and 87.5 kN respectively. Afterwards, the curvature of the beam starts to increase with no increase in moment. The uncracked and cracked flexural stiffness for Beam-U were 15,306.9 kN.m^4/m^2 and 2,687.5 kN.m^4/m^2 respectively.

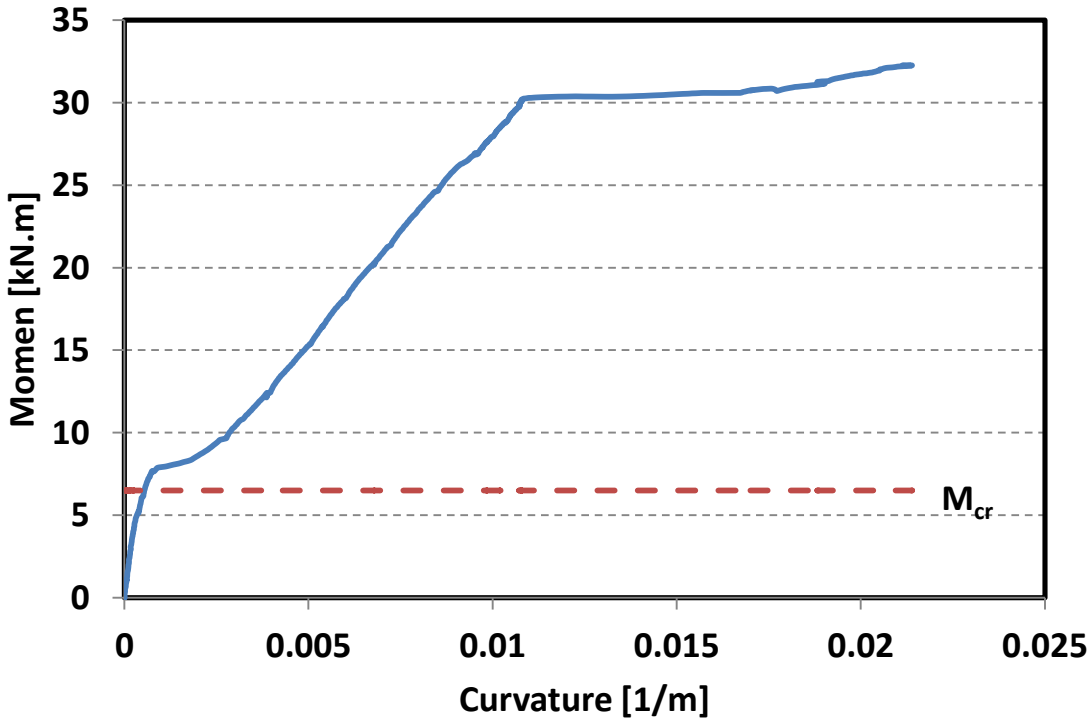

Figure 4.32: Moment-curvature for Beam-U

4.2.2.3 Beam-UF

As for Beam-UF, the first crack observed was near mid-span at load of 33.8 kN. The mid-span displacement when the first crack was observed was 1.9 mm corresponding to a cracking moment of 11.6 kN.m. As the load increases, more vertical cracks were observed along beam span as shown in **Figure 4.33**.

Figure 4.33: Vertical cracks in Beam-UF

The maximum moment carried by Beam-UF at failure was 49.9 kN.m corresponding to a load of 145.5 kN.m. The mid-span displacement at failure was 109.2 mm and the displacement at loading points was 90 mm. **Figure 4.34** shows Beam-UF at failure.

Figure 4.34: Beam-UF at failure

It was obvious that failure of Beam-UF occurred due to debonding between the UHPC layer and the T-section concrete between the support and the loading point as shown in **Figure 4.35**.

Figure 4.35: Debonding of UHPC overlay in Beam-UF at support area

The load-displacement for Beam-UF shows that the beam behavior was linear-elastic until load and displacement of 84.7 kN and 8.6 mm respectively as shown in **Figure 4.36**. The tension strain in the steel rebars at the end of linear-elastic region was 0.0022. The linear region of the load-displacement curve shown in **Figure 4.37** was used to calculate the stiffness of the beam. **Figure 4.38** shows the tensile strain in the rebars Vs. the applied load. It was observed that steel reached the yield at load of 79.8 kN and displacement of 7.8 mm. The strain gauges attached to the steel rebars were detached at load of 98.8 kN.

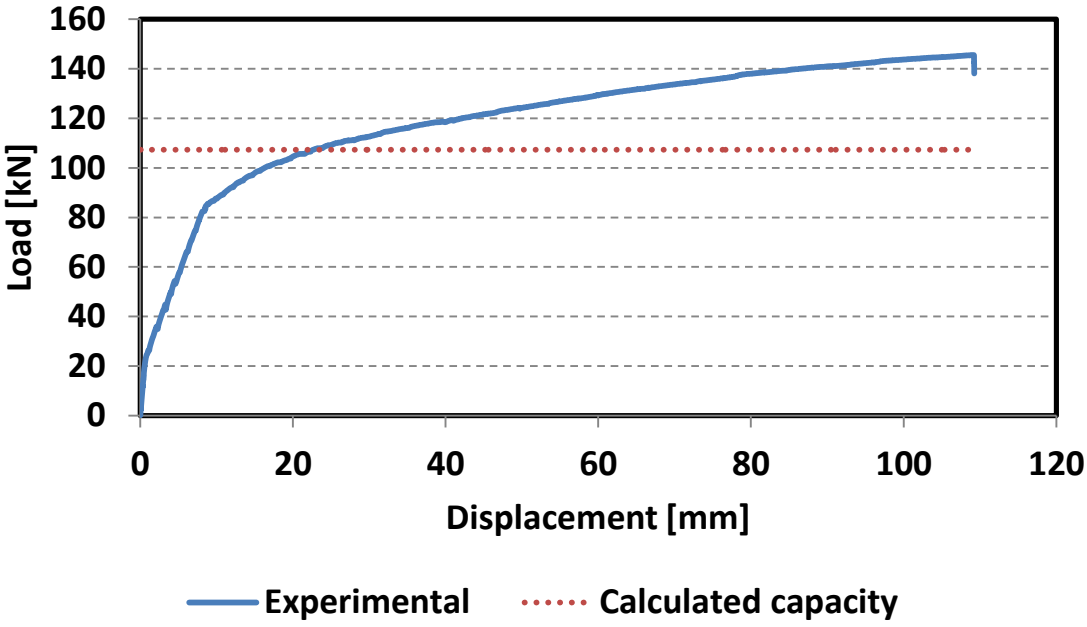

Figure 4.36: Load-Displacement for Beam-UF

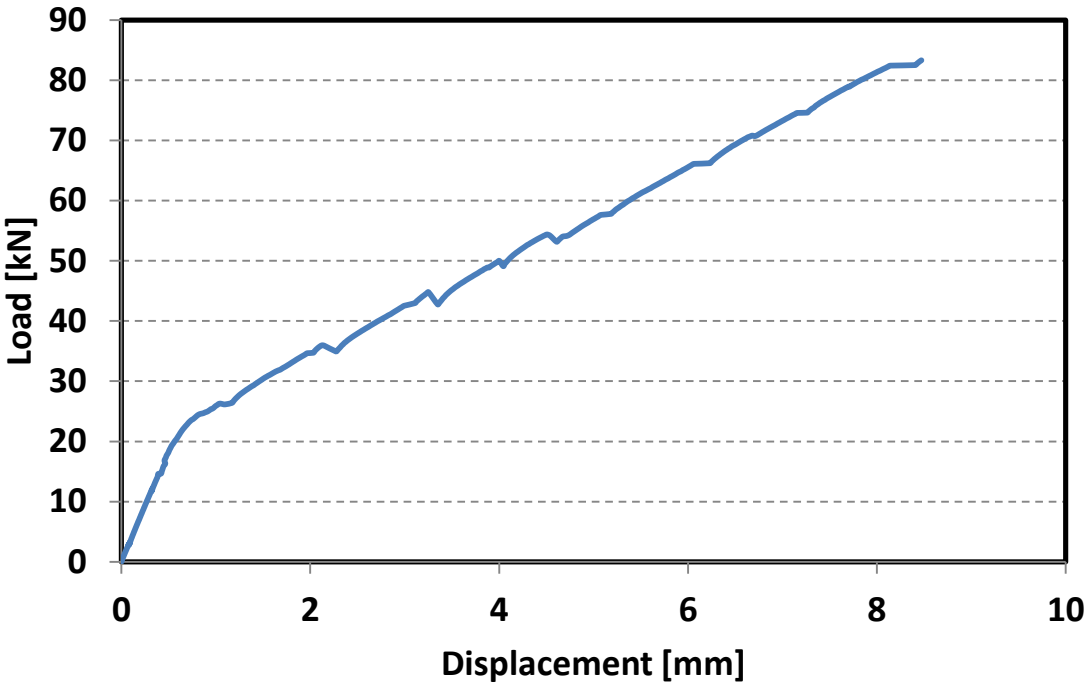

Figure 4.37: Linear part of load-displacement used for calculating Beam-UF Stiffness

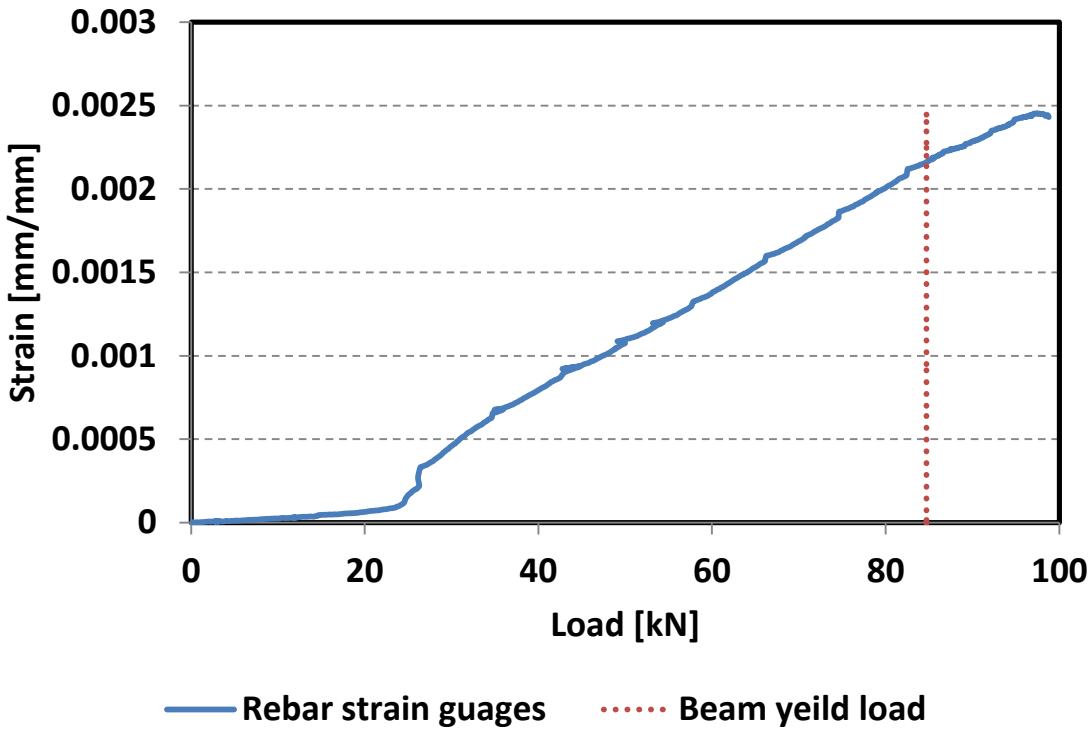

Figure 4.38: Load vs. tensile strain in rebars in Beam-UF

The strain gauges attached to the CFRP laminates were able to read the strain in the CFRP until failure of beam. **Figure 4.39** shows the strain in the CFRP laminates. The figure shows that the CFRP laminates was in compression until the load reached 107.7 kN corresponding to a mid-span displacement of 23 mm. The maximum tensile strain in the CFRP at failure was 0.0031 and the tension force in the CFRP at failure of the beam was 47.3 kN and no failure of CFRP took place. The calculation of the tension force is based on the stress-strain of CFRP laminates observed in our lab (Section 3.2). **Figure 4.40** shows the compressive strain in concrete at the top of the beam. The figure shows that the ultimate compressive strain at concrete at failure was 0.0023.

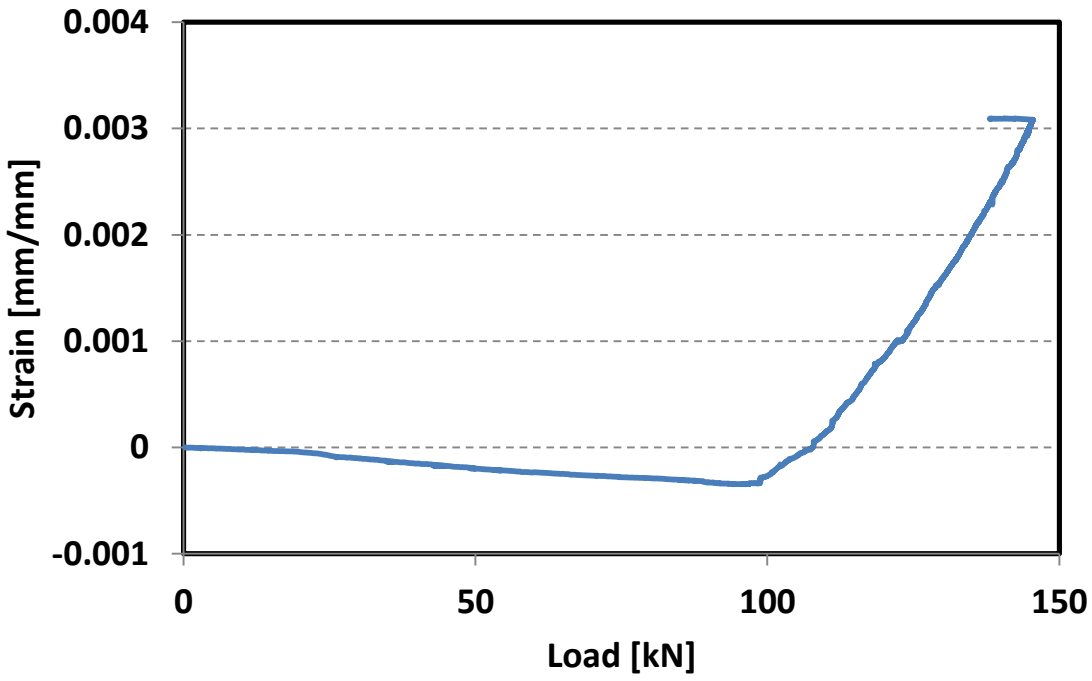

Figure 4.39: Load vs. strain in CFRP laminates in Beam-UF

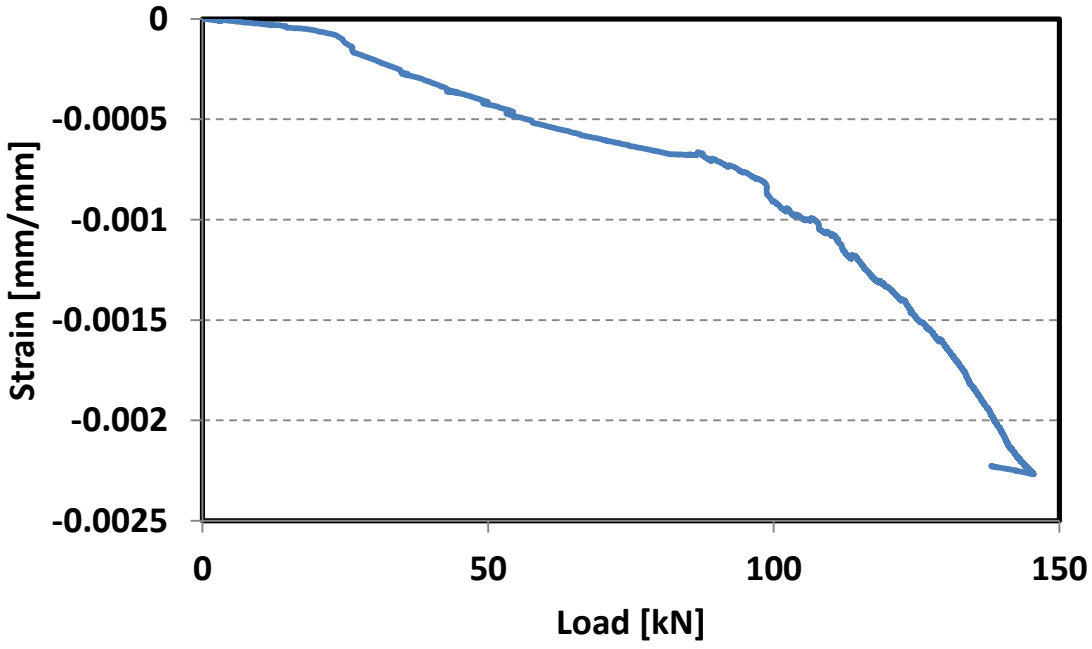

Figure 4.40: Load vs. compressive strain in concrete top fiber in Beam-UF

The curvature of the beam was calculated using equation **4.25**. The strain distribution at mid-span section was obtained using the strain in the concrete, CFRP laminates, and the steel rebars. The depth of compression zone (c) was calculated using equation **4.28** until the load reached 98.8 kN and equation **4.29** until failure.

$$c = \frac{\left(h - t_u\right)\ \varepsilon_f - t_u \varepsilon_s}{\varepsilon_f - \varepsilon_s} \qquad \textbf{(4.28)}$$

$$c = \frac{t_u\ \varepsilon_c}{\varepsilon_c - \varepsilon_f} \qquad \textbf{(4.29)}$$

Figures 4.41 to **Figure 4.43** show the strain distribution on the mid-span section at different values of loads.

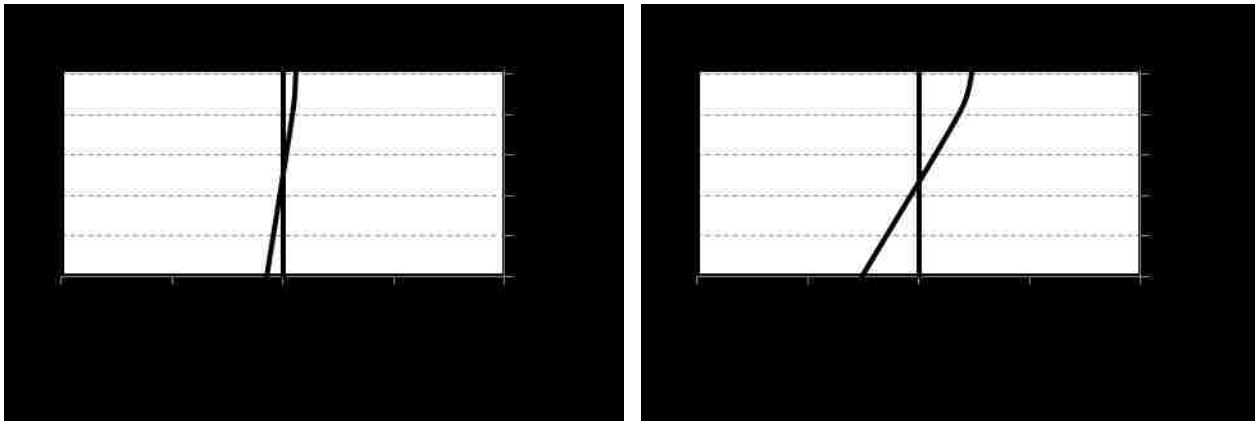

Figure 4.41: Strain distribution at mid-span section of Beam-UF at different loads

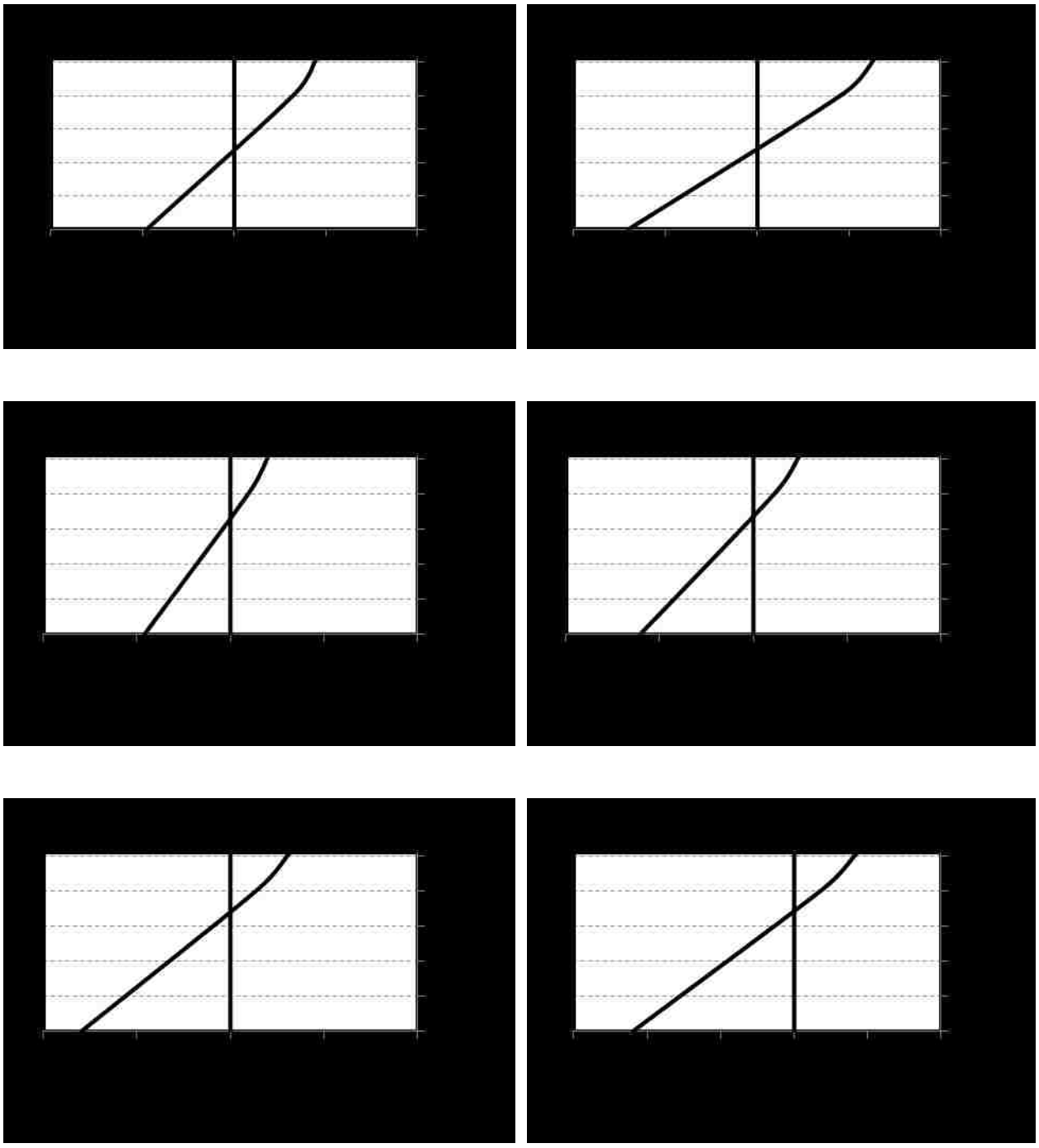

Figure 4.42: Strain distribution at mid-span section of Beam-UF at different loads (Cont.)

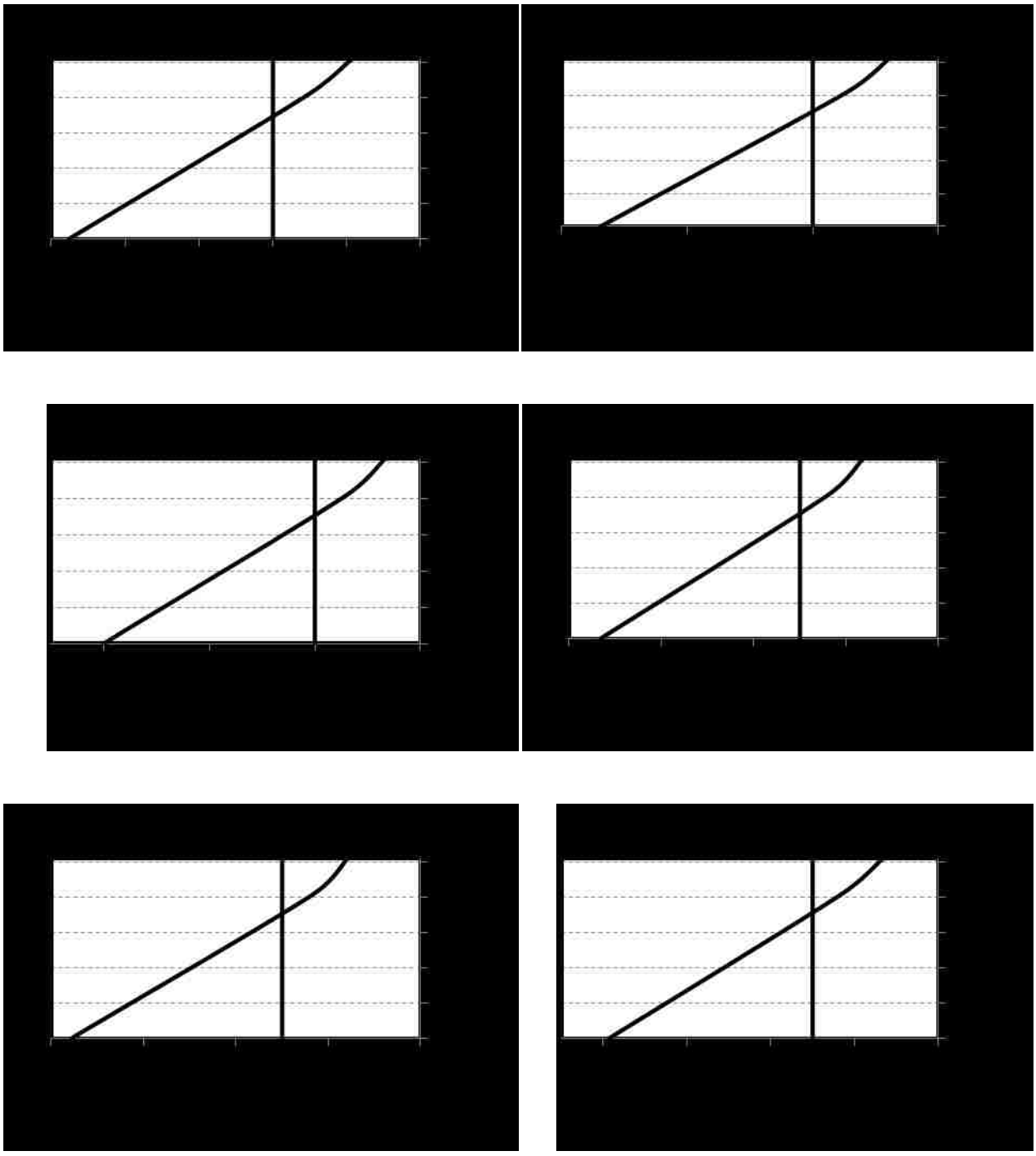

Figure 4.43: Strain distribution at mid-span section of Beam-UF at different loads

(Cont.)

The Moment-curvature for Beam-UF is presented in **Figure 4.44**. The linear part is divided to two parts. The initial stiffness of the beam is calculated from the start of the loading until moment of 8.1 kN.m. The cracked stiffness of the beam was calculated from moment of 8.1 kN.m to moment of 33.9 kN.m. The uncracked and cracked flexural stiffness were 13,937.6 is $kN.m^4/m^2$ and 2,926.2 $kN.m^4/m^2$ respectively.

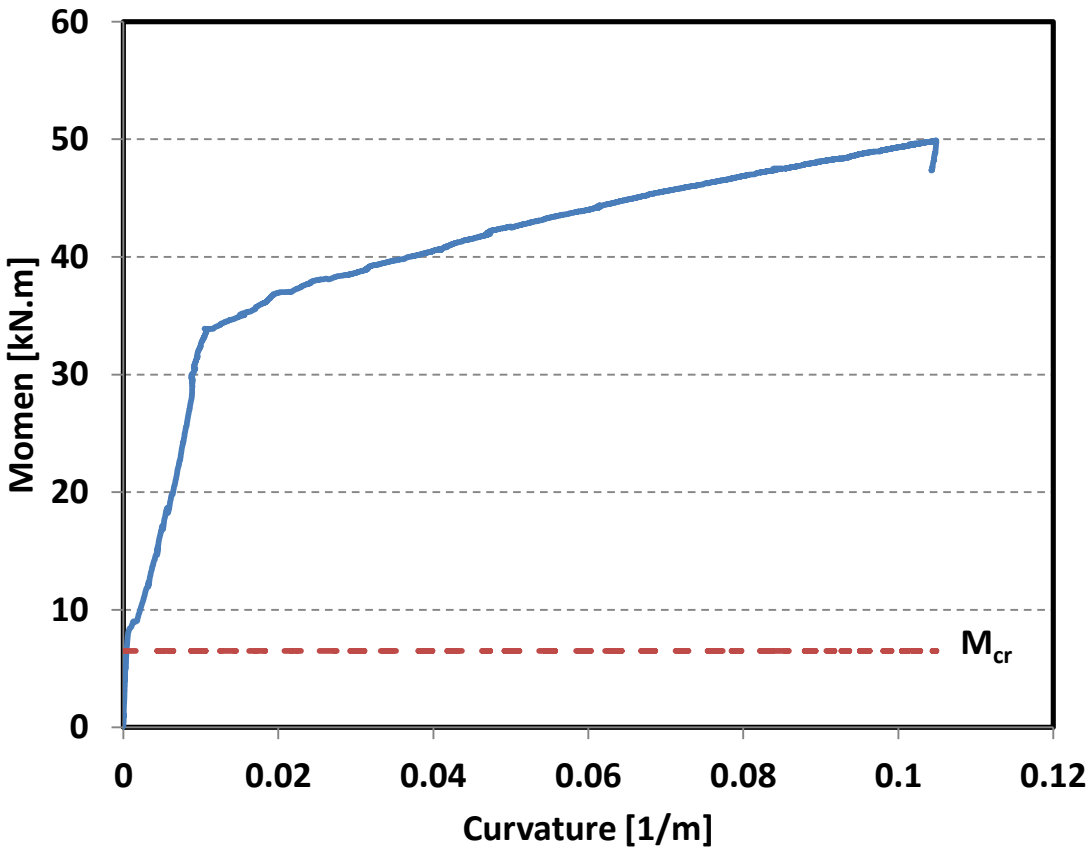

Figure 4.44: Moment-curvature for Beam-UF

4.2.2.4 Beam-MUF

The first crack observed in Beam-MUF was in the middle third of the beam near loading point. The load and the mid-span displacement when the first crack occurred were 32.1 kN and 2.0 mm respectively. The corresponding cracking moment was 11.0 kN.m. As the loading continue, more vertical cracks were observed as shown in **Figure 4.45.**

Figure 4.45: Cracks propagated in Beam-MUF at early loading

The flexural capacity of Beam-MUF was 42.4 kN.m associated with a load of 123.5 kN. The mid-span displacement and the displacement at the loading point at failure were 77.7 mm and 67.5 mm respectively. **Figure 4.46** shows Beam-MUF at failure.

Figure 4.46: Beam-MUF at failure

As shown in **Figure 4.47**, the failure of the beam occurred due to the debonding of the LMUHPC overlay at the mid span of the beam.

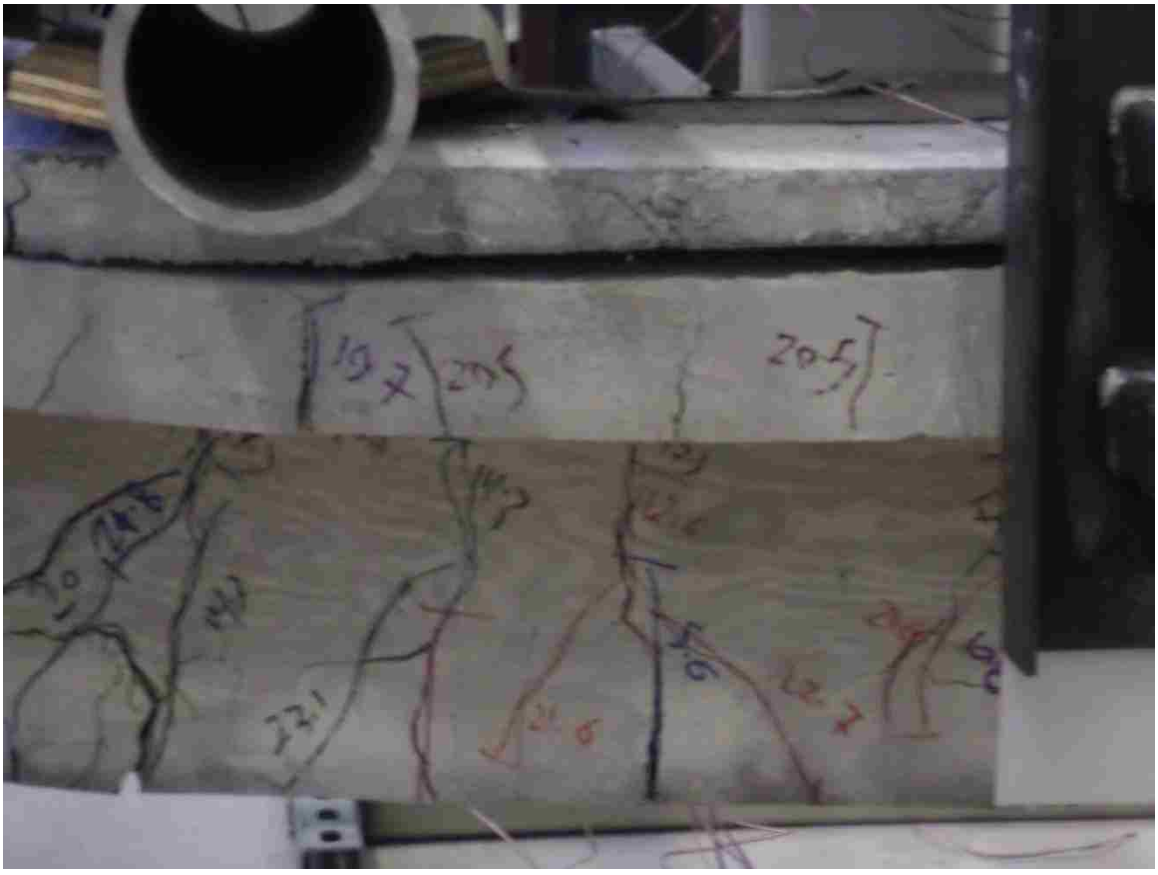

Figure 4.47: Debonding of the LMUHPC layer in Beam-MUF

Figure 4.48 shows the load-displacement for Beam-MUF. The Figure shows that the beams behavior was linear-elastic until the load reached 78.6 kN. The corresponding mid-span displacement was 8.2 mm. The linear elastic part of the load-displacement curve shown in **Figure 4.49** was used to calculate Beam-MUF stiffness. The strain in the steel rebars at the end of the linear-elastic behavior of the beam was 0.0026. The applied load vs the tensile strain in the rebars is presented in **Figure 4.50**. The figure shows that the rebars reached yield at a load of 65.8 kN corresponding to a displacement of 6.5 mm.

The strain gauges attached to the rebars were able to read the strain until they were detached at a load of 100.5 kN.

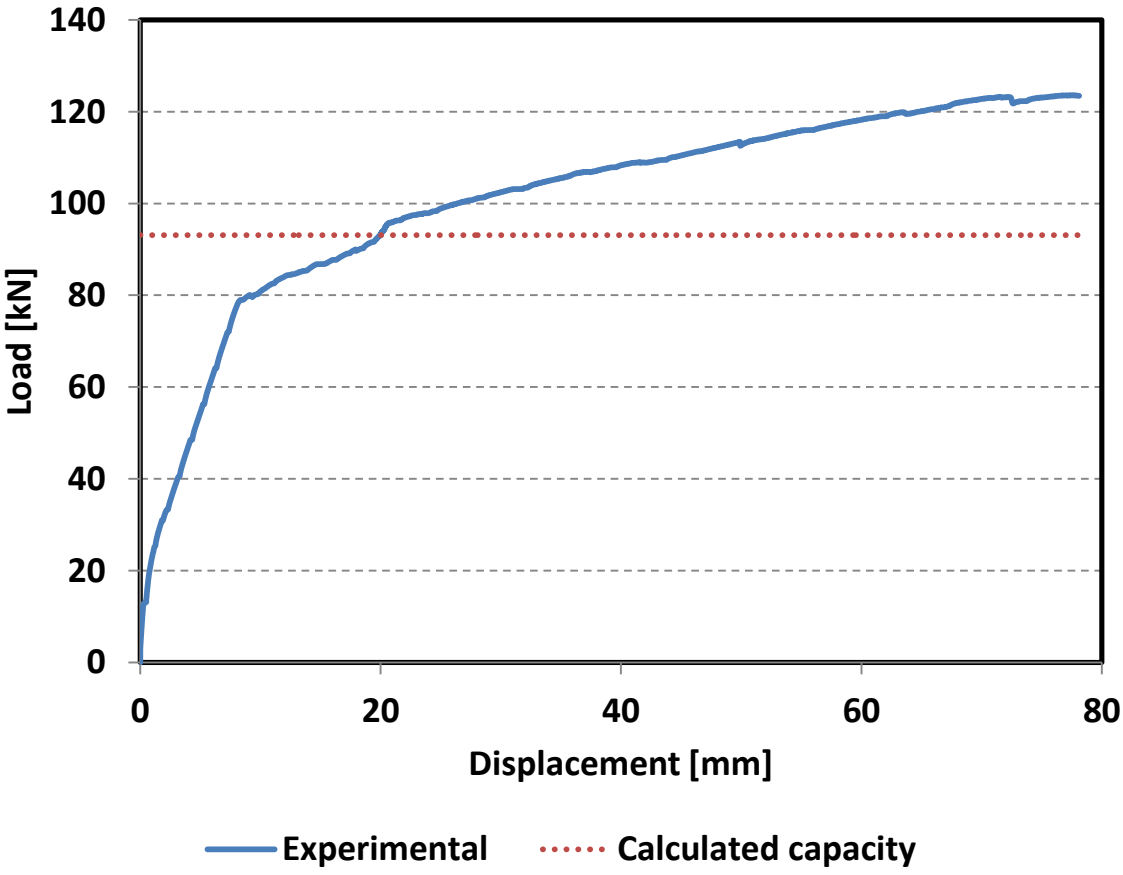

Figure 4.48: Load-displacement for Beam-MUF

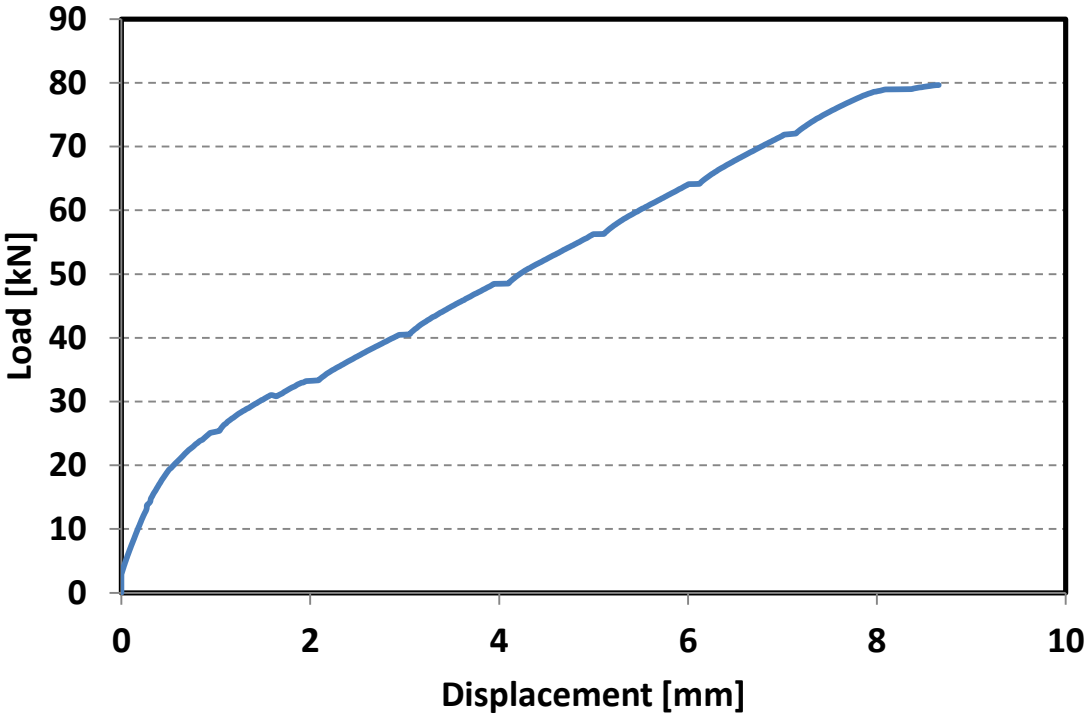

Figure 4.49: Linear part of load-displacement used for calculating Beam-MUF stiffness

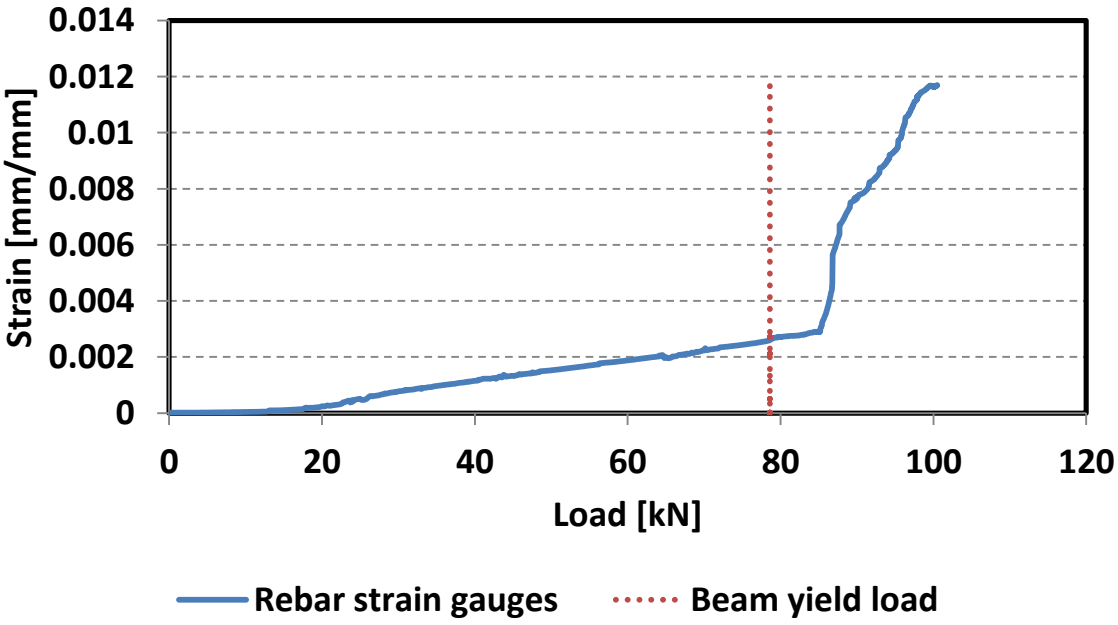

Figure 4.50: Load vs. tensile strain in rebars in Beam-MUF

Load vs the strain in the CFRP laminates is presented in **Figure 4.51**. The strain gauges attached to the CFRP laminates were able to read the strain until failure. The figure shows that the CFRP was in compression and then turned to be under tension at a load of 85.1 kN corresponding to a mid-span displacement of 13.4 mm. The tension strain and the tension force in the CFRP at failure of the beam were 0.0016 and 30.5 kN respectively and no failure of CFRP took place. The maximum compressive strain of the concrete top fiber at failure was 0.0021. Load Vs. compressive strain in top concrete fiber in Beam-MUF is presented in **Figure 4.52**.

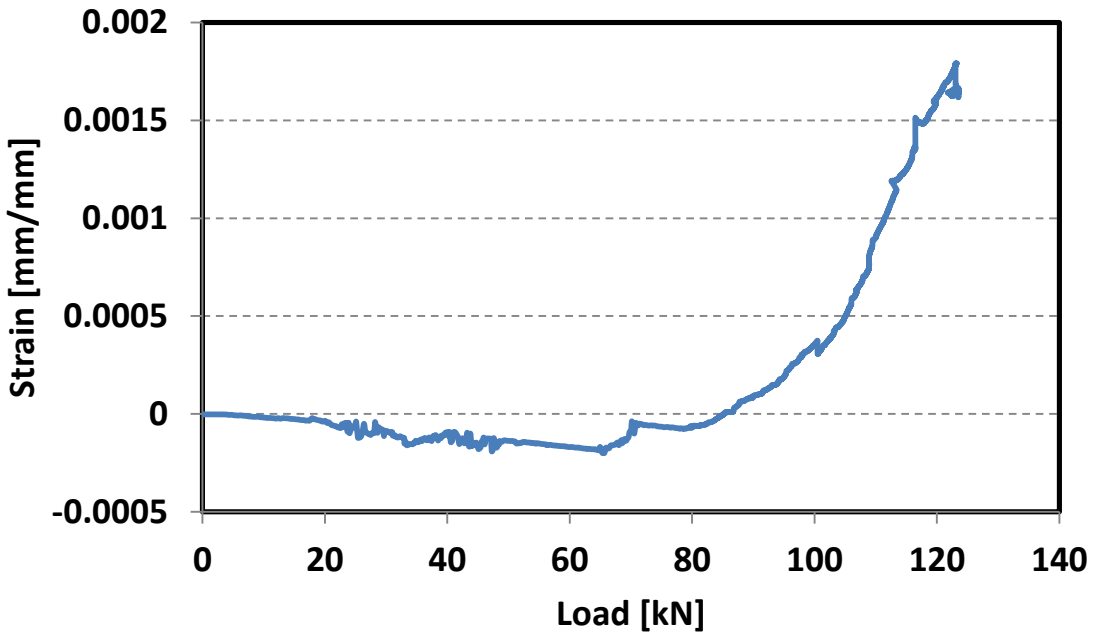

Figure 4.51: Load vs. strain in CFRP laminates in Beam-MUF

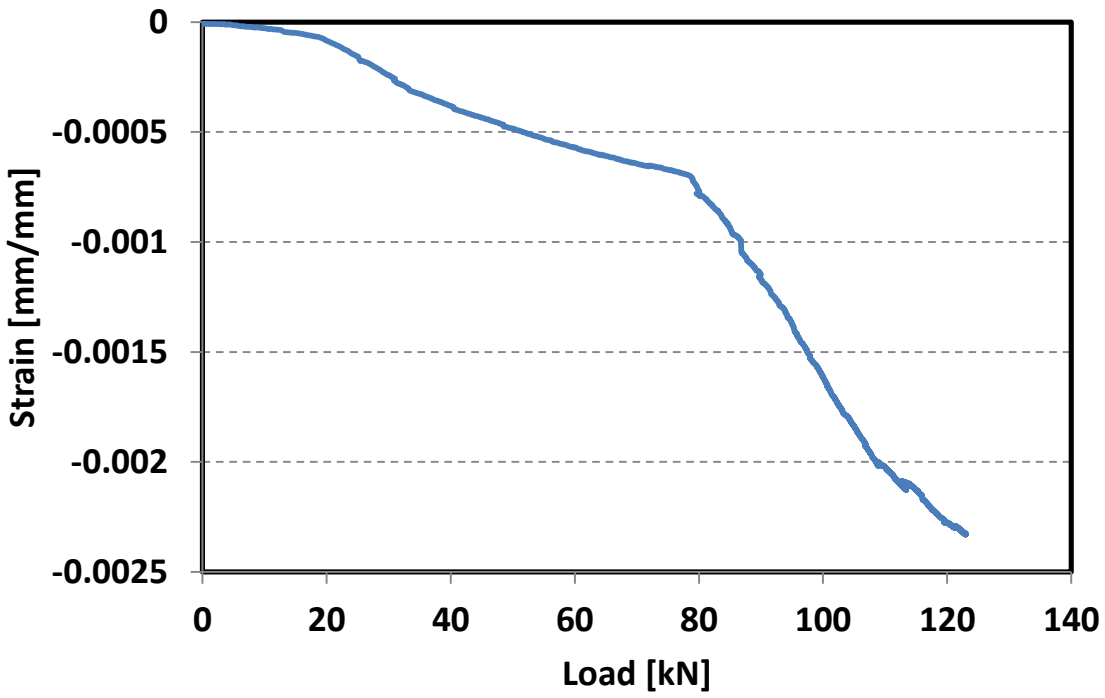

Figure 4.52: Load vs. compressive strain in concrete top fiber in Beam-MUF

The curvature of the beam was calculated using equation **4.25**. The strain distribution at the mid-span section was obtained using the strain in the concrete, CFRP laminates, and the steel rebars. The depth of compression zone (c) was then calculated using equation **4.28** until the strain in the CFRP reversed from compression to tension at a load of 85.1 kN. The calculation was then performed using equation **4.29** until failure. **Figures 4.48** to **4.50** show the strain distribution on the mid-span section at different loads values.

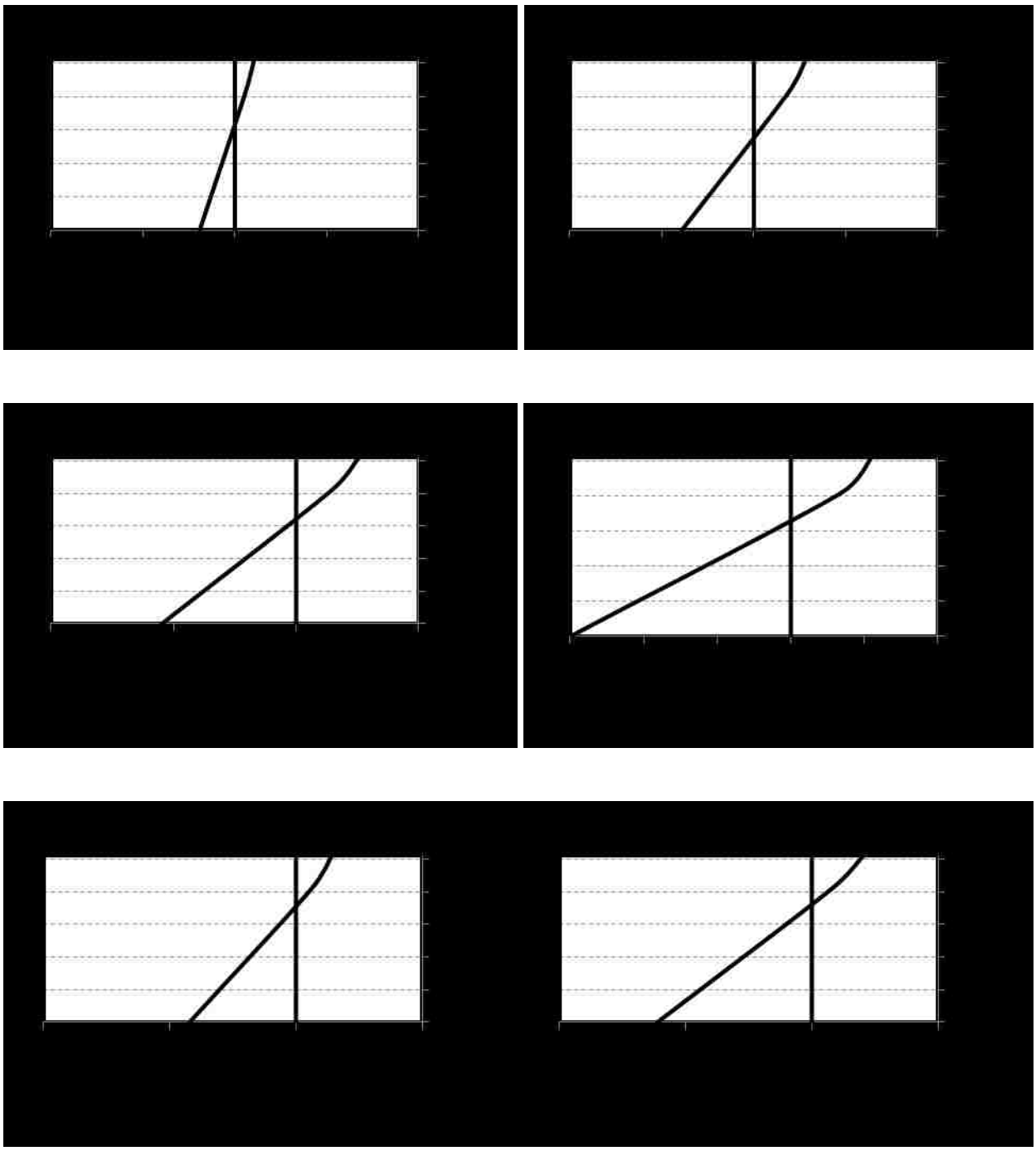

Figure 4.53: Strain distribution at mid-span section of Beam-MUF at different loads

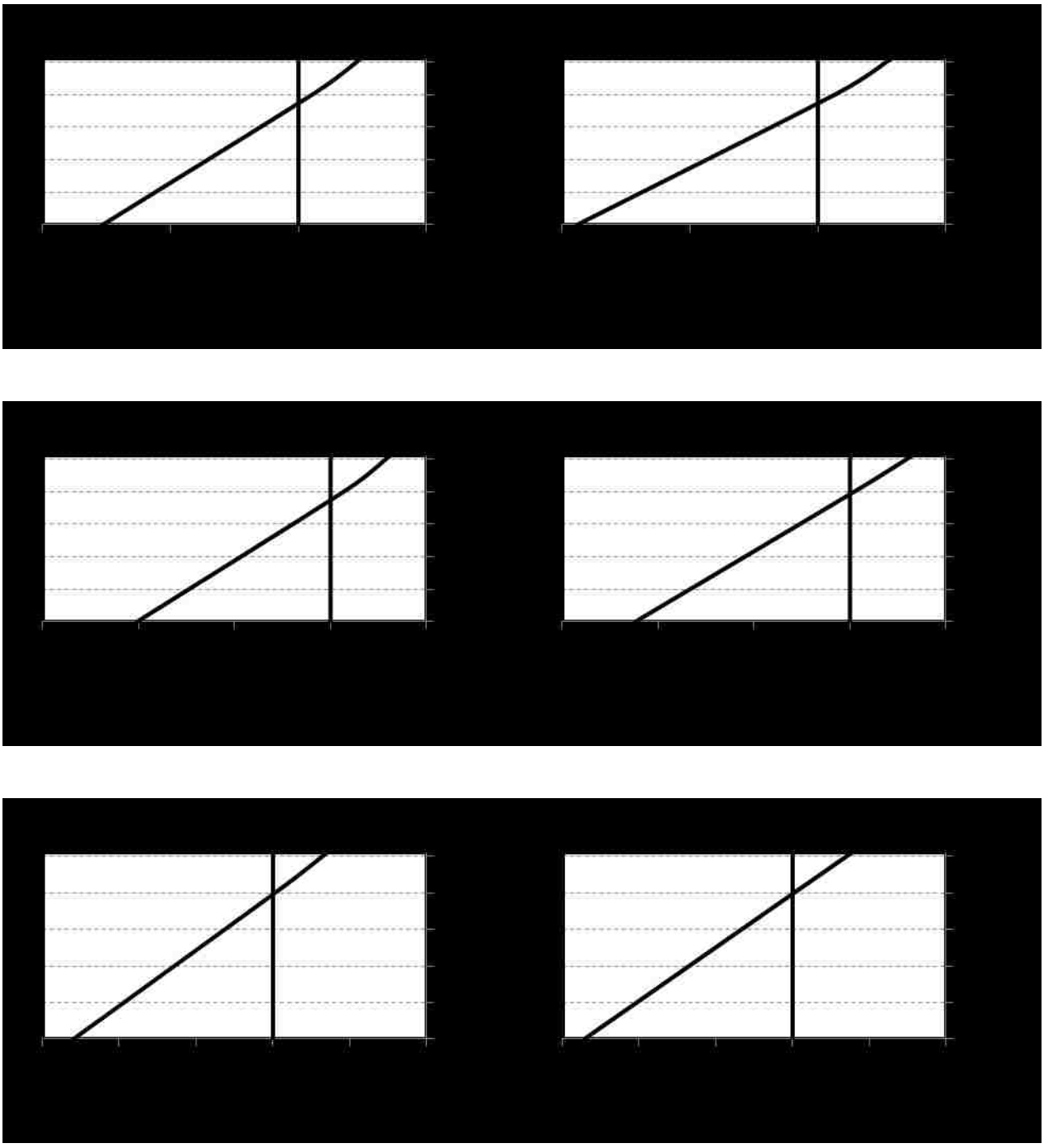

Figure 4.54: Strain distribution at mid-span section of Beam-MUF at different loads

(Cont.)

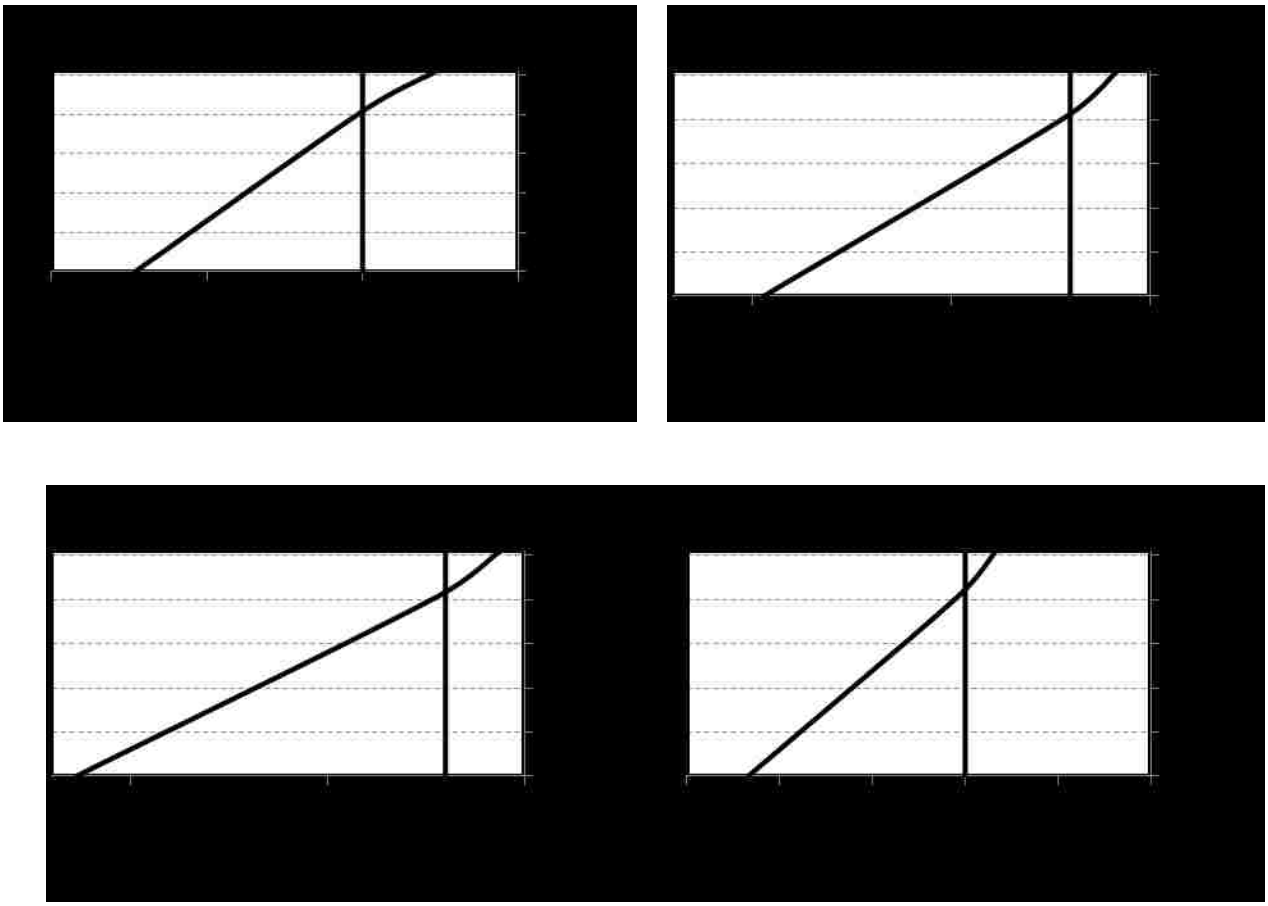

Figure 4.55: Strain distribution at mid-span section of Beam-MUF at different loads (Cont.)

The moment-curvature curve for Beam-MUF is shown in **Figure 4.56**. The flexural stiffness of the beam was calculated following equation **4.27**. Similar to Beam-U and Beam-UF, the flexural stiffness of Beam-MUF changed when the beam cracked. Initial and cracked flexural stiffness for Beam-MUF were 19,536.7 kN.m^2 and 1,809.5 kN.m^2 respectively.

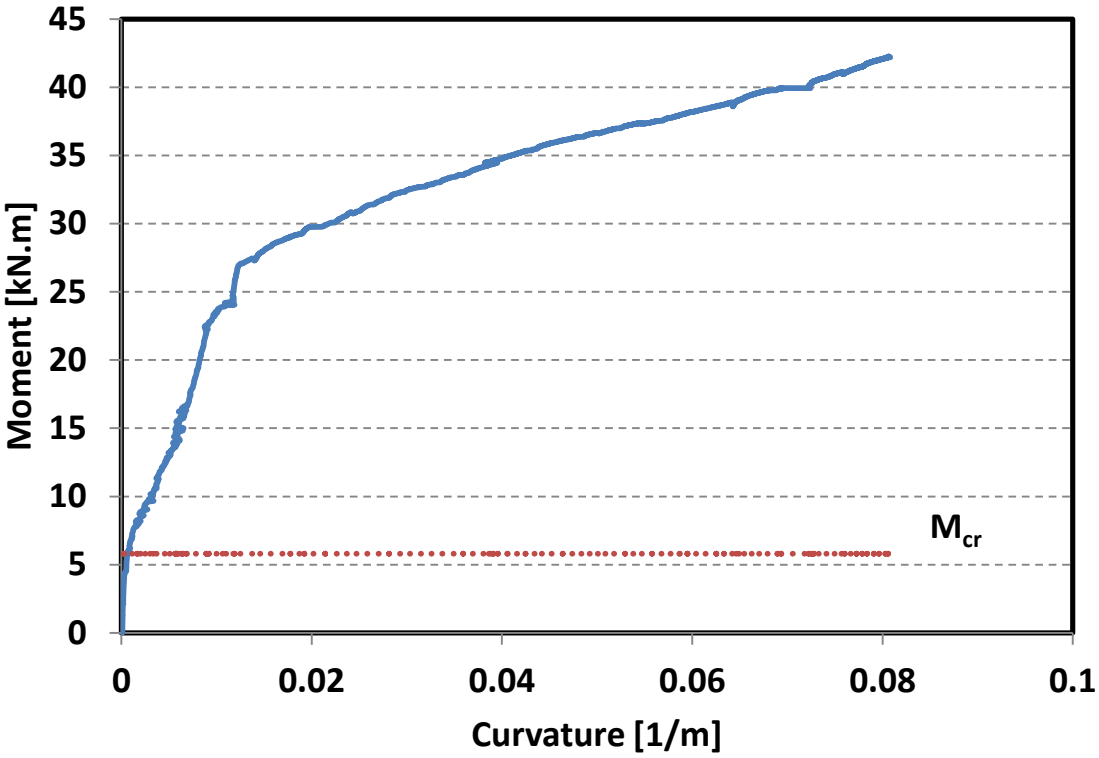

Figure 4.56: Moment-curvature for Beam-MUF

4.3 Comparison and Discussion

In this section, comparison between the control beam and the three beams is presented to show the effect of the modification in each beam on its mechanics and capacity. Moreover, a comparison between Beam-UF and Beam-MUF to shows the deference between the behavior of UHPC and LMUHPC overlays. **Table 4.6** shows the summary of the results for the four beams.

Table 4.6: Summary of the results for the four beams

	Beam-C	**Beam-U**	**Beam-UF**	**Beam-MUF**
Failure				
Mode	Crushing in concrete	Crushing in concrete	Debonding at support	Debonding at mid-span
Load [kN]	133.2	133.3	145.5	123.5
Moment [kN.m]	45.7	45.7	49.9	42.4
Mid-span displacement [mm]	117.8	123.6	109.2	77.7
Capacity increase	N/A	+ 0.07%	+ 9.2%	-7.3%
Loading points displacement [mm]	99.6	100.3	90	67.5
Strain in concrete top fibers	-0.0043	-0.0031	-0.0023	-0.0021
Strain in CFRP laminates	N/A	N/A	0.0031	0.0016
Force in CFRP laminates [kN]	N/A	N/A	47.3	24.4
First observed crack				
Load [kN]	25.6	16.9	33.8	32.1
Mid-span displacement [mm]	2.2	0.5	1.9	2
Linear-elastic limit				
Load [kN]	80.4	77.8	84.7	78.6
Mid-span displacement [mm]	7	7.4	8.6	8.2
Strain in CFRP laminates	N/A	N/A	-0.003	-7.5×10^{-5}
Strain in steel rebars	0.0021	0.0021	0.0022	0.0026
Yield of steel rebars				
Load [kN]	77.2	75.1	79.8	65.8
Mid-span displacement [mm]	6.7	7	7.8	6.5
Strain in CFRP laminates reverse point				
Load [kN]	N/A	N/A	107.7	81.5
Mid-span displacement [mm]	N/A	N/A	23	13.4
Stiffness ($\delta P/\delta \Delta$)				
Initial [kN/mm]	19.8	43.7	30.1	41.5
Cracking [kN/mm]	11.6	8.4	7.1	7.8
Flexural stiffness (EI)				
Initial [$kN.mm^4/mm^2$]	2860.6	15306.9	13937.6	19536.7
Cracking [$kN.mm^4/mm^2$]	2545.1	2687.5	2926.2	1809.5

Beam-U vs Beam-C

Beam-U was tested to investigate the influence of UHPC overlay only with the CFRP laminates on the behavior of the beam. The behavior of Beam-U was similar to the behavior of Beam-C. The increase of the load capacity associated with strengthening the beam with UHPC overlay only is limited to 0.07%. As presented in **Figure 4.57**, the failure in both beams occurred due to crushing in the concrete top fibers. This proves that UHPC overlay only has a limited effect on the beam capacity.

(a) (b)

Figure 4.57: Failure in (a) Beam-C (b) Beam-U

The mid-span displacement at failure in Beam-U was 4.9% higher than the mid-span failure displacement in Beam-C. Load-displacement for both Beam-C and Beam-U are presented in **Figure 4.58**. The toughness for both beams was calculated as the area under the load-displacement curve. The toughness for Beam-C and Beam-U were 13.3 kN.m and 15.4 kN.m respectively.

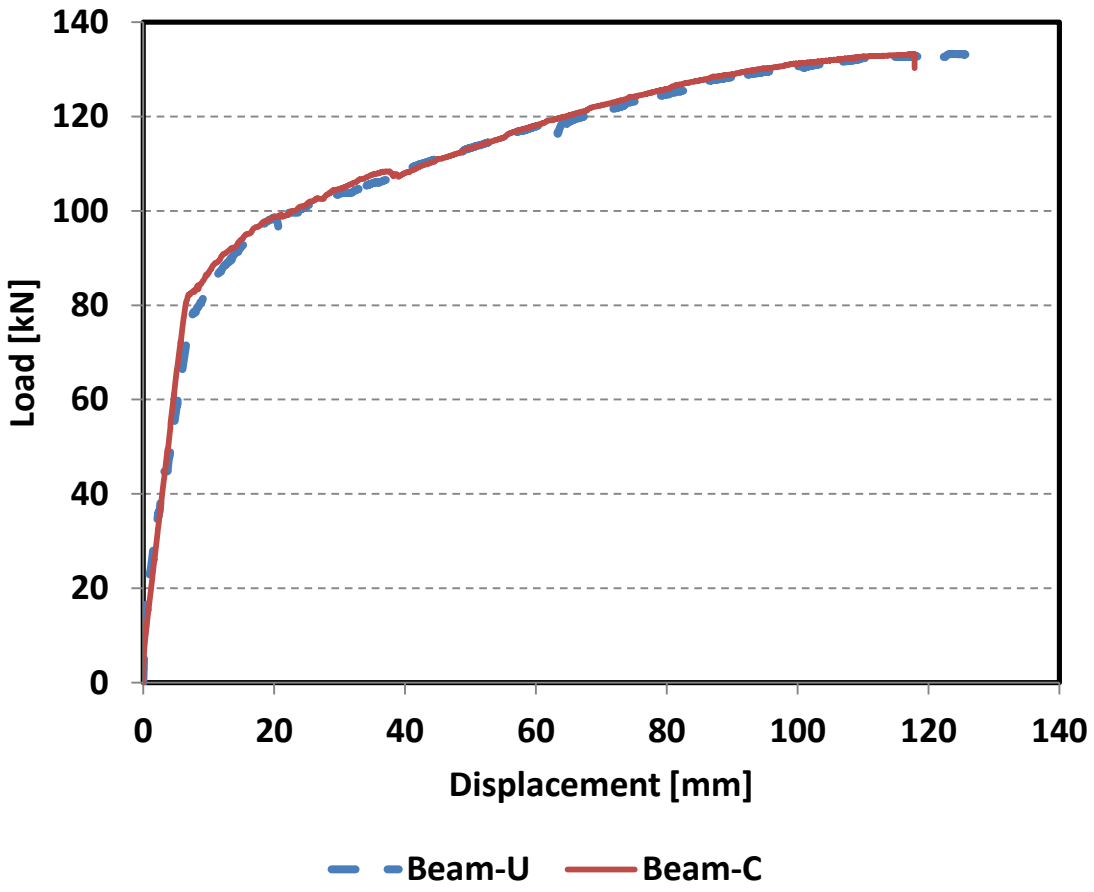

Figure 4.58: Load-displacement for both Beam-C and Beam-U

After yielding of the beams, both beams behaved in the same manner. However, the effect of the UHPC overlay is observed on the linear-elastic part of the load-displacement curve shown in **Figure 4.59**. The initial stiffness $\left(\frac{\delta P}{\delta \Delta}\right)$ of Beam-U was increased by 120.7%. Unlike the initial stiffness, the cracked stiffness of Beam-U was decreased by 27.6%. First part of moment-curvature of both beams up to curvature of 0.02 m^{-1} is presented in **Figure 4.60.** This curvature is corresponding to compressive strain in concrete top fiber of -0.0007 in both beams.

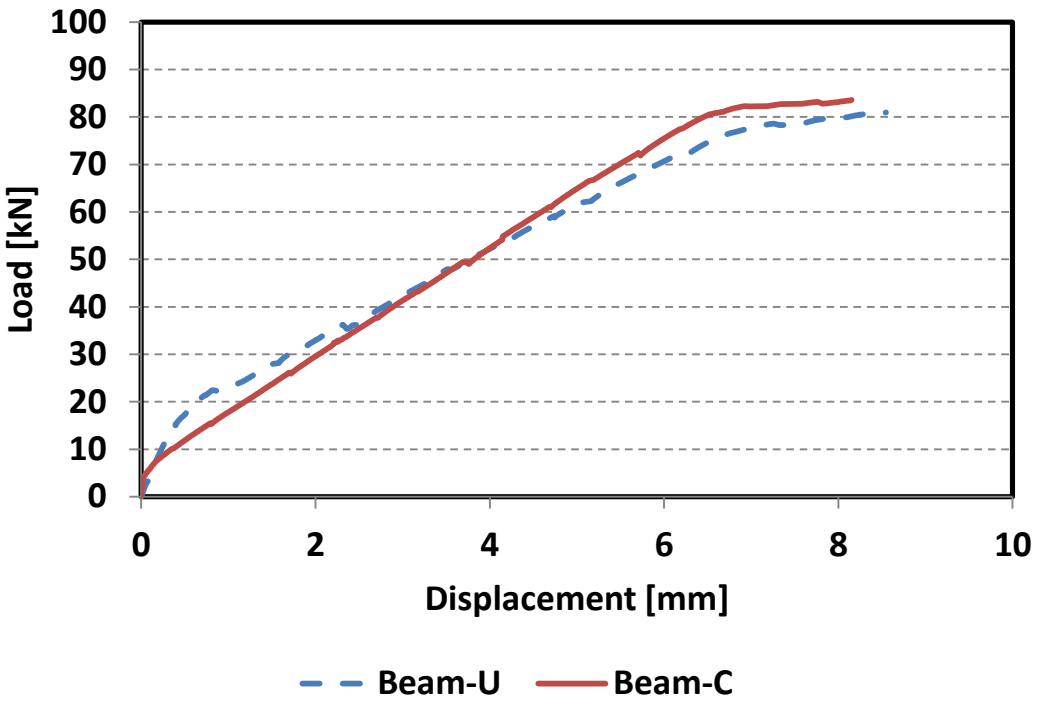

Figure 4.59: Linear-elastic part of the load-displacement for both Beam-C and Beam-U

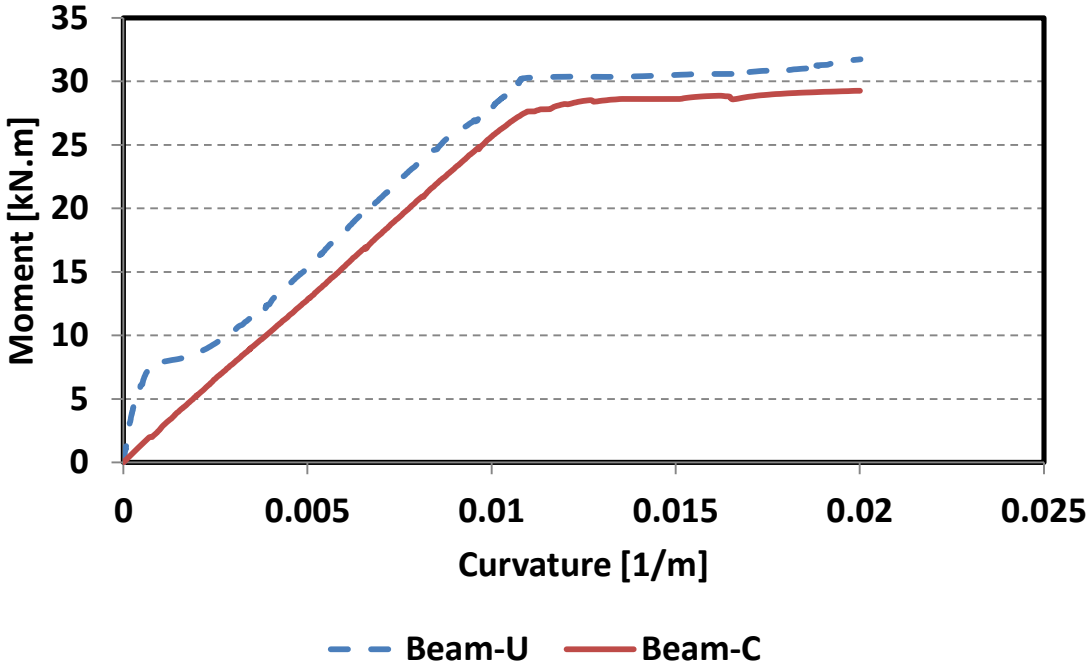

Figure 4.60: First part of moment-curvature for both Beam-C and Beam-U

The change in flexural stiffness (EI) for Beam-C after cracking is very limited and cannot be observed in the moment-curvature curve. Calculations show that the cracked flexural stiffness of Beam-C is 12.4% less than the initial flexural stiffness. For Beam-U, the initial flexural stiffness was increased by 435% due to the UHPC layover. The cracked flexural stiffness for Beam-U is calculated to be 5.6% higher than the cracked flexural stiffness of Beam-C. Moreover, the curves show that Beam-U yielded at a moment 9% higher than the yielding moment of Beam-C. After yielding, both beams behaved in the same manner. A yielding plateau was observed where the curvature of both beams started to increase with no increase in the moment value until the curvature reached 0.18 m^{-1}. Afterwards, the curvature increase was corresponding to a minimal increase in the applied moment.

Beam-UF vs Beam-C

Beam-UF was tested to investigate the new proposed strengthening technique. The beam was strengthened with CFRP laminates and 51 mm UHPC overlay. The load capacity for Beam-UF was 145.5 kN. The increase of the beam capacity associated with the strengthening technique was 9.2%. The mid-span failure displacement was decreased by 7.3%. As shown in **Figure 4.61**, the failure in Beam-UF was associated with shear failure unlike the failure in Beam-C which was associated with flexural failure. The change in the failure mode form crashing concrete top fiber in Beam-C to debonding at the support area associated with shear cracks in Beam-UF proves that Beam-UF was successfully strengthened in flexure and the failure of the beam was due to shear not flexural. Although the calculated shear capacity for Beam-UF was more than 300 kN, the shear failure occurred at a relatively low load due to the tensile demand of the shear force and

the insufficient developing length for the rebars at the support following equation **4.30** [39].

$$A_s f_s \geq \left[\frac{M}{0.9d} + (V_n - 0.5V_s)\cot\theta \right] 10^3 \quad \textbf{(4.30)}$$

Where

f_s: Allowed stress in steel rebars [MPa].

M: Bending moment at distance (d) from the support [kN.m].

V_n: Nominal shear force at distance (d) from the support [kN].

θ: Angle of inclination of the principal diagonal compressive stresses (taken 45°).

$$f_s = \frac{l}{l_d} f_y \quad \textbf{(4.31)}$$

Where

l: Actual provided developing length [m].

l_d: Required developing length [m].

The actual shear force on the beam (V_{max}) at failure was calculated using equation **4.32**

$$V_{max} = V_P + V_{sw} + V_{setup} \quad \textbf{(4.32)}$$

Where

V_P: Shear force due to applied load = P/2 [kN].

V_{sw}: Shear force due to beam self-weight [kN].

V_{setup}: Shear force due to loading setup weights [kN].

The nominal shear capacity calculated from equations **4.30** and **4.31** was75.1 kN. The actual shear for on the beam calculated using equation **4.32** was 75.2 kN. The beam failed just after the maximum shear force passed the nominal shear capacity. This proves that failure was governed by shear and the beam would have been able to carry more load if the steel rebars were will detailed and developed. This observation sheds light on a fact reported by other researcher which is related to potential change in failure mode [5]. From a practical point of view, the development length of rebars in almost all old codes is shorter than current required by ACI 318. Designers might need to pay attention to that fact that flexural strengthening of RC beams might shift the failure mode to be governed by shear. The amount of shear stirrups might not be the critical issue but rather the tension demand on the longitudinal bars. Further research is needed in that area to formulate consecutive load capacity for flexure strengthened RC beams.

(a) (b)

Figure 4.61: Failure mode for (a) Beam-C (b) Beam-UF

Figure 4.62 shows that the debonding in Beam-UF was between the UHPC overlay and the lower concrete part not between the CFRP laminates and the concrete.

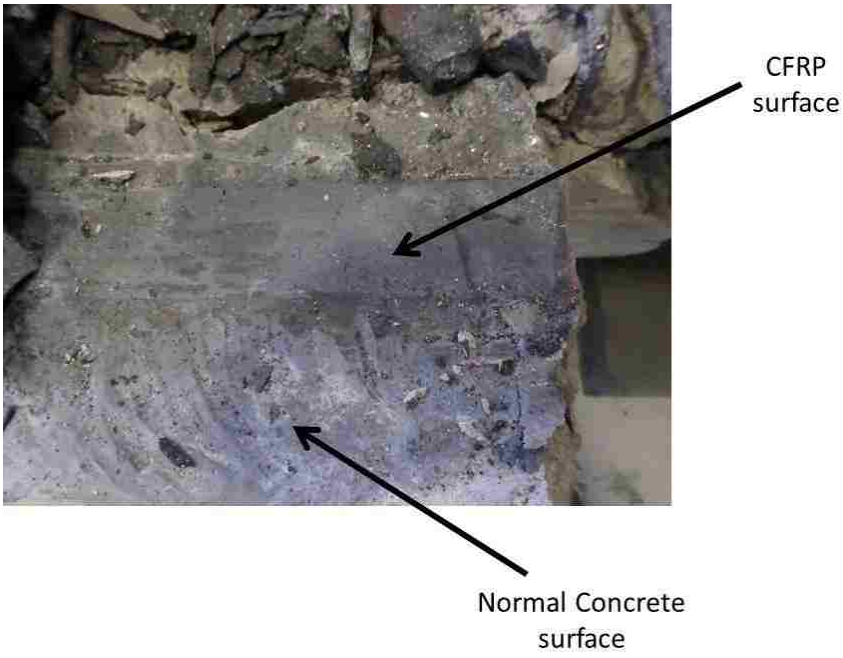

Figure 4.62: CFRP laminates in Beam-UF after failure

Figure 4.63 shows the load-displacement curves for both Beam-UF and Beam-C. The toughness for Beam-UF was 13.1 kN.m. The toughness of Beam-UF was 1.5% less than the toughness of Beam-C. The curves show that Beam-UF was gaining more load after yielding more than in Beam-C. The linear-elastic parts of load-displacement curves shown in **Figure 4.64** show the change in the initial and cracked stiffness of the strengthened beam. The initial stiffness of Beam-UF was increased by 52% and the cracked stiffness was decreased by 38.8%.

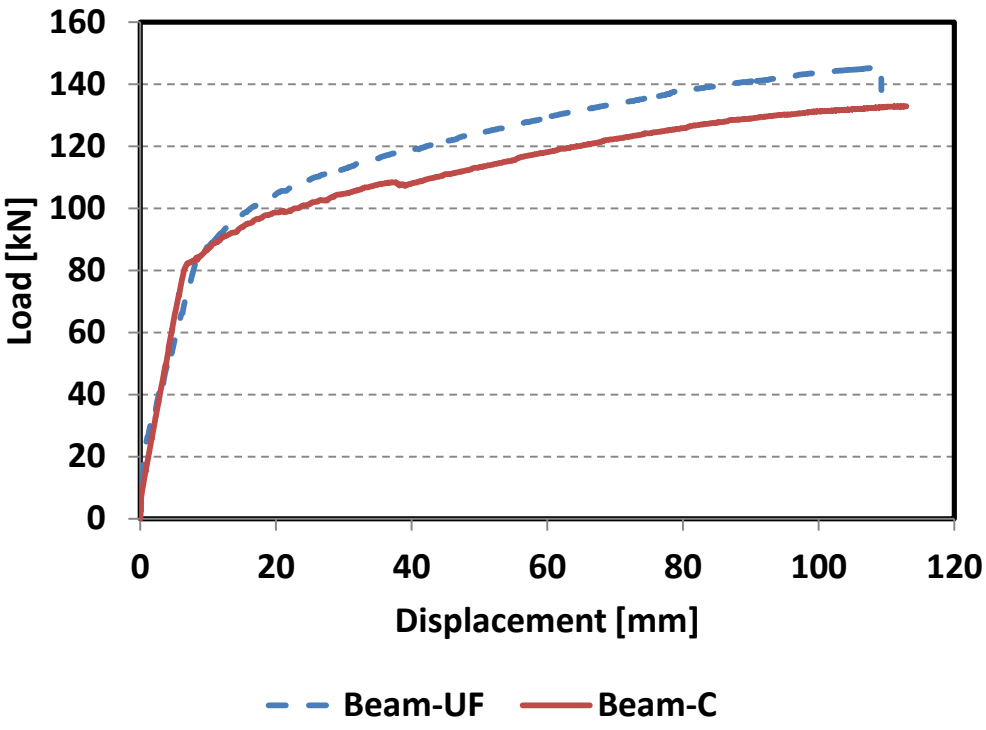

Figure 4.63: Load-displacement curves for both Beam-C and Beam-UF

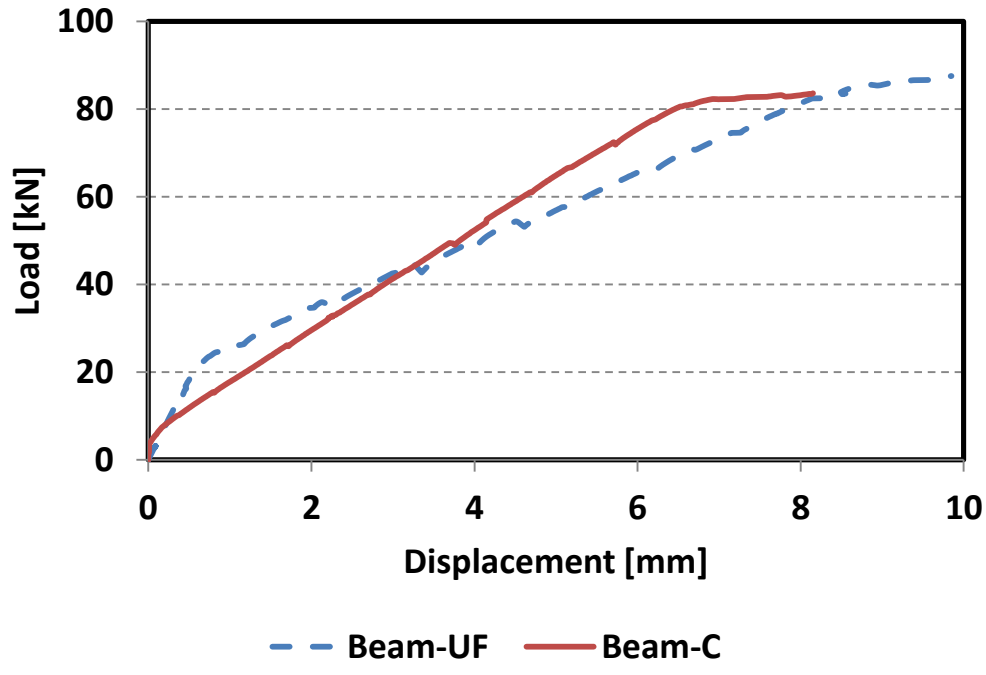

Figure 4.64: Linear-elastic part of the load-displacement curves for both Beam-C and Beam-UF

First part of moment-curvature curves for Beam-C and Beam-UF up to curvature of 0.032 m^{-1} in both beams are presented in **Figure 4.65**. This curvature is corresponding to compressive strain in concrete top fiber of -0.001 and -0.0012 for Beam-C and Beam-UF respectively. The curves show that the initial and cracked flexural stiffness of Beam-UF were increased by 447.6% and 15% respectively. Moreover, the curves show that Beam-UF yielded at a moment 22.8% higher than yield moment of Beam-C. After yield, Beam-UF behavior was slightly deferent than the behavior of Beam-C. The applied moment on Beam-UF continue to increase with the increase of the curvature with lower rate without yielding plateau.

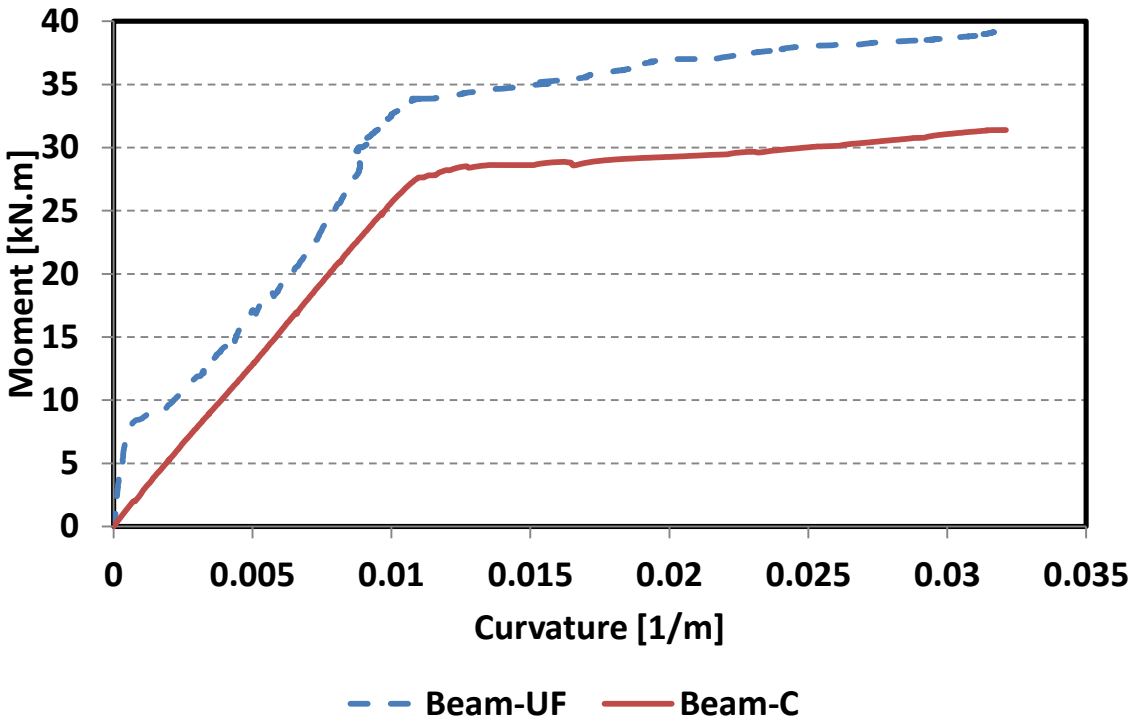

Figure 4.65: First part of moment-curvature for both Beam-C and Beam-UF

Beam-MUF vs Beam-C

Beam-MUF was tested to investigate the influence of the SBR polymer latex on the bonding between the LMUHPC overlay and the normal concrete. The LMUHPC was expected to have more bonding strength than the UHPC and debond at higher load than the UHPC overlay. Despite the expected, the LMUHPC overlay debonded at lower load than the UHPC. Failures of both beams are presented in **Figure 4.66**. Beam-MUF was able to carry a maximum load of 123.5 kN. The load capacity for Beam-MUF was 7.3% less than the control beam. The mid-span failure displacement was decreased by 34%. **Figure 4.67** shows the load-displacement curves for both Beam-C and Beam-MUF. The toughness of Beam-MUF was 40.1% less than the toughness of the control beam.

(a) (b)

Figure 4.66: Failure mode for (a) Beam-C (b) Beam-MUF

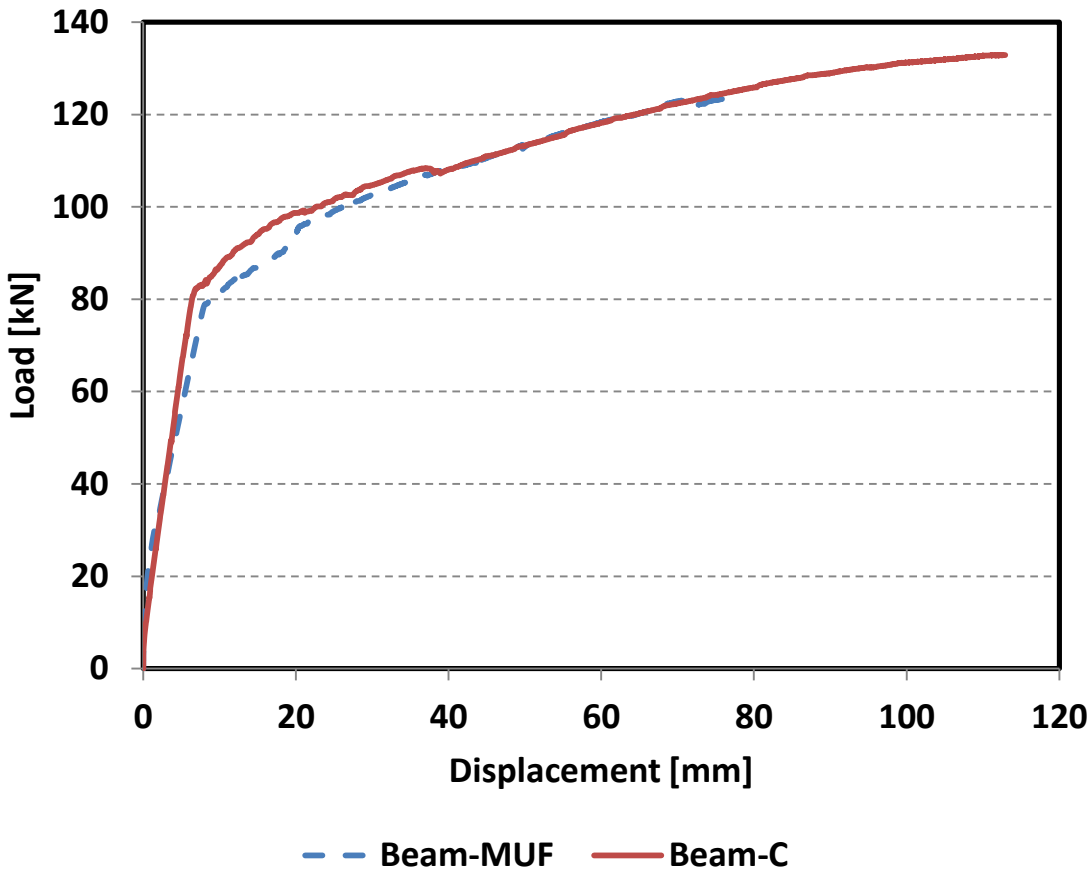

Figure 4.67: Load-displacement curves for both Beam-C and Beam-MUF

The linear-elastic parts of load-displacement curves shown in **Figure 4.68** show the change in the initial and cracked stiffness of the strengthened beam. The initial stiffness of Beam-UF increased by 109.6% and the cracked stiffness decreased by 32.8%.

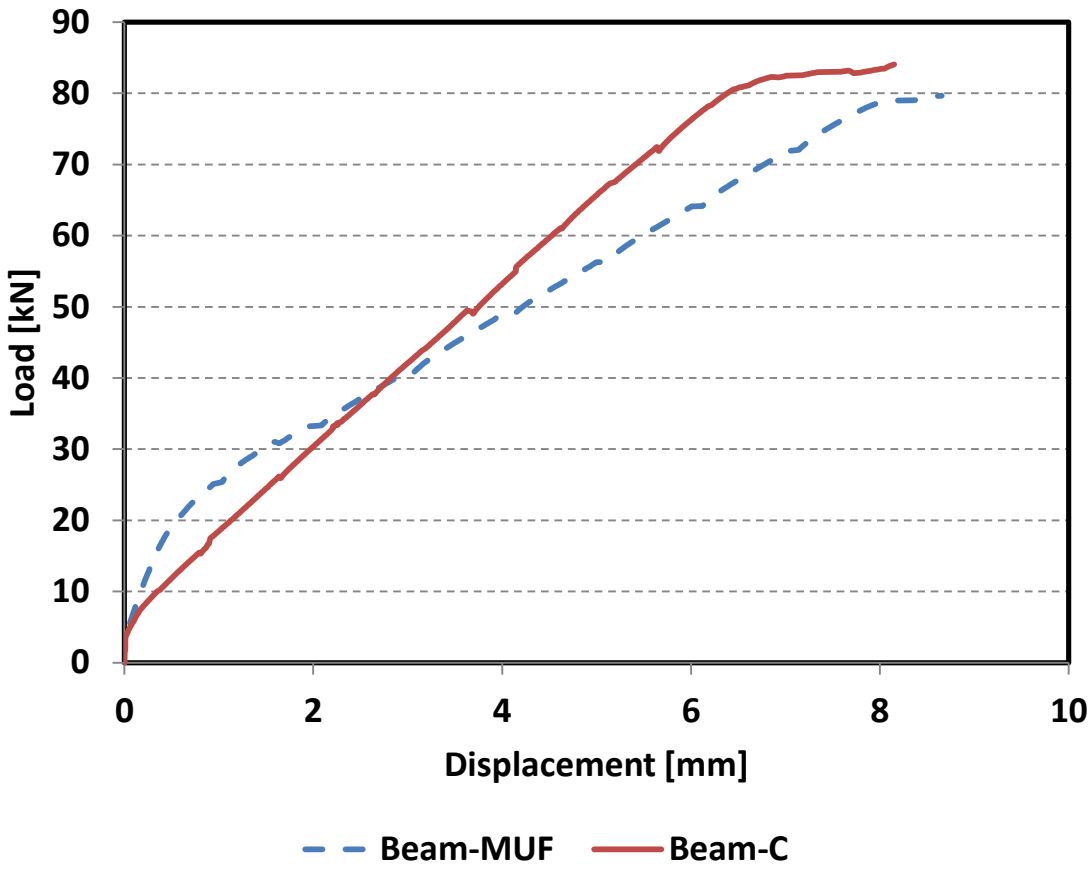

Figure 4.68: Linear-elastic part of the load-displacement curves for both Beam-C and Beam-MUF

Moment-curvature for both Beam-C and Beam-MUF up to curvature of 0.032 m^{-1} in both beams is presented in **Figure 4.69**. This curvature is corresponding to compressive strain in concrete top fiber of -0.001 and -0.0014 for Beam-C and Beam-UF respectively. The curves show that the initial flexural stiffness of Beam-MUF was increased by 667.6% and the cracked flexural stiffness was decreased by 28.9%. Moreover, the curves show that Beam-MUF yielded at a moment 4.7% less than the yielding moment of Beam-C. After yielding, Beam-MUF behavior was similar to the behavior of Beam-UF.

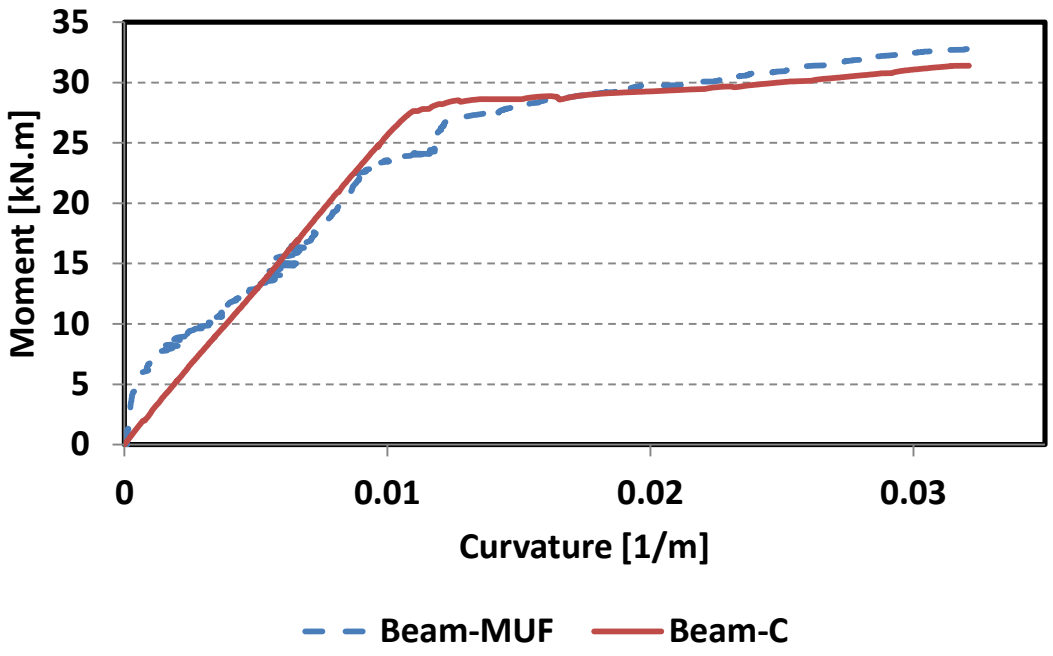

Figure 4.69: First part of moment-curvature for both Beam-C and Beam-MUF

Beam-MUF vs Beam-UF

Contradicting our hypothesis, LMUHPC overlay in Beam-MUF debonded at load 15% less than the failure load of Beam-UF and 7.3% less than the control beam. This low value of debonding load in LMUHPC is due to its relatively low Young's modulus of elasticity and its high deformability. In addition to that, LMUHPC has a higher Poisson's ratio than the normal concrete and UHPC [10, 33]. Equation **4.33** is used to calculate the vertical strain in LMUHPC and UHPC overlays.

$$\varepsilon_v = \frac{p}{EA}10^3 \qquad \textbf{(4.33)}$$

Where

ε_v: Vertical strain under loading point.

P: Applied load at each loading point = P/2 [kN].

A: Effective area of load distribution at the surface between the overlays and the normal concrete [mm^2].

The horizontal strain at the bottom surface of the overlay is related to the vertical strain as shown in equation **4.34**.

$$\varepsilon_h = \nu \varepsilon_v \quad \textbf{(4.34)}$$

Where

ε_h: Horizontal strain at the bottom surface of the overlay.

ν: Poisson's ratio = 0.17 for UHPC and 0.2 for LMUHPC [15, 33]

Substituting equation **4.34** in equation **4.33**, horizontal strain can be calculated using equation **4.35**.

$$\varepsilon_h = \frac{\nu \ p}{EA} 10^3 \quad \textbf{(4.35)}$$

To calculate the effective area in equation **4.33**, a load distributing slope 2 (vertical): 1 (horizontal) in the UHPC and LMUHPC overlays was assumed as shown in **Figure 4.70**.

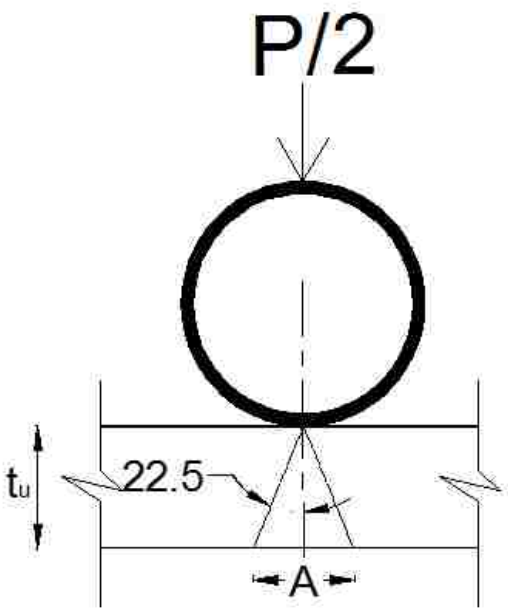

Figure 4.70: Load distribution in UHPC and LMUHPC overlays

A comparison between Beam-UF and Beam-MUF shows the vertical and horizontal strains under loading point in both beams is presented in **Table 4.7**. The comparison is held at the same load corresponding to the load at which the LMUHPC overlay in Beam-MUF started to debond. The high value of horizontal strain in Beam-MUF resulted in premature debonding between the LMUHPC overlay and the normal concrete section. Afterwards, debonding cracks propagated horizontally until the LMUHPC overlay was completely separated from the normal concrete section below as shown in **Figure 4.71.** The T-beam was no longer working as a composite section. On the other hand, the horizontal strain in UHPC overlay in Beam-UF is less than one half of the horizontal strain in LMUHPC overlay in Beam-MUF. This low value of horizontal strain is due to the relatively high modulus of elasticity and its relatively low Poisson's ratio. This deference in the horizontal strain explains why the LMUHPC overlay debonded early

while the UHPC overlay did not debond. A LMUHPC with elastic modulus than used here and with sufficient bond strength might resulted in further improvement in system load carrying capacity

Table 4.7: Vertical and horizontal strains in Beam-UF and Beam-MUF

	Beam-UF	Beam-MUF
P [kN]	122	122
p [kN]	61	61
ε_v	8.7×10^{-5}	1.6×10^{-4}
ε_h	1.5×10^{-5}	3.1×10^{-5}

Figure 4.71: Debonding of LMUHPC overlay in Beam-MUF

Service Load

According to ACI 318, the service bending moment of Beam-C and Beam-UF were calculated to be 25.7 kN.m and 28.1 kN.m corresponding to applied load of 74.9 kN and 81.8 kN respectively. The curvatures for both beams were calculated at service loads to be 0.0088 m^{-1} and 0.001 m^{-1} for Beam-C and Beam-UF respectively as shown in **Figure 4.65**. Although the UHPC overlay was able to reduce the curvature of the beam at service load, the effect of the overlay on the curvature of the beam was limited to 12%. This limited effect is due to the non-significant difference in the modulus of elasticity between

the UHPC and the normal concrete. The modulus of elasticity of the UHPC is only 18.4% higher than the modulus of elasticity of the normal concrete.

CHAPTER 5. Conclusions and Recommendations

In this research, a new proposed technique for strengthening RC T-beam in flexure was proposed and investigated. The new system is a combination of Carbon Fiber Reinforced Polymer (CFRP) laminates with Ultra High performance Concrete (UHPC) overlay applied on the compression side of the beam. Four T-beams were cast and tested under flexural loading to validate the proposed strengthening technique. In this chapter, conclusions based on the experimental observations and analysis are drawn followed by some recommendations for future work.

5.1. Conclusion

The experimental observations show that the proposed strengthening system was able to increase the load capacity of the strengthened T-beam. A combination of the UHPC overlay and CFRP allowed a flexural capacity increase of 9.2%, which pushed the neutral axis up and made the CFRP laminates act under tension. Although the increase in the load capacity was limited to 9.2%, it was observed that the failure mode of the T-beam was changed from flexural failure to shear failure. It was shown that this very limited increase was due to the limited anchorage length of the rebars at the supports and thus the shears capacity of the beam. The system would have been more effective if the beam had more shear capacity than what was used.

Moreover, strengthening the beam with a UHPC overlay only without CFRP had almost no significant effect on the T-beam capacity. The behavior of the T-beam with only UHPC was similar to the behavior of the control T-beam. The failure of the beam was due to crushing of the concrete top fibers and the increase in the load capacity was less

than 1%. This proves that the CFRP laminates had a major contribution in increasing the flexural capacity in the strengthened beam using the presented system.

When the UHPC overlay was replaced with Latex Modified Ultra High Performance Concrete (LMUHPC) to improve the bond strength between the LMUHPC overlay and the normal concrete section, the experimental observations showed that the behavior of this T-beam was opposite what was expected. The T-beam strengthened with CFRP and LMUHPC failed at load 7.3% less than the control beam. The premature failure of the beam was due to debonding between the LMUHPC overlay and the normal concrete surface at the two loading points. This debonding propagated horizontally until the LMUHPC overlay was fully separated from the normal concrete section. Modifying UHPC with Styrene-Butadiene Rubber (SBR) polymer latex resulted in reducing the modulus of elasticity and increasing Poisson's ratio of concrete overlay. The LMUHPC became very deformable compared with the normal concrete underneath. This resulted in high shear stresses that resulted in debonding of the LMUHPC overlay from the normal concrete T-beam.

Finally, it was concluded that the proposed strengthening system is efficient with slabs and shallow and medium depth T-beams. As the depth of the T-beam increases, the efficiency of the strengthening technique decreases due to the limited moment arm that becomes available to the CFRP laminates.

5.2. Recommendations

Further investigation on the efficiency of the strengthening technique is required. It is recommended to investigate the strengthening technique on beams with higher shear

capacity or combine the flexure strengthening with shear strengthening. Moreover, investigating the effect of the strengthening technique on beams with different dimensions and different reinforcement ratios is also recommended. Furthermore, investigating the effect of using LMUHPC with low SBR polymer content (5-7%) is also recommended.

References

[1] The Cement Sustainability Initiative., *Recycling Concrete*. 2009, The Cement Sustainability Initiative.

[2] U.S. Geological Survey, *Mineral Commodity Summaries 2013: U.S. Geological Survey*. 2013. p. 38-39.

[3] Garner, A.P., *Strengthening Reinforced Concrete Slabs Using a Combination of CFRP and UHPC*. 2011, University of New Mexico: Albuquerque, NM, USA.

[4] Mosallam, A., Reda Taha, M.M., Kim, J.J. and Nasr, A., *Strength and ductility of RC slabs strengthened with hybrid high-performance composite retrofit system.* Engineering Structures, 2012. **Vol. 36**: p. 70-80.

[5] Kim, J.J., H-C, NOH, Reda Taha, M.M., Masallam, A., *Establishing Design Limits for RC Slabs Strengthened with Hybrid FRP-HPC Retrofit System.* Journal of Composites. Part B: Engineering, 2013. **Vol. 51**: p. 19-27.

[6] Hag-Elslsafi, O., Alampalli, A., Kunin, J., *Application of FRP laminates for strengthening of a reinforced-concrete T-beam bridge structure.* Composite Structures, 2001. **Vol. 52**: p. 453-466.

[7] Attari, N., Amziane, S., Chemrouk, M., *Flexural strengthening of concrete beams using CFRP, GFRP and hybrid FRP sheets.* Construction and Building Materials, 2012. **Vol. 37**: p. 747-757.

[8] Duthinh, D. and M. Stranes, *Strengthening of Reinforced Concrete Beams with Carbon FRP.* Composites in Constructions, 2001: p. 493-498.

[9] Siddiqui, N.A., *Experimental investigation of RC beams strengthened with externally bonded FRP composites.* Latin American Journal of Solids and Structures, 2009. **Vol. 9**: p. 343 – 362.

[10] Toutanji, H., Zhao, L., and Zhang, Y. *Flexural behavior of reinforced concrete beams externally strengthened with CFRP sheets bonded with an inorganic matrix.* Engineering Structures, 2006. **Vol. 28**: p. 557–566.

[11] ACI Committee 440, *Guide for the Design and Construction of Externally Bonded FRP Systems for Strengthening Concrete Structures*. 2002, American Concrete Institute.

[12] Gravina, R.J. and Smith, S.T., *Flexural behaviour of indeterminate concrete beams reinforced with FRP bars.* Engineering Structures, 2008. **Vol. 30**: p. 2370–2380.

[13] Lau, D. and Pam, H.J., *Experimental study of hybrid FRP reinforced concrete beams.* Engineering Structures, 2010. **Vol. 32**: p. 3857–3865.

[14] Ceroni, F., *Experimental performances of RC beams strengthened with FRP materials.* Construction and Building Materials, 2010. **Vol. 24**: p. 1547–1559.

[15] American Concrete Institute, *ACI 548.4-11: Specification for Latex-Modified Concrete Overlays*. 2012, American Concrete Institute.

[16] Barluengaa, G. and Herna´ndez-Olivares, F., *SBR latex modified mortar rheology and mechanical behaviour.* Cement and Concrete Research, 2004. **Vol. 34**: p. 527-535.

[17] Muhammad, B., Ismail M., Bhutta, M.A.R., Abdul-Majid, Z.., *Influence of non-hydrocarbon substances on the compressive strength of natural rubber latex-modified concrete.* Construction and Building Materials, 2012. **Vol. 27**: p. 241–246.

[18] Wang, R., X.-G. Li, and Wang, P.-M., *Influence of polymer on cement hydration in SBR-modified cement pastes.* Cement and Concrete Research, 2006. **Vol. 36**: p. 1744–1751.

[19] Yun, K.-K. and Choi, P., *Causes and controls of cracking at bridge deck overlay with very-early strength latex-modified concrete.* Construction and Building Materials, 2014. **Vol. 56**: p. 53–62.

[20] Sprinkel, M.M., *Sampling and Testing Latex-Modified Concrete for Permeability to Chloride Ion.* Journal of the Transportation Research Board, 2009: p. 47–52.

[21] BASF Corporation., *Manual for Placement of Latex Modified Concrete*. 2011, BASF Corporation.

[22] Muhammad, B. and Ismail, M., *Performance of natural rubber latex modified concrete in acidic and sulfated environments.* Construction and Building Materials, 2012. **Vol. 31**: p. 129–134.

[23] Kuhlmann, L.A., *Latex modified concrete for the repair and rehabilitation of bridges.* International Journal of Cement Composites and Lightweight Concrete, 1985. **Vol. 7**: p. 241–247.

[24] Reda, M.M., Shrive, N.G., and Gillott, J.E. , *Microstructural investigation of innovative UHPC.* Cement and Concrete Research, 1999. **Vol. 29**: p. 323–329.

[25] Graybeal, B.A., United States. Federal Highway Administration. Office of Infrastructure Research and Development., Turner-Fairbank Highway Research Center., and Performance Systems International (Reston Va.), *Material property characterization of ultra-high performance concrete*. 2006, Federal Highway Administration, Office of Research, Development and Technology: McLean, Va.

[26] Bhanja, S. and Sengupta, B., *Optimum Silica Fume Content and Its Mode of Action on Concrete.* ACI Materials Journal, 2003. **100**(5): p. 407-412.

[27] Schieβl, P., Mazanec, O., and Lowke, D., *SCC and UHPC - Effect of Mixing Technology on Fresh Concrete Properties*, in *Advances in Construction Materials 2007*, C.U. Grosse, Editor. 2007, Springer Berlin Heidelberg. p. 513-522.

[28] Markeset, G., *Ultra High Performance Concrete is Ideal for Protective Structures.* ACI Materials Journal, 2002. **207**(8): p. 125-138.

[29] Graybeal, B.A., *Compressive Behavior of Ultra-High-Performance Fiber-Reinforced Concrete.* ACI Materials Journal, 2007. **104**(2): p. 146-152.

[30] Bierwagen, B.M.A.D. *Ultra High Performance Concrete Highway Bridge*. in *2005 Mid-Continent Transportation Research Symposium*. 2006. Ames, Iowa: Iowa State University.

[31] Vishay Precision Group, *Instruction Bulletin B-129-8*, in *Surface Preparation for Strain Gage Bonding*. 2010, Micro-Measurements.

[32] Vishay Precision Group, *Application Note TT-611*, in *Strain Gage Installation for Concrete Structures*. 2010, Micro-Measurements.

[33] American Concrete Institute, *ACI 318-08: Building Code Requirements for Structural Concrete and Commentary*. 2008, American Concrete Institute.

[34] ASTM International, *ASTM C39 / C39M - 10 Standard Test Method for Compressive Strength of Cylindrical Concrete Specimens*. 2010, ASTM International: West Conshohocken, PA.

[35] ASTM International, *ASTM C496 / C496M - 04e1 Standard Test Method for Splitting Tensile Strength of Cylindrical Concrete Specimens*. 2004, ASTM International: West Conshohocken, PA.

[36] ASTM International, *ASTM C469 / C469M - 10 Standard Test Method for Static Modulus of Elasticity and Poisson's Ratio of Concrete in Compression*. 2010, ASTM International: West Conshohocken, PA.

[37] ASTM International, *ASTM C1064/C1064M – 12 Standard Test Method for Temperature of Freshly Mixed Hydraulic-Cement Concrete*. 2013, ASTM International: West Conshohocken, PA.

[38] ASTM International, *ASTM C231/C231M – 10 Standard Test Method for Air Content of Freshly Mixed Concrete by the Pressure Method*. 2010, ASTM International: West Conshohocken, PA.

[39] Standards Council of Canada, *Canadian highway bridge design code (CHBDC).* Bridge Code. 2013, Canda: Standards Council of Canada.